Structural Response of Balloon type Cross-Laminated Timber at Component and Building
Levels

Kande Thanthrige Gayan Madushan Kandethanthri

A Thesis

In

the Department

of

Building, Civil, and Environmental Engineering

Presented in Partial Fulfillment of the Requirements

For the Degree of

Master of Applied Science (Civil Engineering)

at Concordia University

Montréal, Québec, Canada

May 2024

CONCORDIA UNIVERSITY

SCHOOL OF GRADUATE STUDIES

This is to certify that the thesis prepared

By: Kande Thanthrige Gayan Madushan Kandethanthri

Entitled: Structural Response of Balloon type Cross-Laminated Timber at Component and

Building Levels

and submitted in partial fulfillment of the requirements for the degree of

Master of Applied Science (Civil Engineering)

complies with the regulations of the University and meets the accepted standards with

respect to originality and quality.

Signed by the final examining committee:

_____ Examiner

Dr. Anjan Bhowmick

_____ Examiner

Dr. Behrooz Yousefzadeh

_____ Thesis Supervisor

Dr. Ghazanfarah Hafeez

Approved by

_____

Dr. Chunjiang An, Graduate Program Director

May 2nd, 2024

_____

Dr. Mourad Debbabi, Dean of Faculty

Abstract

Structural Response of Balloon type Cross-Laminated Timber at Component and Building Levels

Kande Thanthrige Gayan Madushan Kandethanthri

This thesis delves into the performance of balloon-type cross-laminated timber buildings. The study focuses on hybrid buildings with balloon-type cross-laminated timber shear walls and steel frames. The effects of mass and vertical geometric irregularities in hybrid buildings are evaluated using Modal Response Spectrum Analysis. The findings reveal that mass irregularities markedly influence inter-story drift, mainly when mass is incorporated at different levels, and that the location of mass addition is vital to the building's seismic response. The vertical geometric irregularity of the building impacts the seismic response uniquely in two orthogonal directions.

Further, the study explores the lateral performance of unbonded post-tensioned balloon-type CLT shear walls. Traditional sensitivity analysis and machine learning models were employed to identify the critical parameters influencing the lateral and uplifting response of the unbonded post-tensioned balloon-type cross-laminated timber shear wall under lateral loading. Various machine learning algorithms were utilised to investigate the best performance model for predicting the critical parameters while applying Shapley Additive explanations (SHAP) to elucidate better the factors influencing lateral and uplifting responses.

The thesis offers valuable perspectives on integrating advanced computational techniques with traditional structural engineering practices, fostering the development of resilient and sustainable building designs.

Acknowledgements

Contribution of Authors

Chapter 3

1- KGM Kandethanthri, Ghazanfarah Hafeez. (2024, April). "Analysing Seismic Performance of Hybrid Structures: The Impact of Vertical and Mass Irregularities on Buildings with Ballone Type Cross-laminated Timber Shear Walls" Journal of Structural Engineering, American Civil Engineering Society Journal (Under review)

Chapter 4

2- KGM Kandethanthri, Ghazanfarah Hafeez, Zhiyong Chen (2024, March). "Structural Performance of Balloon-Type Unbounded Post-Tensioned Cross-Laminated Timber Wall System" Journal of Structural Engineering, American Civil Engineering Society Journal (Under review)

3- KGM Kandethanthri, Ghazanfarah Hafeez. (2024, May 25- 28). "Exploring Machine Learning Techniques for Analyzing Post-Tensioned Cross-Laminated Timber Behavior under Lateral Loads," *Canadian Society for Civil Engineering Annual Conference. 2024* (Accepted)

All authors reviewed the final manuscript and approved of the contents

Table of Contents

List of Figures

List of Tables

List of Abbreviations

CatBoost	Categorical Boosting
CLT	Cross-Laminated Timber
DT	Decision Tree
FE	Finite Element
GBDT	Gradient Boosting Decision Tree
ILS	Initial Lateral Stiffness
IVS	Initial Vertical Stiffness
LLRS	Lateral Load Resisting System
MAE	Mean Absolute Error
MAPE	Mean Absolute Percentage Error
MI	Mass Irregularity
MRSA	Modal Response Spectrum Analysis
NBCC	National Building Code of Canada
R^2	Coefficient of Determination
RF	Random Forest
RMSE	Root Mean Square Error
Ro	Overstrength-related factor
Rd	Ductility-related factor
RSA	Response Spectrum Analysis
RSA-Montreal	Response Spectrum Analysis based on Montréal (City Hall)
RSA-Vancouver	Response Spectrum Analysis based on Vancouver (City Hall)
SHAP	Shapley Additive Explanations

One.   Chapter 1. Introduction

1   General

In the current construction landscape, sustainability is not just a consideration but a necessity, and it has recently shifted towards materials with minimal environmental impact [1] due to the increasing public awareness of environmental issues such as climate change, deforestation, and resource depletion. While eco-friendly construction materials are gaining popularity, structural integrity and safety prerequisites must also be respected. As such, timber construction distinguishes itself as a sustainable option with its capability to lower the CO^2 footprint of timber structures [2] while concurrently demonstrating the capacity for use in residential, commercial, and educational facilities.

CLT was initially presented in Austria and Switzerland in the early 1990s [3]. However, the last decade has witnessed a remarkable popularity of timber in the construction sector, particularly in residential, office buildings, and educational facilities, challenging the dominance of mineral-based construction materials (concrete and brick). This popularity is partly attributed to the adoption of CLT [4]. With the contribution from the research community and timber manufacturing companies, production and standardisation extend beyond Europe to countries like Canada, the United States, Japan, China, and New Zealand [5]. CLT, as a recognised material for construction, has been incorporated in the National Building Code of Canada [6] to serve as the basis for the national safety standard of engineering [7]. Several technical obstacles affected the introduction of CLT to North American markets, including supply-side management [8,9], structural safety, fire resistance [10], and compatibility with the existing building codes [11]. These obstacles invite researchers to innovate, research, and focus on finding solutions to overcome such barriers.

CLT panels are engineered wood products comprising multiple layers of lumber boards stacked in alternating directions, typically at 90 degrees, bonded primarily with adhesives. This configuration can include glueing the boards' wide and narrow faces. Fig. 1-1 illustrated a CLT panel configuration.
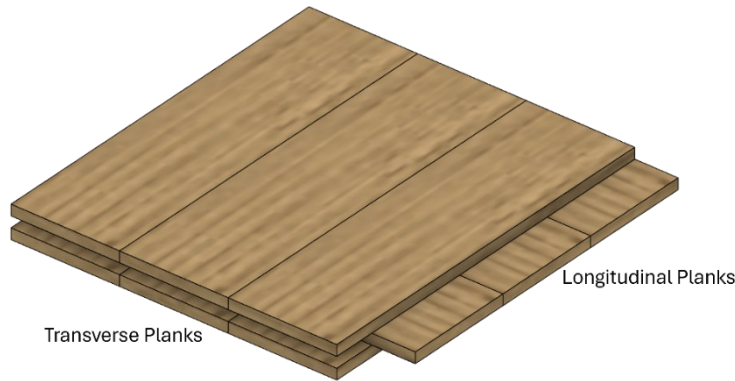
Fig. 1-1 CLT Panel Configuration

The core concept of CLT involves having at least three layers of timber boards with orientations alternating orthogonally to adjacent layers. This process enhances the panel's structural integrity. In terms of application, the orientation of the lumber in CLT panels is strategically selected based on their use within a structure; for walls, the outer layers are usually oriented vertically to support gravity loads effectively, whereas, for floors and roofs, they run parallel to the span direction to optimise load-bearing capacity.

CLT presents numerous benefits over conventional timber and mineral-based materials. From a construction point of view, CLT's prefabrication capabilities lead to efficient on-site assembly [12]. Further, its structural properties, such as high strength, rigidity, and stiffness, ensure durability and stability in building structures. CLT's physical and environmental properties, including low air permeability, significant humidity regulation [12], and thermal energy storage capacity [13], enhance its performance and sustainability in modern building applications. CLT is also well-suited for renovation and construction on weak soils due to its lightweight nature [3]. It allows for the completion of long-span structures combined with other timber or hybrid materials, offering rapid construction times, dry building sites, and precise, slender elements. Rather than merely replacing traditional construction materials, CLT emerges as a valuable alternative.

These benefits offset the increased environmental impact of building operations or maintenance of a CLT structure compared to traditional reinforced concrete buildings. Generally, mass timber buildings have higher operational energy demands and greenhouse gas emissions due to the thermal mass effect. Thermal mass refers to the ability of a material to absorb, store, and release heat. Materials with high thermal mass, such as concrete, can help moderate indoor temperatures by absorbing heat during warmer periods and releasing it during cooler ones, thus reducing the

need for mechanical heating and cooling. CLT has a lower thermal mass, which means it has less capacity to store heat, potentially leading to less natural temperature regulation and higher energy use for heating and cooling. However, despite these operational challenges, CLT structures emit less greenhouse gas emissions and have a greater biomass recovery yield during production, offering significant environmental advantages over the lifecycle of the building.

Two primary techniques for building CLT shear wall structures are balloon-type framing, which integrates floors through various connection techniques with continuous walls running the whole structure height [14,15] and platform-type construction, where each floor acts as a platform for the story above it, with steel brackets and hold-downs connecting walls to floors and foundations (see Fig. 1-2). Although both approaches offer distinct advantages, balloon-type framing is particularly well-suited for CLT construction due to its superior constructability. Further, this method enhances structural integrity, improving seismic performance [16] and boosting acoustic insulation, making it an excellent choice for diverse building applications. Fig. 1-2 illustrates two construction methods for CLT shear walls.

| (a)   (b |
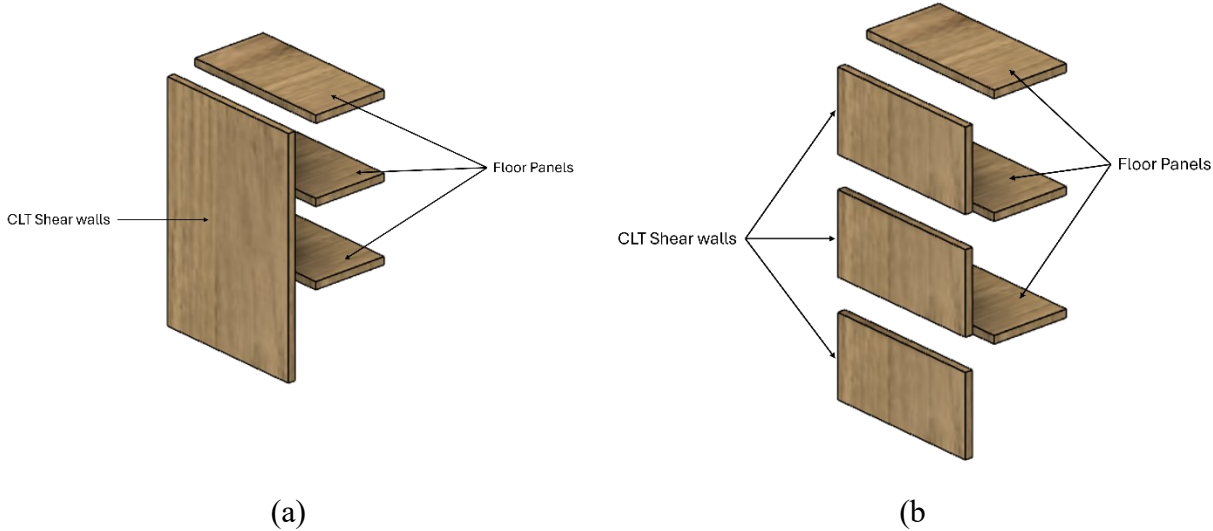
Fig. 1-2 Construction Methods for CLT Shear Wall (a) Balloon-Type CLT Construction (b) Platform-Type CLT Construction

1.1 Lateral Load Resisting System (LLRS)

Wood buildings exhibit a lighter mass than steel and concrete structures, consequently attracting lower seismic loads. However, this reduced mass also increases structural flexibility, rendering

these buildings more susceptible to overturning forces. These forces necessitate robust countermeasures via the LLRS. Shear wall systems are the predominant vertical LLRS in CLT buildings. Concrete LLRS provides strong resistance to lateral forces through its natural mass and stiffness. However, concrete LLRS demonstrates significant production resource usage and a large carbon footprint. Conversely, steel LLRS offers ductility and flexibility, allowing structures to absorb and release energy efficiently during seismic events. Steel systems are highly recyclable and can be engineered for quick construction; however, they require significant energy for production and are prone to corrosion.

A more efficient building solution is presented by introducing balloon-type CLT as a substitute or addition to concrete and steel LLRS that addresses the structural requirements of high-rise construction and the pressing need for sustainability within the built environment. This is achieved by combining wood's rapid renewability and carbon-sequestering capabilities with existing techniques [17,18]. The comparison between different LLRS systems is presented in TABLE 1-1. The guidelines for CLT shear walls outlined in CSA O86 are designed for platform-type construction, as highlighted by the standard's commentary. Nevertheless, balloon-type timber construction research has become increasingly popular in the last decade [14,19–24]. This construction method is widely acknowledged for utilising continuous wall studs extending from the bottom base to the top frame without interruption by floors. The implementation of balloon-type CLT shear walls provides multiple benefits, including the elimination of perpendicular-to-grain bearing between floors, the absence of cumulative perpendicular-to-grain shrinkage across the height of the building, reduced the number of panels required to accomplish a slender panel aspect ratio, a reduction in required connections throughout the building's height, and a low cumulative deformation [25].

TABLE 1-1 Comparison Between Different LLRS Systems

Attribute	CLT LLRS	Concrete LLRS	Steel LLRS
Material Properties	Lightweight, high strength-to-weight ratio	Heavy, inherently strong	Lightweight, high strength-to-weight ratio
Sustainability	Renewable resources sequester carbon, lower environmental impact	High carbon footprint due to cement production	Recyclable, but high energy consumption in production

Construction Pace	Fast, due to prefabrication and ease of assembly	Slow, requires onsite curing	Fast, due to prefabrication and ease of assembly
Fire Resistance	Good with proper design, chars at a predictable rate, providing inherent fire resistance	Excellent, inherent fire resistance without additional treatments	Requires protective coatings to achieve fire resistance
Cost	Competitive, but can be higher due to specialised labour and transport	Generally lower cost, widespread availability, and familiarity	Variable can be competitive but subject to market fluctuations in steel prices
Architectural Flexibility	High, allows for innovative design due to flexibility and esthetics	Moderate, can be bulky and limit design flexibility	High, allows for slender and flexible design options
Moisture Sensitivity	Sensitive requires design consideration for moisture protection and management.	Low, generally not affected by moisture	Moderate corrosion risk requires protective measures
Thermal Performance	An excellent natural insulator, it contributes to building energy efficiency.	Poor, requires additional insulation	Poor, requires additional insulation
Acoustic Performance	Good, with proper design, can achieve high acoustic performance	Suitable, mass provides natural sound damping	Variable depends on design but generally requires additional measures for sound damping

1.1.1 Hybrid Structures

Combining heterogeneous materials- such as steel, concrete, or timber- into hybrid building entities and structures is an established practice within the North American construction industry. For example, the combination of steel and concrete leverages their strengths—such as compressive strength, tensile resilience, and compressive resilience—and their shared thermal expansion coefficients. Furthermore, advancements in steel and timber connections have developed, suggesting increased efficiency when using metal fasteners within timber constructions. Such integrations have earned compliments for their enhanced efficiency in architectural design in recent years. The hybridisation of timber with other materials has only gained significant interest over the past two decades, driven by the unique properties of timber, including its environmental and mechanical benefits [26,27]. A notable application of such hybridity (steel and timber) is incorporating steel moment-resisting frames within timber-framed multi-residential buildings [28].

Hybrid structures can be categorised across components, systems, and building levels. Each category responds to specific structural demands, including permanent and transient loads, to enhance structural resilience to gravitational and lateral forces. Example projects using different hybrid levels are introduced in TABLE 1-2.

TABLE 1-2 Example Project Using Different Hybrid Levels

Hybrid Category	Hybrid Technology Type	Project	Location	Description
Component Level	Timber-Concrete Composite (TCC)	International House Sydney	Sydney, Australia	A commercial building featuring timber-concrete composite floors, highlighting sustainability and aesthetic appeal
System Level	Timber-Steel Hybrid Systems	Arbora Complex	Montreal, Canada	A residential and commercial complex utilises a hybrid system of CLT panels and steel,

				enhancing structural integrity and fire resistance
Building Level	Timber-Hybrid Modular Buildings	Dalston Works	London, K	One of the most significant CLT projects, this residential building uses modular construction techniques, combining timber with other materials for efficiency and sustainability

1.2 Cross-Laminated Timber Connections

The CLT connections are of the essence in making the CLT building's structural reliability and performance. The CLT construction is unique in its sustainability, strength, and adaptability. These connections, which can be designed as concealed [29] or exposed, play a crucial role in assembling CLT panels and ensuring the transfer of loads through the structure. Importantly, these connections also provide ductility, critical for lateral resistance, thereby improving the building's ability to withstand lateral forces. Different methods of fastening are used, such as mechanical fasteners—screws, nails, and dowels—as well as innovative techniques such as glued connections or steel connectors. The design of a CLT connection is critical when designing for structural capacities, such as shear, tension, and compression, as well as fire resistance and acoustic performance. In addition, the effectiveness and quality of these interfaces signify an improvement in castability, appearance, and weather resistance, which results in considering the CLT as one of the contemporary timber structures [3]. TABLE 1-3 Compares angle brackets, hold-downs, and Holz-Stahl-Komposit connections.

TABLE 1-3 Comparison Between Angle Bracks, Holddown And Holz-Schrauben-Klebstoff

Feature/Aspect	Angle Brackets (Fig. 1-3.a)	Hold-Downs (Fig. 1-3.b)	Holz-Stahl-Komposit (Fig. 1-3.c)
Material Composition	Metal, typically steel	Metal, typically steel	Combination of metal screws and adhesive, often with timber
Load Capacity	Moderate to high, depending on size and design	High, designed to resist uplift and lateral forces	High, enhanced by the combination of mechanical and adhesive bonds
Installation Complexity	Relatively simple, requires precise alignment	More complex, often requires tensioning	More complex, involves precise drilling, screwing, and application of adhesive [30]
Aesthetics	Visible, may require concealment for aesthetic purposes	Usually concealed within the structure	It can be almost invisible if designed correctly
Cost	Generally lower cost than specialised hold-downs	Higher cost due to specialised design and materials	Variable, depending on the type of screws and adhesive used

(a)

(b)
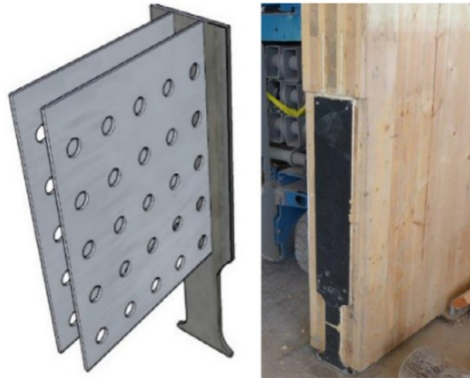
(c)

Fig. 1-3 CLT Connection Types

1.3 Post-Tensioning of Cross-Laminated Timber

Several studies have explored the lateral performance of both single and coupled CLT walls utilising traditional CLT connections, focusing on connections between walls and floors or foundations. The findings of these studies suggest that walls with appropriate height-to-length ratios (not less than 2) exhibit the ability to re-centre themselves following a substantial lateral load event. These walls remain primarily elastic and are significantly impacted by connection behaviour [31,32]. However, while proposing energy dissipation and ductility, these traditional connection systems are limited [33]. Subsequently, the National Building Code in Canada recommends their use under low ductility and modification factors [32,34]. This imposes an elastic design approach, leading to high shear forces at the base and upper story levels, hypothetically resulting in uneconomical designs, especially in high seismic regions [35].

A study conducted by Izzi et al. in 2018 explored the use of platform-type framing systems in multi-story structures. The study discovered significant flexibility and drift due to the slip of CLT panels at different floor levels [36]. Responding to this, researchers investigated unbounded post-tensioning for CLT shear wall panel-to-foundation connections. This research was inspired by the PREcast Seismic Structural System (PRESSS) program designed for concrete structures [37]. This system incorporates an unbounded post-tensioning strand to secure the CLT shear wall to the foundation, as illustrated in Fig 1. When subjected to a lateral force at its corner, the wall panel initiates a rocking motion, causing the post-tensioning strands to elongate and eventually restore the system to its original centre position once the load is removed [38,39].

With developments in timber construction techniques, the Unbounded Post-tension Cross-Laminated Timber (UPTC) shear wall system has appeared as an encouraging solution to increase the ductility of CLT shear walls. This technique offers several advantages, including increased seismic resilience and improved lateral load resistance. CLT shear walls employing this system are tied to the foundation using unbounded post-tensioning strands, as shown in Fig. 1-4.
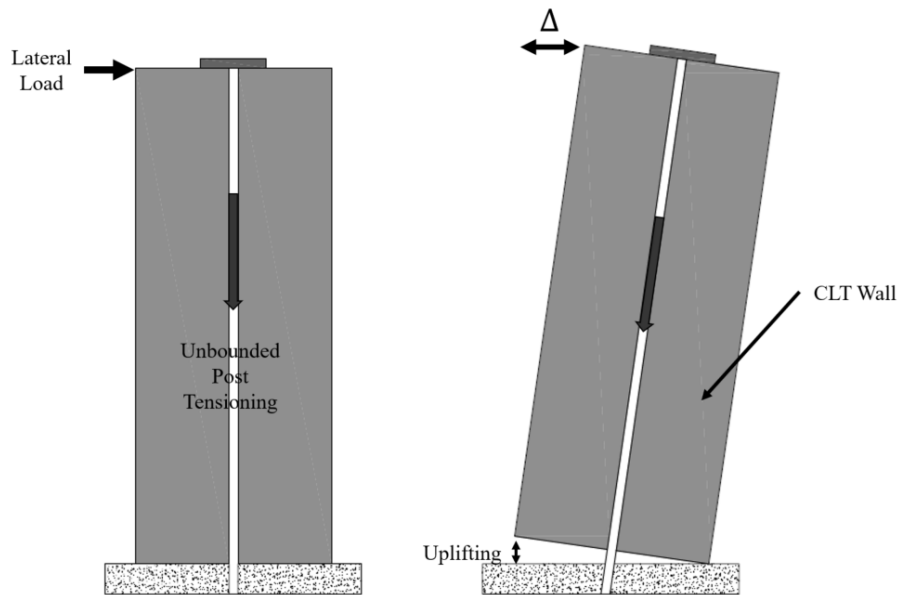
Fig. 1-4 UPTC Shear Wall

1.4   Motivation

1.4.1   CLT Seismic Capacity

Research results reveal a considerable increase in the seismic capacity from the balloon-type CLT compared to the platform-type CLT configurations [23,25]. Additionally, the literature demonstrates that CLT-hybrid structures have better seismic performance than other structures [40,41], emphasising that the balloon-type of CLT can significantly strengthen the structural integrity and resilience of buildings exposed to earthquakes. Extending the investigation's scope and including various buildings that use balloon-type CLT shear walls is required in this context. Hence, an overall analysis of the buildings within a broad spectrum of the CLT shear walls with and without post-tensioning is necessary.

1.4.2 CLT Reinforcement Techniques

Reinforcement techniques have demonstrated [42–45] increased lateral resistance of CLT Ballon-type shear walls. However, unbounded post-tensioning and its unique advantages in enhancing ductility and energy dissipation is a gap in the CLT reinforcement research, and an in-depth examination of the efficacy of various reinforcement strategies is necessary. Given the emerging stage of unbounded post-tensioning in CLT and the lack of related research, a thorough investigation into the factors influencing the UPTC shear wall's lateral stiffness is necessary. This investigation is approached through traditional sensitivity analysis and the application of advanced ML techniques.

1.4.3 Machine Learning Methods

The employment of ML methods in structural engineering is sometimes scrutinised in literature due to their perceived opacity, which complicates the interpretation of results and the understanding of influences on output parameters. To mitigate this issue, the application of SHapley Additive exPlanations (SHAP) analysis has been proposed as a method to clarify the "black box" nature of ML models, facilitating a more transparent comprehension of the variables impacting the lateral resistance of UPTC shear wall [46,47].

1.4.4 Primary Motivation

Exploration of more modern issues in building structures, such as the severity of seismic occurrences across the globe, urges engineers to introduce novel methods of designing and constructing structures that meet the prerequisites of structural integrity, safety, and sustainable development. CLT poses a fascinating opportunity, demonstrating the capability to address seismic design regulations due to its notable lightness, strength and eco-friendliness. The incorporation of CLT remains at the developing and mostly research-driven stage, thus critically necessitating the progressed experimental inquiry to discover a complete functionality.

The primary motivation of this thesis is to contribute significantly to the body of knowledge in structural engineering by offering novel insights into the behaviour of CLT balloon-type systems, mainly by further investigating hybrid (CLT-Steel) structural irregularities. Additionally, it aims to prove that integration with ML can answer some critical questions that have emerged in the

structural engineering research field. The findings are crucial in developing more sustainable and resilient CLT structures, ensuring their efficacy and safety in areas prone to seismic activity, and providing a framework for future research studies to incorporate with ML. This endeavour aligns with academic pursuits and aims to advance structural engineering toward sustainable and safe construction practices.

1.5   Research Objective

The primary purpose of this research is to comprehensively examine the seismic behaviour of hybrid buildings that contain balloon-type CLT shear walls. This research will help understand CLT shear wall capacities by incorporating unbounded post-tensioning techniques into the balloon-type. The research objectives of this thesis are to:

1. Assess the seismic performance of hybrid constructions with balloon-type CLT shear walls, emphasising how mass and vertical irregularities affect the building's structural resilience and sustainability.
2. Validate the unbounded post-tensioned CLT through literature comparison to explore the factors impacting its lateral performance using traditional sensitivity analysis.
3. Develop a machine learning-based predictive model to predict the initial stiffness of an unbounded CLT shear wall and, through SHAP analysis, identify the critical factors affecting the lateral stiffness of an unbounded post-tension CLT shear wall.

1.6   Research Methodology

To achieve the research objectives, Finite Element (FE) modelling software programs (Dlubal RFEM 6.05 and ABAQUS/Standard) were used. Fig. 1-5 illustrates the research framework and how the goals are achieved.
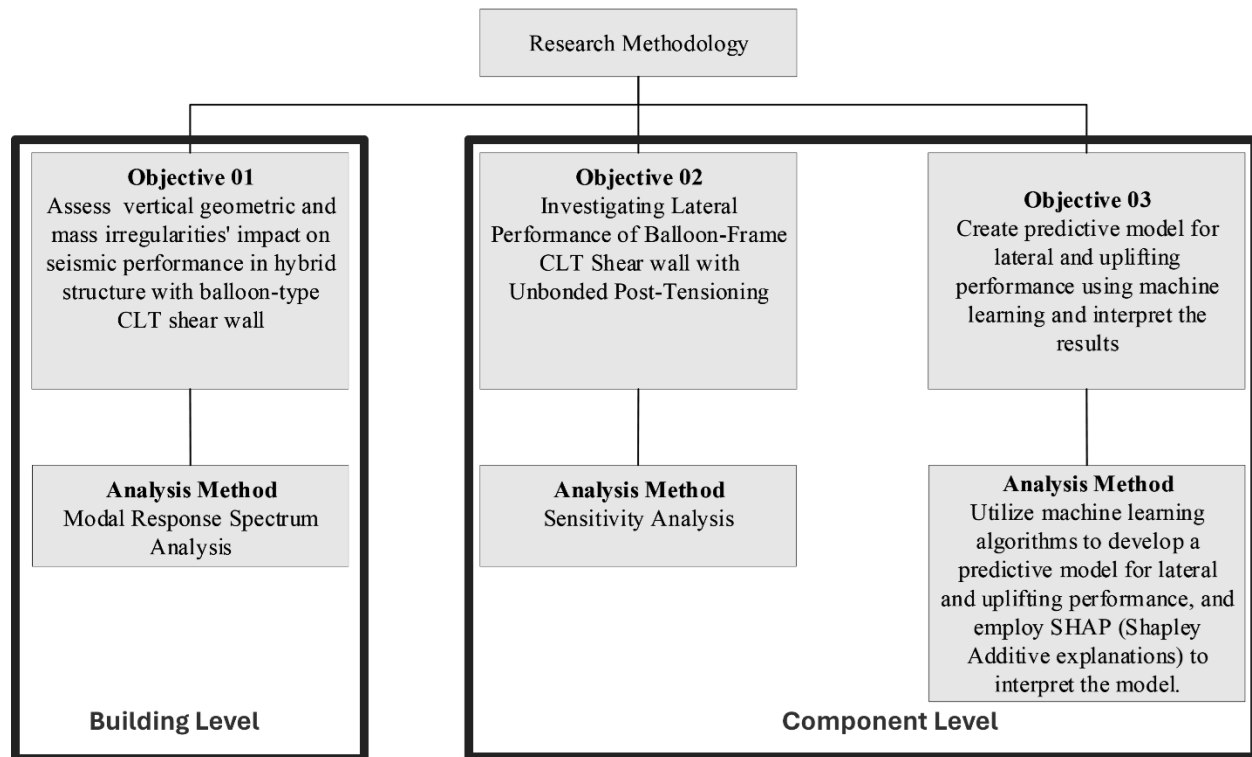
Fig. 1-5 Research Framework

Initially, hybrid structures comprising 8, 12, 16 and 20 stories were modelled to achieve the first objectives, incorporating CLT balloon-type shear walls with different CLT balloon-type shear wall configurations. The validity of hybrid structures was then confirmed through research through available publications and literature [40]. Two approaches were taken to investigate the effect of mass irregularity. First, an increased mass at the middle story of structures with 8, 12, 16 and 20 stories was implemented with modal response spectra to investigate the effect. Then, the location of the increased mass was changed, and the impact was examined. To explore the effects of vertical irregularity, the study utilised setback ratios to distinguish the varying effects of vertical geometric irregularity [48]. This approach involved conducting a model response spectrum analysis (MRSA) to thoroughly investigate these irregularities' influence on structural behaviour.

The second objective was carried out using traditional sensitivity analysis. Model validation is conducted to validate the modelling process of unbounded post-tension balloon-type CLT. This analysis focused on differences in wall thickness, aspect ratios, post-tensioning specifics, and thorough initial lateral stiffness and force-displacement relationship analyses. The aim was to illuminate the complex ways each factor affects the lateral performance of the shear wall. By

systematically evaluating the impact of various design parameters, the study aimed to discover insights for optimising balloon-type CLT shear wall systems to improve seismic resilience.

The third objective was accomplished by creating a detailed database of unbounded post-tensioned CLT walls, including both input and output parameters. Different machine learning algorithms were used to identify the best prediction model within the dataset. Integrating SHAP identified the critical factors for the lateral performance of an unbounded post-tension shear wall.

1.7   Thesis Organization

This thesis consists of six chapters, including this one.

Chapter 1 provides a foundational overview of balloon-type CLT, outlining the research's motivation, objectives, and methodology.

Chapter 2 presents a comprehensive literature review on the balloon-type CLT industry and hybrid structures, covering aspects like experimental tests, finite element modelling, and analytical models.

Chapter 3 presents the first paper submitted to the Journal of Structural Engineering, American Society of Civil Engineers (ASCE), "Analyzing Seismic Performance of Hybrid Structures: The Impact of Vertical and Mass Irregularities on Buildings with Ballone Type Cross-laminated Timber Shear Walls", and the information on various models and their labelling nomenclature are provided in Appendix A.

Chapter 4 presents the second paper submitted to the Journal of Structural Engineering, American Society of Civil Engineers (ASCE), titled "Structural Performance of Balloon-Type Unbounded Post-Tensioned Cross-Laminated Timber Wall System." The information on FE model validation is included in Appendix B.

Chapter 5 presents an additional investigation of the mass irregularity of hybrid buildings with different shear wall configurations and story heights. Appendix C illustrates models.

Chapter 6 summarises the discussion, concluding the thesis objectives and future recommendations.

1.8   References

[1]   B. D'Amico, F. Pomponi, J. Hart, Global potential for material substitution in building construction: The case of cross-laminated timber, J Clean Prod 279 (2021) 123487. https://doi.org/10.1016/j.jclepro.2020.123487.

[2]   G. Churkina, A. Organschi, C.P.O. Reyer, A. Ruff, K. Vinke, Z. Liu, B.K. Reck, T.E. Graedel, H.J. Schellnhuber, Buildings as a global carbon sink, Nat Sustain 3 (2020) 269–276.

[3]   R. Brandner, G. Flatscher, A. Ringhofer, G. Schickhofer, A. Thiel, Cross laminated timber (CLT): overview and development, European Journal of Wood and Wood Products 74 (2016) 331–351.

[4]   M. Wieruszewski, B. Mazela, Cross Laminated Timber (CLT) as an Alternative Form of Construction Wood., Wood Industry/Drvna Industrija 68 (2017).

[5]   H.E. Ilgın, M. Karjalainen, P. Mikkola, Views of Cross-Laminated Timber (CLT) Manufacturer Representatives around the World on CLT Practices and Its Future Outlook, Buildings 13 (2023) 2912.

[6]   E. Karacabeyli, S. Gagnon, Fpi. (Institut), Canadian CLT Handbook:, National LIBRARY OF CANADA, 2019. https://books.google.ca/books?id=Yk14zQEACAAJ.

[7]   C.C. on B. and F. Codes, N.R.C. of Canada, National Building Code of Canada, 2015, National Research Council Canada, 2015. https://books.google.ca/books?id=1H61DAEACAAJ.

[8]   K. Jones, J. Stegemann, J. Sykes, P. Winslow, Adoption of unconventional approaches in construction: The case of cross-laminated timber, Constr Build Mater 125 (2016) 690–702.

[9]   H. Quesada-Pineda, R. Smith, G. Berger, Drivers and barriers of cross-laminated timber (Clt) production and Commercialization: a case of study of Western Europe's Clt industry, BioProducts Business (2018) 29–38.

[10]   J. Schmid, M. Klippel, A. Just, A. Frangi, M. Tiso, Simulation of the fire resistance of cross-laminated timber (CLT), Fire Technol 54 (2018) 1113–1148.

[11]   S. Kurzinski, P. Crovella, P. Kremer, Overview of cross-laminated timber (CLT) and timber structure standards across the world, Mass Timber Construction Journal 5 (2022) 1–13.

[12]   E. Gasparri, A. Lucchini, G. Mantegazza, E.S. Mazzucchelli, Construction management for tall CLT buildings: From partial to total prefabrication of façade elements, Wood Mater Sci Eng 10 (2015) 256–275. https://doi.org/10.1080/17480272.2015.1075589.

[13]   L. Setter, E. Smoorenburg, S. Wijesuriya, P.C. Tabares-Velasco, Energy and hygrothermal performance of cross laminated timber single-family homes subjected to constant and variable electric rates, Journal of Building Engineering 25 (2019) 100784. https://doi.org/10.1016/j.jobe.2019.100784.

[14]   Z. Chen, M. Popovski, Mechanics-based analytical models for balloon-type cross-laminated timber (CLT) shear walls under lateral loads, Eng Struct 208 (2020) 109916. https://doi.org/10.1016/j.engstruct.2019.109916.

[15]   E. Karacebeyli, B. Douglas, CLT Handbook: Cross-Laminated Timber—US Edition, FPInnovations, Pointe-Claire, Quebec, Canada (2013).

[16]   Z. Li, X. Wang, M. He, Experimental and Analytical Investigations into Lateral Performance of Cross-Laminated Timber (CLT) Shear Walls with Different Construction Methods, Journal of Earthquake Engineering 26 (2022) 3724–3746. https://doi.org/10.1080/13632469.2020.1815609.

[17]   E. Karacabeyli, S. Gagnon, Cross laminated timber (CLT) handbook, FPInnovations: Vancouver, BC, Canada (2019).

[18]   E. Karacabeyli, B. Douglas, F.P.L. (U.S.), Fpi. (Institute), B.S.L. Council, CLT Handbook: Cross-laminated Timber, FPInnovations, 2013. https://books.google.ca/books?id=ogdFAQAACAAJ.

[19]   D. Xing, D. Casagrande, G. Doudak, Investigating the deformation characteristics of balloon-type CLT shearwall, Canadian Journal of Civil Engineering (2023). https://doi.org/10.1139/cjce-2023-0233.

[20]   E. Ferdosi, Seismic damage assessment for balloon-type shear wall timber structures, 2024. https://open.library.ubc.ca/collections/24/items/1.0440683.

[21]   C. Dickof, M. Shahnewaz, N. Bevilacqua, T. Tannert, Experimental investigations on balloon frame CLT shearwalls, in: World Conference on Timber Engineering, 2021.

[22]   T.Y. Yang, S. Lepine-Lacroix, J.A.R. Guerrero, J.B.W. McFadden, M.A.Q. Al-Janabi, Seismic performance evaluation of innovative balloon type CLT rocking shear walls, Resilient Cities and Structures 1 (2022) 44–52. https://doi.org/10.1016/j.rcns.2022.03.004.

[23]   M. Shahnewaz, C. Dickof, T. Tannert, Seismic behavior of balloon frame CLT shear walls with different ledgers, Journal of Structural Engineering 147 (2021) 04021137.

[24]   Z. Chen, M. Popovski, Theoretical Building Height Limits of Balloon Mass Timber Shear Wall Systems, Journal of Structural Engineering 150 (2024). https://doi.org/10.1061/JSENDH.STENG-12726.

[25]   H. Daneshvar, J. Niederwestberg, C. Dickof, J.-P. Letarte, Y.H. Chui, Cross-laminated timber shear walls in balloon construction: Seismic performance of steel connections, Modular and Offsite Construction (MOC) Summit Proceedings (2019) 405–412.

[26]   A. Asiz, I. Smith, Connection system of massive timber elements used in horizontal slabs of hybrid tall buildings, Journal of Structural Engineering 137 (2011) 1390–1393.

[27]   P. Clouston, A. Schreyer, Design and use of wood–concrete composites, Practice Periodical on Structural Design and Construction 13 (2008) 167–174.

[28]   A.M. Abdel Aziz, Successful delivery of public-private partnerships for infrastructure development, J Constr Eng Manag 133 (2007) 918–931.

[29]   R.Y. Je Too, H. Isoda, Seismic Performance of CLT Shear Wall Infilled Hybrid Steel Frames with Concealed Steel Plates and Drift Pin Connections, Journal of Structural Engineering 149 (2023) 04023111.

[30]   G. Fini, L. Pozza, C. Loss, T. Tannert, Design of a mass-timber building with different seismic bracing technologies, Atti Del XVII Convegno ANIDIS L'ingegneria Sismica in Italia: Pistoia, 17-21 Settembre 2017.-(Studi in Tema Di Internet Ecosystem) (2017) 52–62.

[31]   I. Gavric, M. Fragiacomo, A. Ceccotti, Cyclic behavior of CLT wall systems: Experimental tests and analytical prediction models, Journal of Structural Engineering 141 (2015) 04015034.

[32]   A. Ceccotti, C. Sandhaas, M. Okabe, M. Yasumura, C. Minowa, N. Kawai, SOFIE project–3D shaking table test on a seven-storey full-scale cross-laminated timber building, Earthq Eng Struct Dyn 42 (2013) 2003–2021.

[33]   R. Ganey, J. Berman, T. Akbas, S. Loftus, J. Daniel Dolan, R. Sause, J. Ricles, S. Pei, J. van de Lindt, H.-E. Blomgren, Experimental investigation of self-centering cross-laminated timber walls, Journal of Structural Engineering 143 (2017) 04017135.

[34]   T. Connolly, C. Loss, A. Iqbal, T. Tannert, Feasibility study of mass-timber cores for the UBC tall wood building, Buildings 8 (2018) 98.

[35]   S. Pei, M. Popovski, J.W. van de Lindt, Analytical study on seismic force modification factors for cross-laminated timber buildings, Canadian Journal of Civil Engineering 40 (2013) 887–896. https://doi.org/10.1139/cjce-2013-0021.

[36]   M. Izzi, A. Polastri, M. Fragiacomo, Investigating the hysteretic behavior of Cross-Laminated Timber wall systems due to connections, Journal of Structural Engineering 144 (2018) 04018035.

[37]   M.J.N. Priestley, S. (Sri) Sritharan, J.R. Conley, S. Stefano Pampanin, Preliminary Results and Conclusions From the PRESSS Five-Story Precast Concrete Test Building, PCI Journal 44 (1999) 42–67. https://doi.org/10.15554/pcij.11011999.42.67.

[38]   A. Palermo, S. Pampanin, A. Buchanan, M. Newcombe, Seismic design of multi-storey buildings using laminated veneer lumber (LVL), (2005).

[39]   A. Iqbal, S. Pampanin, A. Palermo, A.H. Buchanan, Performance and Design of LVL Walls Coupled with UFP Dissipaters, Journal of Earthquake Engineering 19 (2015) 383–409. https://doi.org/10.1080/13632469.2014.987406.

[40]   M. Khajehpour, Y. Pan, T. Tannert, Seismic analysis of hybrid steel moment frame CLT shear walls structures, Journal of Performance of Constructed Facilities 35 (2021) 04021059.

[41]   A. ALIBASIC, V. VOCAL, Design of floor-to-wall connections in hybrid structures-Study of robustness in CLT floor to concrete wall connections, (2021).

[42]   Y. Kurama, S. Pessiki, R. Sause, L.W. Lu, Seismic behavior and design of unbonded post-tensioned precast concrete walls, PCI Journal 44 (1999) 72–89. https://doi.org/10.15554/PCIJ.05011999.72.89.

[43]   A.W. Wilson, C.J. Motter, A.R. Phillips, J.D. Dolan, Modeling techniques for post-tensioned cross-laminated timber rocking walls, Eng Struct 195 (2019) 299–308. https://doi.org/10.1016/J.ENGSTRUCT.2019.06.011.

[44]   A.W. Wilson, C.J. Motter, A.R. Phillips, J.D. Dolan, Seismic response of post-tensioned cross-laminated timber rocking wall buildings, Journal of Structural Engineering 146 (2020) 04020123.

[45]   K.M. Twigden, S. Sritharan, R.S. Henry, Cyclic testing of unbonded post-tensioned concrete wall systems with and without supplemental damping, Eng Struct 140 (2017) 406–420. https://doi.org/10.1016/j.engstruct.2017.02.008.

[46]   D.-C. Feng, W.-J. Wang, S. Mangalathu, E. Taciroglu, Interpretable XGBoost-SHAP machine-learning model for shear strength prediction of squat RC walls, Journal of Structural Engineering 147 (2021) 04021173.

[47]   S. Mangalathu, S.-H. Hwang, J.-S. Jeon, Failure mode and effects analysis of RC members based on machine-learning-based SHapley Additive exPlanations (SHAP) approach, Eng Struct 219 (2020) 110927.

[48]   M. Pirizadeh, H. Shakib, Probabilistic seismic performance evaluation of non-geometric vertically irregular steel buildings, J Constr Steel Res 82 (2013) 88–98.

Two.   Chapter 2. Literature Reviews

2   Literature Review

The literature review systematically investigates two critical domains for developing this research endeavour. Initially, the primary emphasis is on hybrid structures, particularly highlighting the integration of Cross-Laminated Timber (CLT), thereby underscoring their relevance and utility in contemporary structural engineering. Subsequently, the review rigorously assesses the secondary literature regarding the application of post-tenting techniques to CLT, evaluating their efficacy in enhancing structural integrity.

2.1 Literature Review on Hybrid Structures

Combining heterogeneous materials such as steel, concrete, or timber into hybrid building entities and structures is an established practice within the North American construction industry. For example, the combination of steel and concrete leverages their strengths, such as compressive strength, tensile resilience, and compressive resilience and their shared thermal expansion coefficients. Furthermore, advancements in steel and timber connections have developed, suggesting increased efficiency when using metal fasteners within timber constructions. Such integrations have earned compliments for their enhanced efficiency in architectural design in recent years. The hybridisation of timber with other materials has only gained significant interest over the past two decades, driven by the unique properties of timber, including its environmental and mechanical benefits [1,2]. A notable application of such hybridity (steel and timber) is incorporating steel moment-resisting frames within timber-framed multi-residential buildings [3]. Numerous studies have proven the environmental and structural benefits of hybrid CLT structures. Shin et al. (2023) show that hybrid CLT structures demonstrate a significantly reduced global warming potential compared to concrete structures, which average 26.5%, excluding biogenic carbon emissions. When traditional walls (concrete) are replaced with CLT hybrid alternatives, a significant reduction in environmental impact, averaging 35%, is demonstrated [4].

Cyclic and seismic load resistance capacity is a standard requirement for many design guidelines. Consequently, hybrid structures combining steel, concrete, and CLT emphasise performance under

cyclic or seismic loads. In seismic scenarios, structural capacities depend mainly on mechanical properties (stiffness and strength) employed in the principal structural elements such as walls, frameworks, and connections[5]. CLT panels provide a natural earthquake resistance and lightweight nature, which are beneficial when combined with other building materials (steel, concrete) that demonstrate a higher weight and less shear resistance. Kuilen et al. (2011) demonstrated that numerically integrating CLT with concrete core shear walls for the architectural design of skyscrapers ascending to 150 meters indicates the viability of these hybrid systems [6]. Some finite element and experimental studies have been employed to investigate hybrid structures. Khajehpour et al. (2021) conducted a comparative analysis to compare traditional steel moment frames to hybrid structures, demonstrating that hybrid steel structures could reduce total steel requirements by 40-50% with the 60% inter-story drift compared to traditional steel moment frames. Additionally, using FEMA P695, the author proposed the hybrid system's overstrength elated factors (Ro) as 1.57 and ductility-related factors (Rd) as 3.87 [7]. Hashemi et al. (2017) have investigated the hybrid steel-timber lateral load system coupled with Resilient Slip Friction (RSF) through numerical and experimental investigation. The authors found that the lateral load-resisting system employing CLT walls and RSF joints significantly improves seismic resilience by offering considerable energy dissipation and self-centring capabilities [8]. Further, Tesfamariam et al. (2014) assessed seismic vulnerability in a hybrid structure comprising a steel moment reactive frame with CLT infill and found that the fundamental period and seismic vulnerability are reduced significantly as more bays are infilled [9]. Zhang et al. (2021) employed experimental and numerical methods to investigate the stiffness of connections (hold-downs and vertical and horizontal shear connections) in tall CLT-glulam hybrid buildings [10]. The authors found horizontal shear connections critical in assessing the seismic performance of CLT-glulam hybrid buildings, suggesting that optimising these connections can significantly enhance the seismic resilience of tall timber structures.

Wang et al. (2023) introduced two new Engineering Design Parameters (EDPs) to assess hybrid structures, namely Maximum Connection Damage Index (MaxCDI) and Maximum Inter-story CLT Shear Wall Damage Index (MaxISWDI). Employing these EDPs, the authors investigated 12 prototype CLT-glulam hybrid buildings utilising nonlinear time-history analyses. They found that MaxISDR and MaxRDR effectively capture damage to glulam frame subsystems, while the

Maximum Inter-story CLT Shear Wall Damage Index is suited for CLT shear wall subsystems [11].

2.2 Literature Review on Post-Tensioned CLT Shear Walls

The post-tensioned CLT shear wall structure represents an innovative solution for earthquake-resilient structures. The structural seismic performance affects the post-tension force of these post-tensioned CLT shear walls. Over the structure's service life, the post-tension force changes due to the time-dependent elastic, creep, and environmental deformations of wood [12].

Post-tension rocking walls have traditionally been applied on precast concrete structures [13–15]. A variety of approaches to enhance energy dissipation in post-tension precast concrete rocking walls have been used, including the integration of energy-dissipating connectors between adjacent walls, connections to nearby columns through dissipaters, and the anchorage of mild steel bars to the foundation for energy dissipation at the base of the wall [1,14,16,17]. Post-tension precast concrete rocking walls have been applied to other materials, notably Laminated Veneer Lumber (LVL) and post-tension CLT rocking walls [18,19].
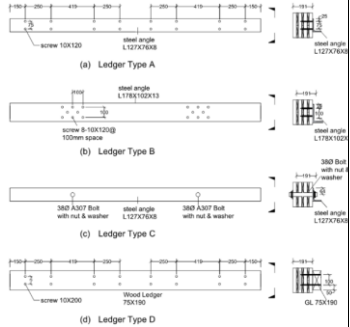
Setting the post-tensioning tendons provides rocking and re-centring capabilities for post-tensioned CLT shear walls [20]. Different types of dampers, such as elastoplastic, viscous, or frictional, may be employed at the foundation of the shear walls or between two walls to dissipate energy and reduce damage. Numerous scholars have identified the effectiveness of resisting lateral loads of post-tensioned CLT shear walls.

Wilson et al. (2021) assessed the economic losses associated with earthquake damage to nonstructural components of buildings with post-tension CLT rocking walls using FEMA P-58 methodology. The author identified the economic aspects by considering discount factors, including repair costs, the probability of exceeding repair costs, and the expected annual loss [21]. Further, Wilson et al. (2020) conducted nonlinear time history analyses of 5-story and 12-story prototype buildings using post-tensioned CLT rocking walls coupled with U-shaped flexural plates (UFPs) as the lateral force-resisting system. The author concluded that near-fault ground motions with directivity effects resulted in the most significant demands for the 5-story building. The mid-height rocking joint in the 12-story building diminished the influence of ground motion directivity effects. Both buildings confirmed the efficacy of UFPs at different heights in energy dissipation, suggesting a viable seismic design alternative for buildings in high-seismic regions [22].

Hossain et al. (2019) investigated the lateral load performance of unbonded post-tensioned CLT rocking walls for potential use as a lateral load-resisting system in tall wood buildings in high seismic regions. The study found that the walls displayed satisfactory performance regarding force-displacement response and re-centring ability, with residual drifts less than 0.3% - to 5% drift [23]. The study by Ho et al. (2017) investigates a hybrid system combining post-tensioned CLT panels and light-frame wood shear walls. The study assessed the hybrid system under cyclic loading and compared the outcomes with the traditional light-frame wood system. The study found that the hybrid system significantly enhances seismic resilience by leveraging the strength of both CLT and light-frame wood shear walls and suggested further exploration into the behaviour of such systems under larger lateral displacements beyond the elastic limits of materials [24].

Akbsa et al. (2017) conducted cyclic experiments on single-panel and multipanel post-tensioned CLT shear walls, summarising critical structural limit states under lateral loading compared to test results [25]. Additionally, Ganey et al. (2017) explored U-shaped flexural plates in post-tensioned CLT shear walls, showing that these walls possess remarkable self-centring capabilities even after experiencing significant lateral drifts exceeding 0.1. Ho et al. (2024) conducted a performance-based design procedure using pushover analysis for a hybrid system combining post-tensioned CLT and light-frame wood shear walls. The study validated a six-story building's design through nonlinear time history analyses, demonstrating its ability to meet predetermined seismic performance levels while emphasising the CLT panels' self-centring capacity and robust lateral load resistance [26]. Kivekäs et al. (2024) investigated the structural non-seismic design of post-tensioned CLT shear walls using both the Winkler Spring Analogy (WSA) and Material-Based Model (MBM). They showed a significant impact of CLT's orthotropy and fabrication defects on wall deformation, especially at the bottom. Further, the study demonstrated the effectiveness of post-tensioning configurations, mainly when at least two bars were included at opposite ends of the cross-section. Post-tensioned bar materials with higher elastic moduli performed better, influencing the manufacturing drilling by allowing for smaller bar diameters [27].

2.3   Summary and Additional Literature Review

Study	Objectives	Research Gap	Results	Conclusion
Studies Background: Ballone Type CLT				
Li et al. (2022) [28]	To investigate the lateral performance of CLT shear walls with platform and balloon construction methods, conduct cyclic loading tests, and develop analytical prediction models.	Most research focused on platform-type CLT structures, with limited studies on balloon construction methods.	It was found that balloon-type CLT shear walls have higher initial lateral stiffness than platform-type shear walls, but both have similar ultimate load-resisting capacities.	This study determines the effectiveness of both construction methods (Balloon type and platform type) for CLT shear walls and provides validated analytical models for estimating their lateral load-resisting performance.
Daneshvar et al. (2019) [29]	Initiate seismic design of tall wood buildings using balloon Balloon framing, focusing on the behaviour of connections during seismic events.	Limited research on seismic behaviour of balloon construction CLT structures and their connections in high seismic regions.	The authors designed an experimental program to investigate various connections' yielding and failure mechanisms.	The research helps understand the seismic behaviour of prefabricated mass timber buildings and assists in designing high-rise timber structures.

Dickof et al. (2021) [30]	Compare the behaviour of balloon frame CLT shearwalls to platform-type and determine differences in ductility.	Limited research comparing balloon frame to platform construction in CLT shearwalls.	Found that ledgers do not significantly impact the remaining load-carrying capacity of ledgers.	Demonstrates efficacy of balloon frame CLT shear walls for low-rise construction, contributing to design flexibility and efficiency.
Xing et al. 2023 [31]	Investigate the lateral deformation and kinematic behaviour of balloon-type CLT shear wall systems, developing a simplified analytical model for lateral displacement.	Existing building codes and standards lack provisions for designing and detailing balloon-type CLT shear wall systems.	A validated finite element model was used to analyse critical factors affecting shear wall behaviour, and a simplified analytical model was developed and verified against numerical models.	The study's analytical model provides a less than 4.7% average error in predicting top lateral displacement, offering a reliable tool for engineering design of balloon-type CLT shearwalls.

Yang et al. (2022) [32]	Assess the seismic performance of four 12-story balloon-type CLT rocking shear walls using the performance-based design procedure.	Limited research on balloon-type CLT rocking shear walls; lack of guidance for such systems.	The prototype balloon-type CLT rocking shear walls have sufficient adjusted collapse margin ratios (ACMR) compared to the acceptable limits recommended by FEMA P695.	Balloon-type CLT rocking shear walls are a valid seismic force-resisting system, and the performance-based design procedure is efficient for designing robust seismic systems.
Studies Background: Hybrid Structures				
Hashemi et al. (2017) [8]	To develop a hybrid steel-timber lateral load resisting system (LLRS) using CLT walls coupled with (Resilient Slip Friction) RSF joints and boundary steel columns to minimise post-earthquake damage and maintenance.	Existing systems either lack self-centring behaviour or do not efficiently dissipate energy. Traditional friction joints in seismic design do not offer sufficient self-centring to prevent residual displacements after an earthquake.	The research showed that the LLRS, employing CLT walls and RSF joints, significantly improves seismic resilience by offering considerable energy dissipation and self-centring capabilities. Through numerical models and experimental tests, the system's effectiveness has been	The proposed hybrid system represents a new generation of resilient LLRS for various structures. It offers energy dissipation and self-centring capabilities, making it a viable solution for seismic damage avoidance. Further experimental validation is recommended.

			validated in a simulation of a four-story prototype building.	
Zhang et al. (2021) [10]	To investigate the effect of the stiffness of hold-downs, vertical, and horizontal shear connections on tall CLT buildings' dynamic and seismic performance.	The study addresses the lack of a detailed understanding of how connection stiffness impacts the seismic performance and dynamic properties of tall buildings made from CLT, especially considering various types of connections (hold-downs, vertical, and horizontal shear connections).	Horizontal shear connections notably induce building stiffness and interstorey drifts, potentially reducing stiffness by 20% and increasing drifts by up to 47% under certain ground motions. In contrast, the stiffness of vertical connections barely affects these parameters, altering them by less than 1%. Adjustments in hold-down stiffness have a minor effect, leading to roughly a 2% decrease in stiffness and a 3% rise in drifts. Moreover, the	The study concludes that the stiffness of connections, especially horizontal shear connections, plays a significant role in tall CLT buildings' dynamic properties and seismic performance. However, the impact is less than the traditionally applied 50% stiffness reduction of mass-timber LLRS used by practitioners to account for connections, suggesting a need for refined design considerations.

			impact of connection stiffness on the building diminishes as the building height increases.	
Khajehpour et al. (2021) [7]	Evaluate a hybrid system combining Steel Moment Frame (SMF) with CLT shear walls for mid- to high-rise buildings against seismic activity.	Lack of studies on seismic performance of balloon framed CLT shear walls.	Hybrid systems reduced steel use by 40%-50% and interstory drifts by up to 60% compared with SMF buildings.	The hybrid system offers a promising solution for economically and sustainably enhancing the seismic performance of mid- to high-rise buildings.
Tesfamariam et al. (2014) [33]	Conduct seismic vulnerability assessment on a novel hybrid structure (steel moment resisting frame with CLT infill panels).	To provide a vulnerability assessment for hybrid steel-timber structures, which is currently lacking.	The study found that the fundamental period and seismic vulnerability are reduced significantly as more bays are infilled.	Different performance objectives can be met within performance-based earthquake engineering by varying the CLT configuration.

Wang et al. (2023) [11]	Assessment of engineering demand parameters (EDPs) for seismic analyses of CLT-glulam hybrid structures.	Limited information on the effectiveness of EDPs in representing structural damage for hybrid structures or subsystems.	The Maximum Connection Damage Index (MaxCDN) effectively characterised connection damage. Connection damage of glulam frame subsystems was limited, and the construction type of CLT shear wall subsystems significantly impacted it.	Maximum Inter-story Drift Ratios (MaxISDR) and Maximum Roof Drift Ratios (MaxRDR) effectively capture damage to glulam frame subsystems, while Maximum Inter-story CLT Shear Wall Damage Index (MaxISWDI) is suited for CLT shear wall subsystems. None of the EDPs could capture the damage to both subsystems due to their distinct deformation modes.
Studies Background: Post-tension CLT				
Wilson et al. (2021) [21]	To assess the economic losses associated with earthquake damage to nonstructural components of buildings with PT CLT	Prior studies have not conducted earthquake risk analysis following FEMA P-58 guidelines for buildings with PT CLT rocking walls.	Identified the economic factors, including repair costs, probabilities of exceeding repair costs, and expected annual loss, by considering discount factors. Found lower	Mid-rise buildings have a lower probability of nonstructural damage for shorter periods than low-rise buildings. Indicated that the economic risk is lower for mid-rise buildings over short-term investment periods

	rocking walls using FEMA P-58 methodology		ratios of non-structural repair cost to total building cost for low-rise buildings compared to mid-rise buildings	
Wilson et al. (2020) [22]	To conduct nonlinear time history analyses for 5-story and 12-story prototype buildings using post-tensioned CLT rocking walls coupled with U-shaped flexural plates (UFPs) as the lateral force-resisting system.	While gravity load-resisting CLT components are included in US building codes, seismic lateral force-resisting CLT systems have not yet been established.	The study subjected building models to far-field and near-fault ground motions scaled to the design earthquake and maximum considered earthquake levels. It was found that UFPs higher up dissipated more energy compared to those closer to the base.	Near-fault ground motions with directivity effects resulted in the most significant demands for the 5-story building. The mid-height rocking joint in the 12-story building diminished the influence of ground motion directivity effects. Both buildings confirmed the efficacy of UFPs at different heights in energy dissipation, suggesting a viable seismic design alternative for buildings in high-seismic regions.
Hossain et al. (2019) [23]	To investigate the lateral load performance of	Limited comprehensive design guidelines and understanding of the	The study found that the walls displayed satisfactory performance	The post-tensioned CLT rocking walls demonstrate promising performance characteristics for

| | unbonded post-tensioned CLT rocking walls for potential use as a lateral load-resisting system in tall wood buildings in high seismic regions. | performance of post-tensioned CLT rocking walls in the context of their recentering capabilities, energy dissipation, and suitability for tall wood building construction in seismic areas. | regarding force-displacement response and re-centring ability, with residual drifts less than 0.3% for up to 5% drift. Wall base slip was minimal for most specimens, with significant contributions from flexural bending and shear deformation to total top displacement. Mechanical connections between vertically stacked walls using steel angles and lag screws proved effective. The energy dissipation capacity of the system was found to be around 2.5% to 6%. | use in tall wood buildings in seismic zones. Attention to base slip prevention and additional energy dissipation methods is necessary for optimal design. The study paves the way for developing design guidelines and broader application of this system in seismic-resistant construction. |

2.4 References

[1]   A. Asiz, I. Smith, Connection system of massive timber elements used in horizontal slabs of hybrid tall buildings, Journal of Structural Engineering 137 (2011) 1390–1393.

[2]   P. Clouston, A. Schreyer, Design and use of wood–concrete composites, Practice Periodical on Structural Design and Construction 13 (2008) 167–174.

[3]   A.M. Abdel Aziz, Successful delivery of public-private partnerships for infrastructure development, J Constr Eng Manag 133 (2007) 918–931.

[4]   B. Shin, S. Wi, S. Kim, Assessing the environmental impact of using CLT-hybrid walls as a sustainable alternative in high-rise residential buildings, Energy Build 294 (2023) 113228. https://doi.org/10.1016/j.enbuild.2023.113228.

[5]   Y.-L. Shen, J. Schneider, S. Tesfamariam, S.F. Stiemer, Z.-G. Mu, Hysteresis behavior of bracket connection in cross-laminated-timber shear walls, Constr Build Mater 48 (2013) 980–991.

[6]   J.W.G. Van De Kuilen, A. Ceccotti, Z. Xia, M. He, Very tall wooden buildings with cross laminated timber, Procedia Eng 14 (2011) 1621–1628.

[7]   M. Khajehpour, Y. Pan, T. Tannert, Seismic analysis of hybrid steel moment frame CLT shear walls structures, Journal of Performance of Constructed Facilities 35 (2021) 04021059.

[8]   A. Hashemi, P. Quenneville, P. Zarnani, Seismic resilient structures with Cross Laminated Timber (CLT) walls coupled with innovative Resilient Slip Friction (RSF) joints, in: Proc. New Zeal. Soc. Earthq. Eng. Conf.(NZSEE), Wellington, New Zeal, 2017.

[9]   C. Dickof, S.F. Stiemer, M.A. Bezabeh, S. Tesfamariam, CLT–steel hybrid system: Ductility and overstrength values based on static pushover analysis, Journal of Performance of Constructed Facilities 28 (2014) A4014012.

[10]   X. Zhang, Y. Pan, T. Tannert, The influence of connection stiffness on the dynamic properties and seismic performance of tall cross-laminated timber buildings, Eng Struct 238 (2021) 112261.

[11]   X. Wang, M. He, Z. Li, Evaluation of engineering demand parameters for seismic analyses of CLT-glulam hybrid structures, Eng Struct 296 (2023) 116958.

[12] S. Nakashima, A. Kitamori, T. Mori, K. Komatsu, Propose alternative design criteria for dowel type joint with CLT, in: Materials and Joints in Timber Structures: Recent Developments of Technology, Springer, 2014: pp. 739–748.

[13] M.J.N. Priestley, S. (Sri) Sritharan, J.R. Conley, S. Stefano Pampanin, Preliminary Results and Conclusions From the PRESSS Five-Story Precast Concrete Test Building, PCI Journal 44 (1999) 42–67. https://doi.org/10.15554/pcij.11011999.42.67.

[14] Y. Kurama, S. Pessiki, R. Sause, L.W. Lu, Seismic behavior and design of unbonded post-tensioned precast concrete walls, PCI Journal 44 (1999) 72–89. https://doi.org/10.15554/PCIJ.05011999.72.89.

[15] F.J. Perez, S. Pessiki, R. Sause, Experimental Lateral Load Response of Unbonded Post-Tensioned Precast Concrete Walls., ACI Struct J 110 (2013).

[16] T. Holden, J. Restrepo, J.B. Mander, Seismic Performance of Precast Reinforced and Prestressed Concrete Walls, Journal of Structural Engineering 129 (2003) 286–296. https://doi.org/10.1061/(ASCE)0733-9445(2003)129:3(286).

[17] J.I. Restrepo, A. Rahman, Seismic Performance of Self-Centering Structural Walls Incorporating Energy Dissipators, Journal of Structural Engineering 133 (2007) 1560–1570. https://doi.org/10.1061/(ASCE)0733-9445(2007)133:11(1560).

[18] F. Sarti, A. Palermo, S. Pampanin, Quasi-Static Cyclic Testing of Two-Thirds Scale Unbonded Posttensioned Rocking Dissipative Timber Walls, Journal of Structural Engineering 142 (2016). https://doi.org/10.1061/(ASCE)ST.1943-541X.0001291.

[19] G.Q. Ganey, M.G. Loso, A.B. Burgess, R.J. Dial, The role of microbes in snowmelt and radiative forcing on an Alaskan icefield, Nat Geosci 10 (2017) 754–759.

[20] X. Zheng, M. He, Z. Li, Q. Luo, Long-term performance of post-tensioned cross-laminated timber (CLT) shear walls: hygro-mechanical model validation and parametric analysis, Archives of Civil and Mechanical Engineering 22 (2022) 68. https://doi.org/10.1007/s43452-022-00389-6.

[21] A.W. Wilson, A.R. Phillips, C.J. Motter, J.Y. Lee, J.D. Dolan, Seismic loss analysis of buildings with post-tensioned cross-laminated timber walls, Earthquake Spectra 37 (2021) 324–345.

[22]   A.W. Wilson, C.J. Motter, A.R. Phillips, J.D. Dolan, Seismic response of post-tensioned cross-laminated timber rocking wall buildings, Journal of Structural Engineering 146 (2020) 04020123.

[23]   K. Hossain, M.E. Kreger, K.J. Fridley, T.N. Dao, M.E. Barkey, EXPERIMENTAL INVESTIGATION OF LONG TERM AND LATERAL LOAD BEHAVIOR OF CLT SHEAR WALLS FOR MID-RISE WOOD BUILDINGS, 2019.

[24]   T.X. Ho, T.N. Dao, S. Aaleti, J.W. van de Lindt, D.R. Rammer, Hybrid system of unbonded post-tensioned CLT panels and light-frame wood shear walls, Journal of Structural Engineering 143 (2017) 04016171.

[25]   T. Akbas, R. Sause, J.M. Ricles, R. Ganey, J. Berman, S. Loftus, J.D. Dolan, S. Pei, J.W. van de Lindt, H.-E. Blomgren, Analytical and experimental lateral-load response of self-centering posttensioned CLT walls, Journal of Structural Engineering 143 (2017) 04017019.

[26]   T.X. Ho, T.N. Dao, J.W. van de Lindt, S. Pryor, Performance-Based Design of Posttensioned Cross-Laminated Timber and Light-Frame Wood Shear Wall Hybrid System, Journal of Structural Engineering 150 (2024). https://doi.org/10.1061/JSENDH.STENG-12778.

[27]   M. Kivekäs, E. Ilgin, S. Pajunen, Structural Non-Seismic Design of Post-Tensioned CLT Shear Walls, (2024).

[28]   Z. Li, X. Wang, M. He, Experimental and Analytical Investigations into Lateral Performance of Cross-Laminated Timber (CLT) Shear Walls with Different Construction Methods, Journal of Earthquake Engineering 26 (2022) 3724–3746. https://doi.org/10.1080/13632469.2020.1815609.

[29]   H. Daneshvar, J. Niederwestberg, C. Dickof, J.-P. Letarte, Y.H. Chui, Cross-laminated timber shear walls in balloon construction: Seismic performance of steel connections, Modular and Offsite Construction (MOC) Summit Proceedings (2019) 405–412.

[30]   C. Dickof, M. Shahnewaz, N. Bevilacqua, T. Tannert, Experimental investigations on balloon frame CLT shearwalls, in: World Conference on Timber Engineering, 2021.

[31]   D. Xing, D. Casagrande, G. Doudak, Investigating the deformation characteristics of balloon-type CLT shearwall, Canadian Journal of Civil Engineering (2023). https://doi.org/10.1139/cjce-2023-0233.

[32]   T.Y. Yang, S. Lepine-Lacroix, J.A.R. Guerrero, J.B.W. McFadden, M.A.Q. Al-Janabi, Seismic performance evaluation of innovative balloon type CLT rocking shear walls, Resilient Cities and Structures 1 (2022) 44–52. https://doi.org/10.1016/j.rcns.2022.03.004.

[33]   S. Tesfamariam, S.F. Stiemer, C. Dickof, M.A. Bezabeh, Seismic vulnerability assessment of hybrid steel-timber structure: Steel moment-resisting frames with CLT infill, Journal of Earthquake Engineering 18 (2014) 929–944.

Three. Chapter 3.

3 Analysing Seismic Performance of Hybrid Structures: The Impact of Vertical and Mass Irregularities on Buildings with Balloon-Type Cross-Laminated Timber Shear Walls

KTGM Kandethanthri, Ghazanfarah Hafeez

3.1 Abstract

This study examines the seismic performance of hybrid structures with balloon-type cross-laminated timber shear walls. It specifically focuses on investigating the effects of mass and vertical geometric irregularities. The modal response spectrum methodology has been employed to estimate the seismic response. The study reveals a positive correlation between increased mass at the middle story and the inter-story drift in hybrid structures. Additionally, this effect is less for upper levels. The research also emphasises the role of mass distribution in seismic resilience, where the location of mass within a structure alters its seismic response. A higher concentration of mass at lower levels leads to a higher response in upper levels, while an upper-level results in a localised effect. Furthermore, the study underscores the importance of directional analysis in buildings with vertical irregular structures to avoid underestimating seismic danger.

Keywords: Cross Laminated Timber, Modal Response Spectrum Analysis, Vertical Geometrical Irregularity, Mass Irregularity

3.2 Introduction

Cross Laminated Timber (CLT), once seen as a niche product in the North American construction sector, is now recognised as an eco-friendly timber solution for non-residential structures [1–3]. The timber sector, academic researchers, and industry professionals are increasingly realising that CLT has the potential to transform lower-grade wood into premium products, thereby adopting economic growth in rural areas [4–6]. While challenges such as material availability, structural

integrity, serviceability, fire resistance, and regulatory approval remain, the adoption of CLT in pilot projects across the United States and Canada since its North American debut in the early 2000s is evidence of its promising future. CLT's widespread acceptance and use in the construction industry hinges on establishing unified and efficient building codes. With its unique composition of several layers of lumber boards glued together at orthogonal angles, CLT offers superior in-plane strength and rigidity [7,8]. It can effectively resist lateral wind and seismic forces when used as floor and roof diaphragms and shear walls, making it a viable option for earthquake-prone regions [9].

Structures made from CLT can be erected using platform-type or balloon-type framing. In platform construction (Fig. 3-1(a)), the structure of each floor acts as the base for the construction of the story above, with the walls being anchored to the foundation and floors through steel brackets and hold-downs. Conversely, balloon framing features (Fig. 3-1(b)) continuous walls extending over multiple stories unimpeded by the limitations of compression strength perpendicular to the grain. The integration of mass timber construction into building codes is evident with its inclusion in the 2015 National Building Code of Canada (NBCC) for encapsulated mass timber structures up to 12 stories [10] and the 2021 International Building Code, allowing for buildings up to 18 stories [11]. The Canadian Standard for Engineering Design in Wood CSA-O86 also provides guidelines for shear walls in platform-type CLT constructions, including design prerequisites that ensure wall rocking mechanisms exhibit energy-dissipative behaviour. Compliance with these standards enables the NBCC to apply ductility and overstrength seismic design force reduction factors of R_d = 2.0 and R_o = 1.5. Given that CLT panels in shear walls do not impart ductility, achieving the required energy dissipation of the Lateral Load-Resisting System (LLRS) relies on the design of the connections [12,13]. The construction of balloon-type CLT shear walls eliminates perpendicular-to-grain bearings between floors. It involves fewer panels to accomplish slender aspect ratios and fewer connections over the building height due to collective perpendicular-to-grain shrinkage. This method offers significant benefits compared to platform-type construction.
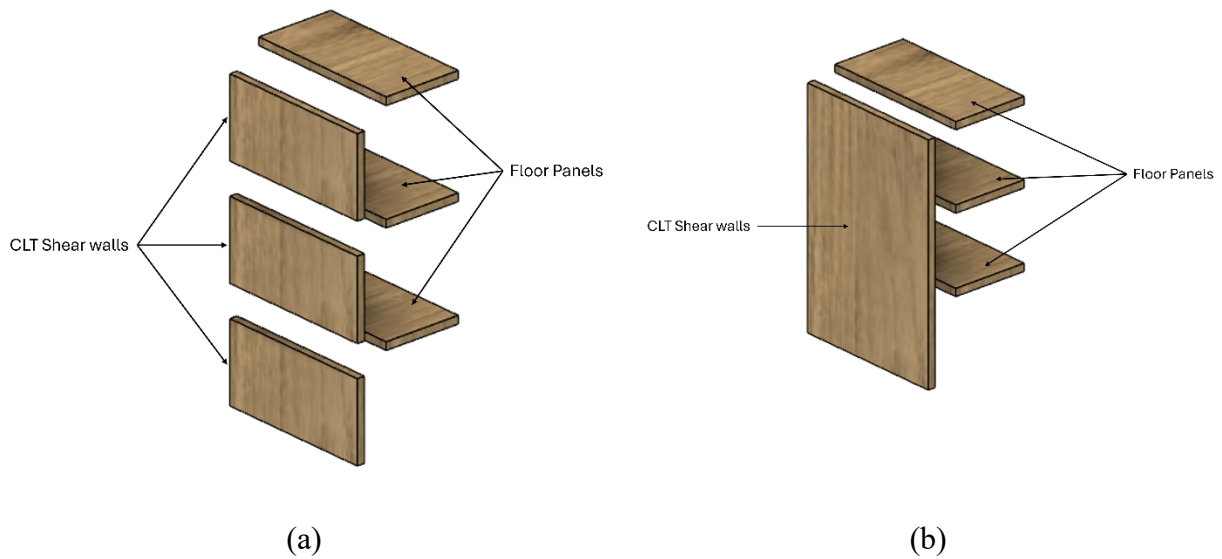
Fig. 3-1 (a) Platform Type CLT Construction (b) Ballone Type CLT Construction

CLT connections play a critical role in the structural integrity and performance of CLT assemblies in modern construction [14]. These mechanical or adhesive-based connections are designed to transfer loads efficiently across panels and elements, creating vast, open spaces and complex structures. CLT is more dimensionally stable and more substantial than other materials, allowing for thinner and lighter connections. The Holz-Stahl-Komposit (HSK) is an innovative connecting method of CLT panels, known for its advanced and efficient design, particularly when combined with steel and CLT hybrid buildings. HSK connections are a significant advancement in construction technology [14–17]. In CLT-steel hybrid structures, HSK connections facilitate the assembly of prefabricated timber elements with steel components, allowing for rapid construction while continuing high degrees of accuracy and structural integrity. The hybrid approach exploits the sustainable benefits of timber and the high strength-to-weight ratio of steel, which also specifies enhanced fire resistance, acoustic performance, and seismic resilience. HSK connections involve using a glued-in perforated steel plate for connecting CLT panels [18,19]. Further, in the HSK system, the adhesive bond facilitates the required load transfer into the CLT panels, and the perforations allow for the formation of adhesive dowels and a weakened steel section, enabling ductile steel failure.

Hybrid systems, prevalent across different structures, adeptly merge multiple structural materials to withstand loads effectively. Frequently encountered are steel and concrete hybrid members,

consisting of reinforced concrete columns paired with structural steel beams alongside dual frame-wall systems. In these systems, steel frames and reinforced concrete walls collaboratively counteract lateral loads. Although less widespread, steel and timber hybrid systems present considerable benefits, particularly when employing CLT as a lightweight option for floor systems [20–23]. Steel provides critical strength and ductility in such hybrid systems, which is indispensable for enduring seismic events [24]. Meanwhile, timber, despite being weaker and necessitating prominent structural elements, adds to the overall stiffness of the system and is lauded for its environmental benefits [23].

An essential matter in the hybridisation of integrating steel moment frames with CLT infill walls. This composition has been examined to increase strength and stiffness while keeping ductility simultaneously [25]. The integration of CLT panels in steel moment frames through static pushover and dynamic analysis demonstrates a linear enhancement of the system strength and stiffness with the addition of CLT panes, which thus can be a way forward in steel structure engineering [25,26]. Combining materials like steel, concrete, and timber, hybrid systems have shown significant benefits in structural engineering, providing strength, ductility, and environmental advantages [27]. Developments in integrating these materials, especially with the growing use of CLT in steel frameworks, offer improved seismic resilience and system stiffness.

3.2.1 Mass Irregularity and Vertical Geometric Irregularity

In the seismic design, two critical irregularities that require special attention are mass and vertical geometric irregularities. The uneven mass is the variation of mass distribution in a structure and can be one of the primary factors in response to seismic forces. Irregular mass distributions, a feature of buildings with asymmetric layouts or concentrated masses at certain levels, can cause amplified responses to seismic shaking, making them prone to potential structural vulnerabilities [28]. In vertical geometric irregularity, the vertical configuration of a building is irregular. These geometrical variations can result in additional eccentricities in the distribution of seismic forces that can cause uneven load distributions and, thus, can amplify the response of the building during seismic events [29].

Design codes, including the NBCC, quantify irregularity based on mechanical properties and classify them into various types. TABLE 3-1 details the criteria for the weight (mass) and vertical geometric irregularities outlined in the NBCC 2015, including their specific conditions.

TABLE 3-1. Regulatory Constraints On Irregularities Specified By The NBCC

Irregularity Type	Description	Limit
Weight(mass) Irregularity	The floor weight is significantly heavier than the one below.	>50% heavier
Vertical Geometric Irregularity	The floor's dimensions greatly exceed those of the floor below.	>30% larger

It has been observed that buildings with certain structural irregularities are at a higher risk of sustaining significant damage during moderate to high seismic hazards. Various studies have documented this vulnerability, emphasising a significant risk to these structures during seismic events [30,31]. Despite the recognised importance of addressing the seismic resilience of buildings with such irregularities, limited research has focused on investigating the performance of structures that incorporate CLT shear walls in their construction and how mass and vertical geometric irregularities might impact seismic response. Further exploration into the behaviour of CLT structures, particularly those with irregular designs, under seismic conditions remains an area that warrants further investigation, highlighting a critical gap in the current knowledge within seismic engineering.

This study examines mass and vertical geometry irregularities of hybrid structures. To achieve this, the author first validated a hybrid structure using Dlubal RFEM 6.05 with the literature (Khajehpour et al., 2021). Two approaches were utilised to investigate the mass irregularity. Initially, the dead load of the middle story was increased by 1.5, 2.0, and 2.5 times and conducted a modal response spectrum analysis to examine the impact. Second, the author investigated the mass irregularity by increasing the dead load for each story across the height and conducted modal response spectrum analysis. To investigate the vertical geometric irregularity, the author used setback ratio (R_H) to differentiate structures with vertical geometric irregularity and conducted the modal response spectrum.

3.3 Model Creation and Validation

To validate the procedure, a hybrid structure with CLT and steel with HSK connections was developed and validated with the literature [32]. The validated building was symmetric, featuring three bays, each spanning 9 meters in all directions and with a story height of 3 meters, resulting in a building dimension of 27 meters by 27 meters across 12 stories. These buildings were constructed using 175-mm thick (5-ply) CLT panels with an additional 100-mm concrete topping. The building's middle bay core is reinforced with CLT balloon-framing shear walls to enhance structural integrity. These walls utilised 7-ply CLT panels, 245 mm thick, 3 meters wide, and 12 meters tall, effectively spanning the 9-meter middle bay. The panels, conforming to the E1M5 grade, met the in-plane shear strength standards as per CSA 086-19 [7]. The view of these panels in the section is illustrated in Fig. 3-2. The structure consisted of steel beams and columns with varying dimensions across different stories: from the 1st to 3rd stories, W310 × 179 beams paired with BOX450 × 30 columns; from the 4th to the 9th stories, the dimensions shifted to W310 × 158 for beams and BOX450 × 25 for columns; and for the 10th to 12th stories, W310 × 107 beams and BOX450 × 20 columns were used.
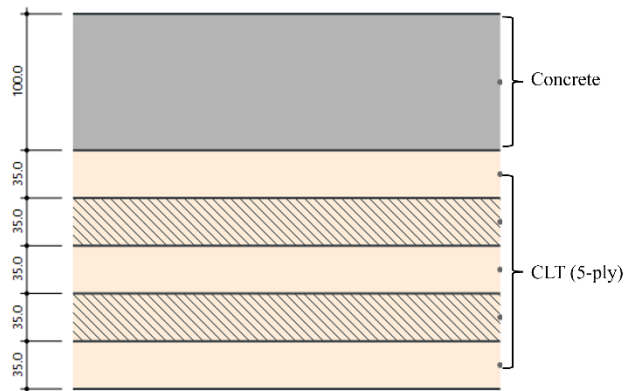
(a)
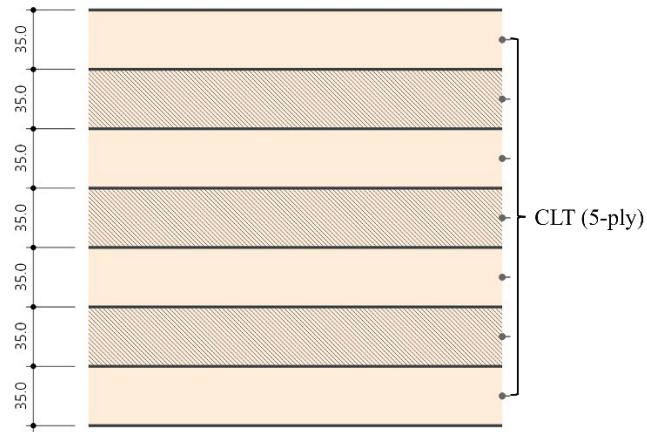
(b)

Fig. 3-2 a) CLT-Concrete Floor Panel Section (B) CLT Shear Wall Section

Considering loading factors, the typical floors were designed with a total dead load of 4.6 kN/m^2 and included partitions and flooring. The roof was designed to withstand snow loads of 1.64 kN/m^2. The steel components were chosen for their 350 MPa yield strength, 200 GPa Young's modulus, and 0.01 taken for strain hardening ratio. The design strategy was based on a rigid link between the steel beams and columns, reached by welding or bolting. HSK connection technology was utilised to join the panels with steel columns, connect the panels, and fasten Hold-Downs (HD) to the foundation. Four distinct types of HSK connections were used in the system: HSK1 to provide the connection along CLT panels in the vertical direction, HSK2 to join CLT panels and steel columns at the interface, HSK2 to provide horizontal connections among CLT panels, and HD to fix the CLT panels to the foundation. In these connections, HSK1 and HLD were the ones that should dissipate the energy, whereas HSK2 vertical connections and HSK2 horizontal connections were intended to be non-dissipative, contributing to the overall seismic resilience of the structure. The effectiveness of these connections, particularly in terms of shear and tension for HSK1 and uplift behaviour for HD, was tested by FPInnovation [15] and adopted their parameters in this study. Detailed backbone parameters for modelling these connections were provided in Fig. 3-3 (a), and Fig. 3-3(b) shows the connection definition at RFEM 6.05 Dlubal. Details on the specific modelling parameters for these connections are provided in TABLE 3-2.

(a)   (b)
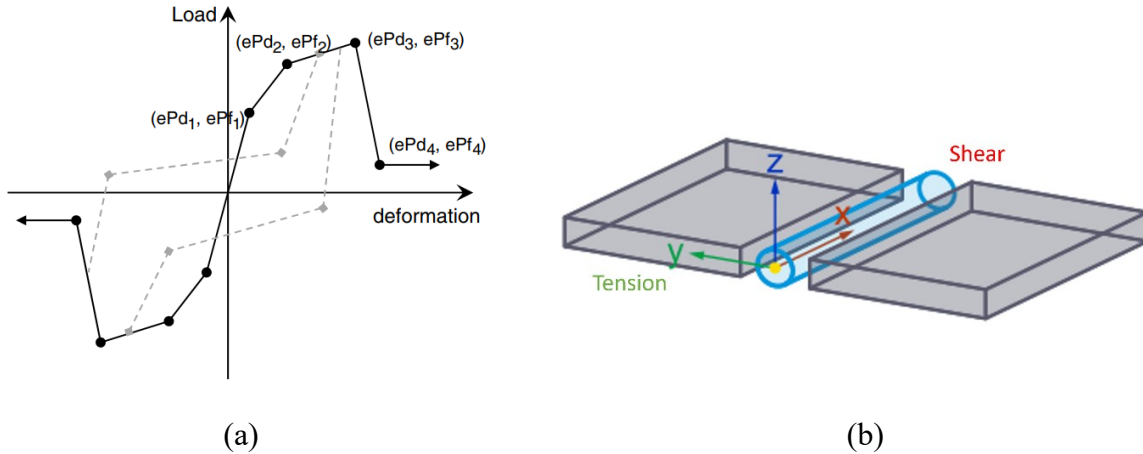
Fig. 3-3 (a) Backbone Curves For HSK Connections (B) Definition Of Connection At RFEM 6.05 Dlubal

TABLE 3-2. Backbone Parameters For Connection Modelling

Parameter	HLD	HSK1 Shear	HSK1 Tension ($\perp$)	HSK2 Shear	HSK2 Tension ($\perp$)	HSK2 Tension ($\parallel$)
ePf1 (kN) / ePd1 (mm)	77 / 0.4	25 / 0.5	6 / 0.8	49 / 0.3	10 / 0.8	8 / 1.2
ePf2 (kN) / ePd2 (mm)	138 / 5	37 / 14	68 / 3.5	65 / 2.5	112 / 3.5	128 / 4.2
ePf3 (kN) / ePd3 (mm)	180 / 19.9	34 / 25.4	61 / 3.9	81 / 10.3	101 / 3.9	133 / 4.7
ePf4 (kN) / ePd4 (mm)	180 / 20	4 / 29.4	7 / 4.3	8 / 18.6	11 / 4.4	13 / 7

Modal analysis of the modelled hybrid building was carried out to ensure the procedure's validity by comparing the results of the fundamental period with the literature [32]. The outcome of the modal analysis yielded a natural period of 0.863s, as opposed to the 0.87s documented in the literature, leading to a percentage error of 0.08%, attributable to the assumed boundary conditions of the model.

3.4 Analysis of Structure with Regular and Irregular Configurations

Following the validation process, the models underwent redesigning to investigate hybrid structures characterised by vertical geometric and mass irregularities, with the configurations of five bays and for three building heights of 8, 12 and 16 stories. The details of the beams and columns of these buildings are presented in TABLE 3-3. For each building model, the load considerations stayed consistent, including a dead load/roof of 3.4 kPa, a live load/roof of 1.48 kPa, a snow load of 1.64 kPa, a dead load/typical floor of 4.5 kPa, and a live load/ typical floor of 2.4 kPa were used in the design. Plan views for 8, 12, and 16 stories are illustrated in Fig. 3-4.

TABLE 3-3. The Member Dimensions of 8, 12, and 16-Story Buildings

Stories	External Beams	Internal Beams	Stories	External Columns	Internal Columns
8 Stories					
1 to 2	W310 × 179	W310 × 129	1 to 2	BOX350 × 20	BOX350 × 30
3	W310 × 158	W310 × 107	3	BOX350 × 15	BOX350 × 20
4 to 8	W310 × 158	W310 × 107	4 to 8	BOX350 × 15	BOX350 × 15
12 Stories					
1 to 3	W310 × 179	W310 × 179	1 to 3	BOX450 × 30	BOX450 × 30
4 to 9	W310 × 158	W310 × 158	4 to 9	BOX450 × 25	BOX450 × 25
10 to 12	W310 × 107	W310 × 107	10 to 12	BOX450 × 20	BOX450 × 20
16 Stories					
1 to 4	W310 × 253	W310 × 253	1 to 3	BOX450 × 30	BOX450 × 40

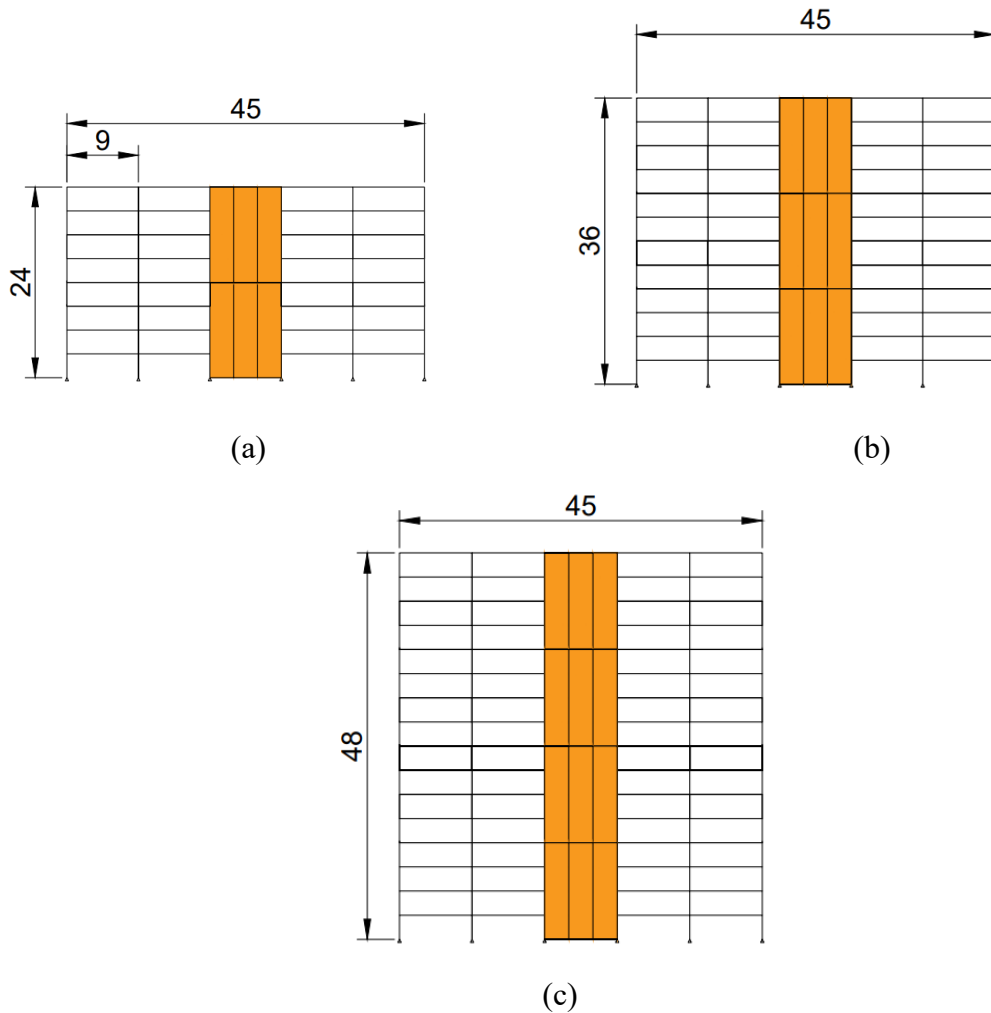| 5 to 10	W310 × 202	W310 × 202	3 to 5	BOX450 × 25	BOX450 × 35
11 to 12	W310 × 179	W310 × 179	6 to 7	BOX450 × 25	BOX450 × 30
13 to 16	W310 × 107	W310 × 107	8 to 9	BOX450 × 25	BOX450 × 25
			10 to 16	BOX450 × 20	BOX450 × 30

Fig. 3-4 Vertical Elevation: (a) 8-Story, (b) 12-Story, (c) 16-Story

Fig. 3-5 illustrates a framework for analysing Mass Irregularity (MI) configurations, offering a thorough comparison across different scenarios. The methodology further categorises the structures, labelling each model according to the dead load increase and the building's story height.

For example, a model of a 12-story hybrid building that has experienced a 2.0-fold increase in dead load is designated as "16-MI-CLT_H-2.0D," facilitating a clear and systematic approach to examining the effects of MI on structural behaviour during seismic events.

```
┌─────────────────────────────┐
│ Increased Dead Load : X 150% │
├─────────────────────────────┤
│ Increased Effective Load : X │
│            138%              │
└─────────────────────────────┘
              ▲
              │
┌─────────────────────┐        ┌─────────────────────────────┐
│  Mass Irregularity  │───────▶│ Increased Dead Load : X 200% │
│   Increased Mass    │        ├─────────────────────────────┤
│    Configuration    │        │ Increased Effective Load : X │
└─────────────────────┘        │            176%              │
              │                └─────────────────────────────┘
              ▼
┌─────────────────────────────┐
│ Increased Dead Load : X 250% │
├─────────────────────────────┤
│ Increased Effective Load : X │
│            276%              │
└─────────────────────────────┘
```
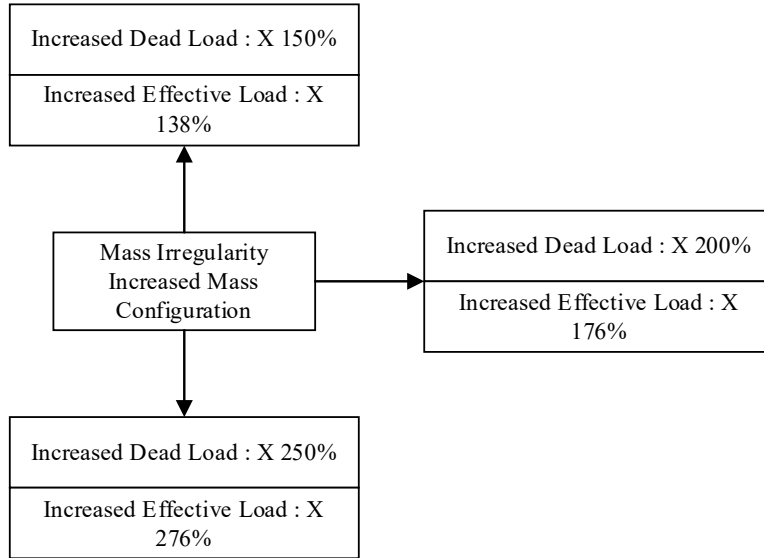
Fig. 3-5 Framework For Analysis Of MI

Furthermore, the author explored an investigation of MI, focusing on the impact of increased mass on seismic performance across different stories throughout the building height. The chosen mass increase was 2.5 times the dead load. The analysis is conducted for 8, 12, and 16 stories. The 8 stories with different MI configurations are illustrated in Fig. 3-6. A systematic naming convention was employed to maintain clarity and precision in identifying the various models based on the floor where the mass increase occurred. For instance, a model of a 12-story hybrid building that featured a mass increase on the second floor was labelled as "12-MI-CLT_H-2.5D-FL_02", indicating the building's height, the nature of irregularity (MI), the factor of dead load increase (2.5D), and the specific floor of the mass incrementation (FL_02). This approach allowed for a detailed analysis of the impact of localised mass increases on structural behaviour under seismic conditions.
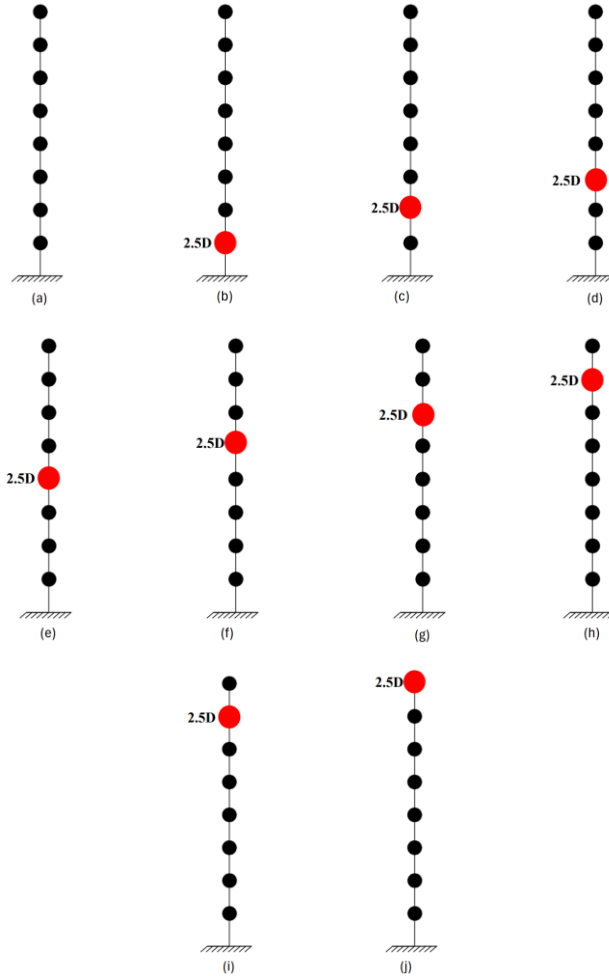
Fig. 3-6 MI Configuration (Along the Height) (A) 8-Basemodel-CLT_H (B) 8-MI-Hybrid-2.5D_FL_01 (C) 8-MI-Hybrid-2.5D-FL_02 (D) 8-MI-Hybrid-2.5D-FL_03 (E) 8-MI-Hybrid-2.5D_FL_04 (F) 8-MI-Hybrid-2.5D_FL_05 (G) 8-MI-Hybrid-2.5D_FL_06 (H) 8-MI-Hybrid-2.5D-FL_07 (I)8-MI-Hybrid

To explore the seismic response of hybrid buildings with Vertical Geometric Irregularities (VGI), 18 models with MI were introduced with three base models (models without irregularities). The investigation extended to two configurations of CLT shear walls, detailed in Fig. 3-7.
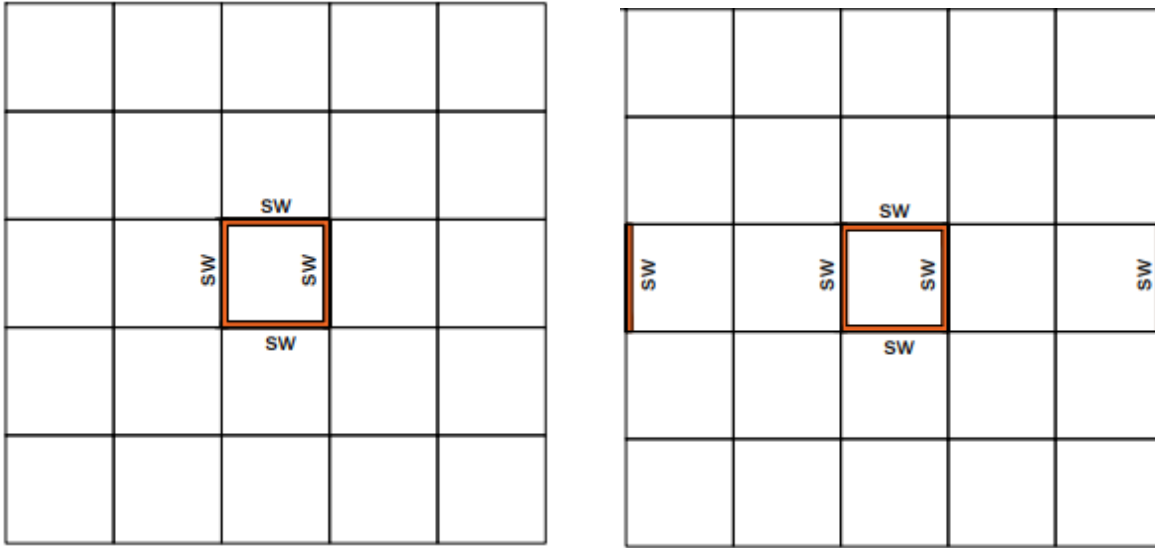
(a)   (b)

Fig. 3-7 (a) SW Configuration -1 (b) SW Configuration -2

The setback ratio (R_H), introduced by Pirizadeh & Shakib (2013), used to differentiate buildings with VGI, is depicted in Fig. 3-8 Definition of Rh
is employed in the analysis.

$$R_H = \frac{Tower\ Height}{Base\ Height}$$

Fig. 3-8 Definition of R_h
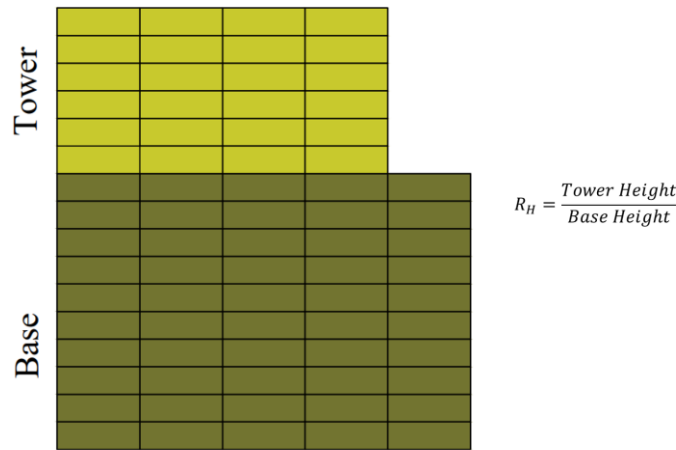
Fig. 3-9 presents a schematic approach for evaluating the seismic response of hybrid buildings with vertical irregularity. Buildings of 8 stories, 12 stories, and 16 stories, considering varying R_H factors, were modelled, and the configuration of steel beams and columns, CLT shear walls, and connections were maintained consistently with the base models (without any irregularity).
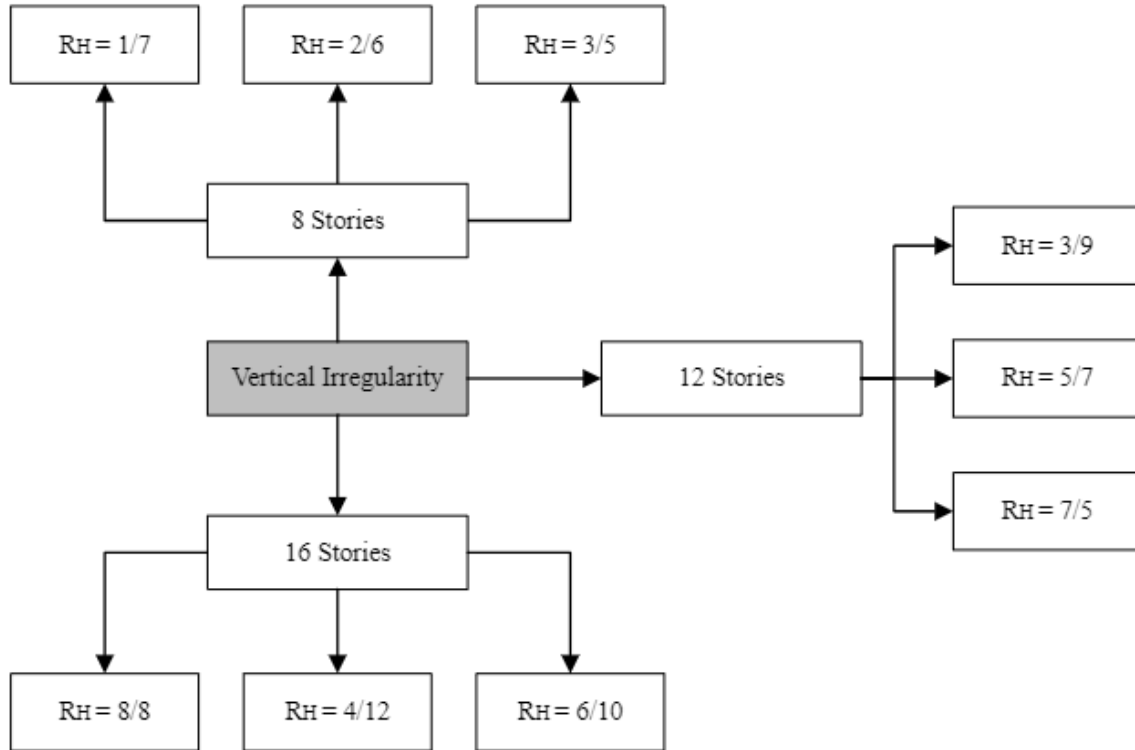
48

Fig. 3-9 Framework For Analysis Of VGI

Based on the R_H definition (Tower height/base height), nine hybrid models with configuration-1 and nine hybrid models with configuration-2 were modelled using Dlubal RFEM. All models with VGI labels are based on the R_h, the number of stories, and the shear wall configuration. Configuration 1 is denoted as "CLT_H," and configuration 2, which includes CLTASW_H, is integrated into the code. For example, a model with 12 stories, a R_h of 8/8, and configuration two is labelled as "8-VI-CLTASW_H-8/8

3.5 Methodology

Modal Response Spectrum Analysis (MRSP) is used to analyse the structure employing Dlubal RFEM 6.05. MRSP employs a dynamic analysis that identifies the highest response from all relevant modes comprising the overall seismic reaction. MRSP calculates deformations and forces induced by seismic events using dynamic equilibrium equations based on the structure's elasticity model to integrate its dynamic properties for a more precise outcome than linear static analyses. Each mode's site-specific design spectrum-derived period value calculates the maximum response in every mode. The overall response of the structure is determined via statistical consolidation of these peak responses in each mode. The building structure locations were assumed in Montréal

(City Hall) and Vancouver (City Hall), and the seismic response design data for those locations is shown in TABLE 3-4 as per NBCC. The labelling of the response spectrum analysis is based on Montréal (City Hall) as "RSA-Montreal" and that based on Vancouver (City Hall) as "RSA-Vancouver". A normal importance factor and Site class C were chosen as the presumptive factors for the analysis. In a recent study by Khajehpour et al. (2021), it was suggested that for hybrid structures, the ductility-related factor (R_d) and the overstrength-related factor (R_o) should be set at $R_d = 3.87$ and $R_o = 1.57$. These force modification factors have been incorporated into this analysis. The SRSS Modal Combination Rule was applied for periodic responses, with the response spectrum analysis being conducted in both the X and Y directions considering orthogonal effort (100% of the prescribed seismic forces in one direction plus 30% of the prescribed forces in the perpendicular direction [34]). Further, the study assumed that all the maximum modal values are statically independent. For this analysis, the first ten modes were selected with a Modal Participation Factor (MPF) for these modes exceeding 90%.

TABLE 3-4. Seismic Design Data for RSA-Montreal and RSA-Vancouver

Spectral Acceleration Parameters	RSA-Montreal	RSA-Vancouver
Spectral Response Acceleration for period 0.2 s	0.595	0.848
Spectral Response Acceleration for period 0.5 s	0.311	0.751
Spectral Response Acceleration for period 1.0 s	0.148	0.425
Spectral Response Acceleration for period 2.0 s	0.068	0.257
Spectral Response Acceleration for period 5.0 s	0.018	0.08
Spectral Response Acceleration for period 10.0 s	0.0062	0.029

Due to the symmetrical nature of the building models, the directional response was disregarded in the analysis of MI, simplifying the analysis by assuming that mass irregularities do not significantly impact the building's behaviour in different horizontal directions. The scenarios change noticeably when addressing VGI analysis as the direction becomes more significant in determining and assessing the structure's behaviour. Comparing MI, VGI often results in an irregular allocation of stiffness and strength across the elevation of a building, which can profoundly affect its response to lateral forces. This irregular distribution can cause varying responses in different directions, necessitating an orientation-based examination to capture the structural behaviour accurately. These directional orientations are maintained constantly across all models to ensure a uniform basis for comparison and analysis [35]. Therefore, the analysis can

more accurately reflect the actual performance of the structure with vertical geometrical irregularities, offering insights into potential vulnerabilities and the effectiveness of various design strategies to mitigate them. Consistent directions (X and Y direction) are established for all the VGI structures and illustrated in Fig. 3-10 to investigate the directional response.
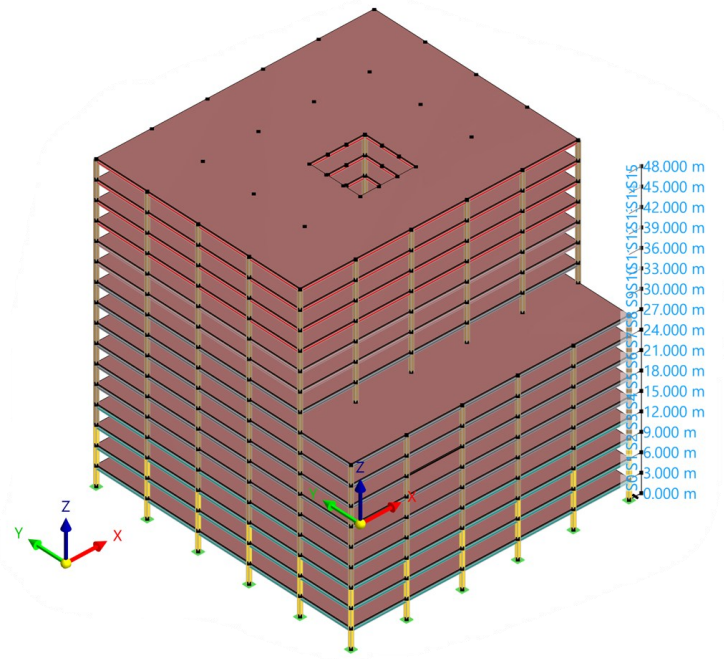

Fig. 3-10 Definition of the Directional Axes (X And Y Directions)

3.6 Evaluation of Mass Irregularity (Increased Mass at the Mid-Level of the Structure)

As discussed, an MRSP analysis was conducted, utilising the first ten modes to analyse the hybrid structures with MI. The MPF for these modes exceeded 90% for all the models, indicating a significant representation of the structure's dynamic behaviour within these modes. Steel columns and beams were also checked per the Steel Design (CSA S16,2019). The inter-story drift distributions along the height of models exhibiting MI were compared and depicted in Fig. 3-11 Maximum Inter-Story Drift Distribution across the Height Hybrid Models with MI: (a) 8 Story (RSA- Montreal) (b) 8 Story (RSA- Vancouver) (c) 12 Story (RSA- Montreal) (d) 12 Story (RSA-Vancouver) (e) 16 Story (RSA- Montreal) (f) 16 Story (RSA- Vancouver)
, with the inter-story drift observed in regular building configurations, recognising the influence of MI on the overall structural performance under seismic loading conditions.

Fig. 3-11 illustrates hybrid structures of 8, 12, and 16 stories with and without (base model) MI. The graph demonstrates a correlation between increasing mass in the middle story (1.5D, 2D and 2.5D) and increasing inter-story drift in a building. The trend becomes more noticeable in buildings with low stories (particularly 8-story structures), suggesting that the building experiences more significant drifts when more mass is added irregularly – indicating a higher risk of damage during seismic events. Additionally, it was observed that the upper levels of the structure are less influenced by the increased mass in the middle story than the lower levels. The lower levels bear the cumulative weight of the structure above them, which means that any alterations at these levels can profoundly affect the building's response to seismic activity.

In analysing structures with 8, 12, and 16 stories, the RSA-Montreal model, which is representative of Montreal, and the RSA-Vancouver model, which has been designed to capture Vancouver's seismic conditions, were used. A significant difference between the two locales was observed. RSA-Vancouver has shown that maximum drift ratios increase three times in all irregular cases, revealing the dominant effect of geographical seismic properties on structural behaviour compared to RSA-Montreal.

In conclusion, it was observed that there is a tangible relationship between the magnitudes of increased mass and inter-story drift. Further, the upper levels of the buildings show a negligible correlation with the increased mass, indicating a diminishing effect of mass increases on upper levels. It also revealed that geographic seismic characteristics significantly influence story drift, as demonstrated in the RSA-Montreal and RSA-Vancouver case studies.
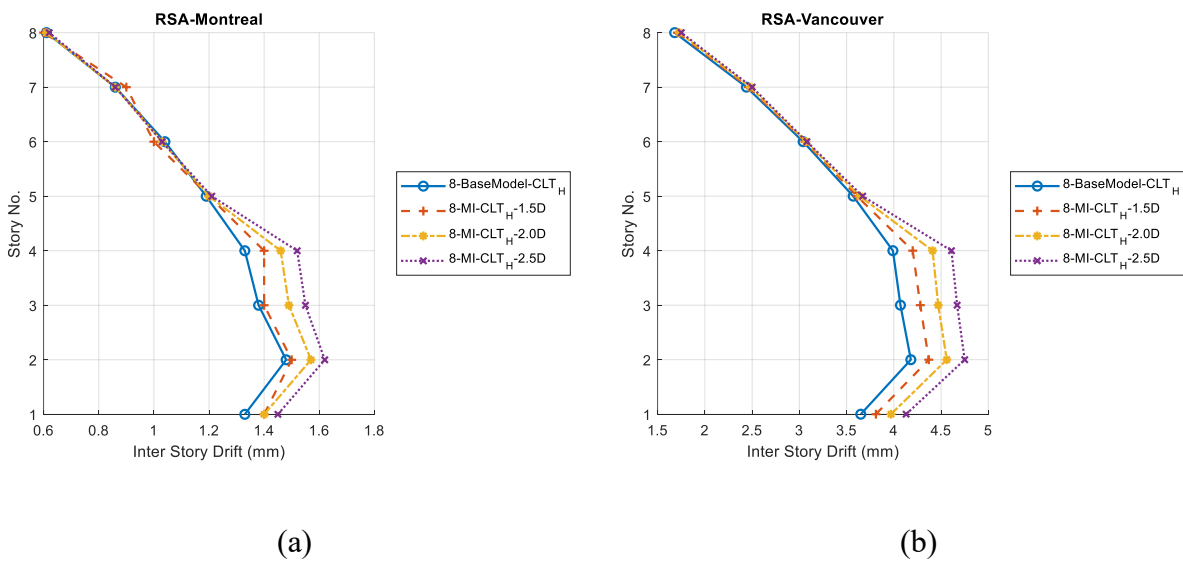
(a)   (b)
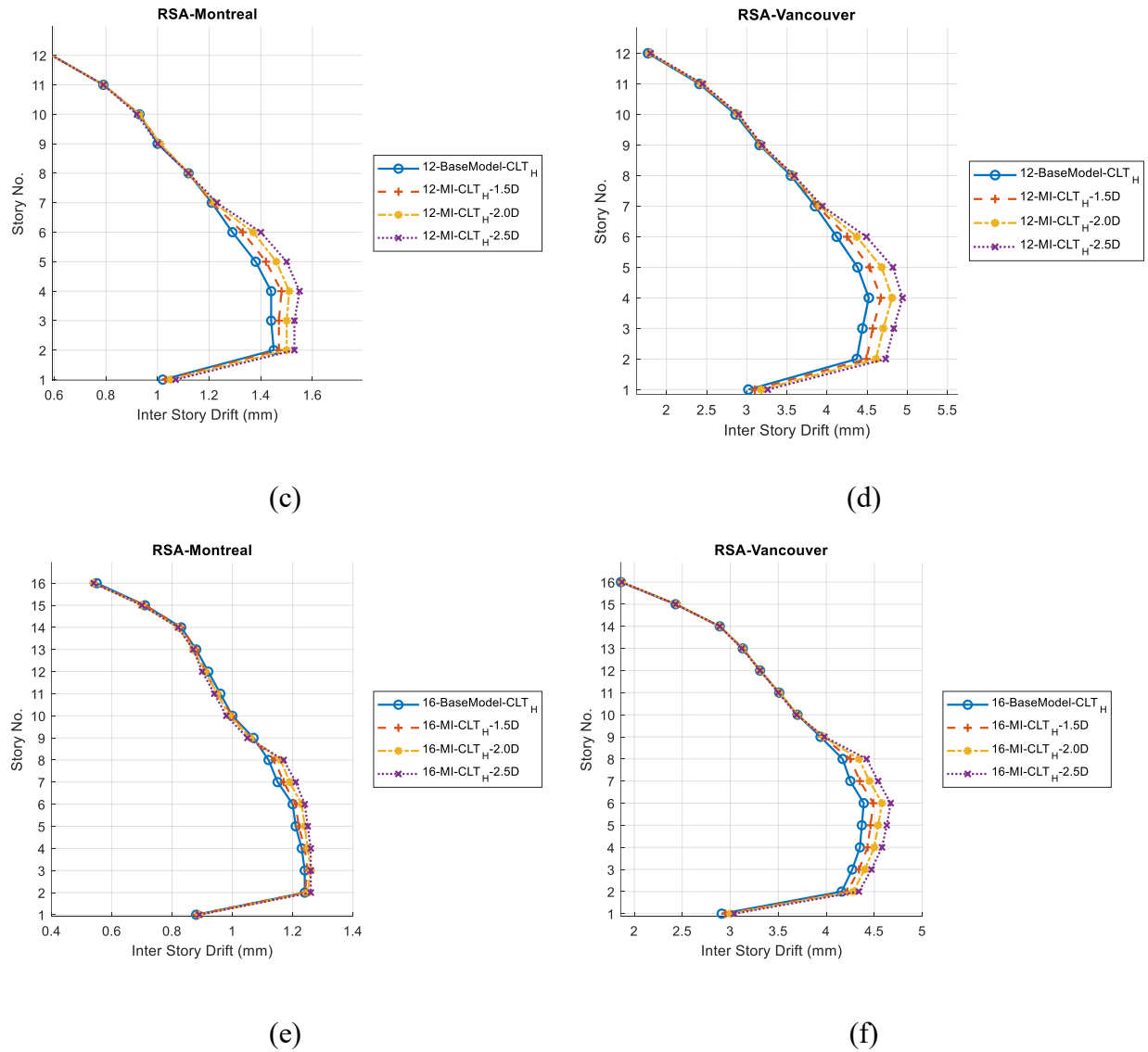
Fig. 3-11 Maximum Inter-Story Drift Distribution across the Height Hybrid Models with MI: (a) 8 Story (RSA- Montreal) (b) 8 Story (RSA- Vancouver) (c) 12 Story (RSA- Montreal) (d) 12 Story (RSA- Vancouver) (e) 16 Story (RSA- Montreal) (f) 16 Story (RSA- Vancouver)

3.7   Variation of Increased Mass along the Height of the Structure

The MRSP analysis used the ten modes to examine the hybrid structures with MI and the variation of increased mass along the structure's height. The building structure is assumed to be in Vancouver (City Hall). The MPF for these modes exceeded 90% for all models, demonstrating a significant representation of the structure's dynamic behaviour within these modes. The inter-story drift distributions along the height of models exhibiting MI were depicted in Fig. 3-12, with the

inter-story drift observed in regular building configurations. This comparison was essential to recognise the influence of MI on the overall structural performance under seismic loading conditions.

Fig. 3-12 shows the inter-story drift for different models, demonstrating the effect of MI on inter-story drift. The nomenclature of the models is provided earlier. The drift values change as the location of the increased mass changes, illustrating the impact of MI (increased mass at a particular floor) on the building's inter-story drift. Trends in drift are observed, indicating that stories located above floors with increased mass tend to exhibit greater drift values in most cases. For example, more significant drift in upper levels is noted when increased mass is positioned on lower levels. At the same time, drift tends to be more contained in upper levels, affecting lower levels less when mass is added to upper levels. The sensitivity of the upper levels is highlighted, with the top story often presenting the highest drift values across most models. This is attributed to the top of the building being typically more sensitive, thus undergoing more significant movement. However, variations in drift values are more pronounced in some models than in others, suggesting a substantial impact of mass distribution on the movement of the uppermost stories.

The stability of the lower levels is also observed, showing less drift variation than the upper levels. However, an increase in the drift of lower levels is observed when mass is added to the lower levels, indicating that mass addition at lower levels impacts the stability of the lower levels, influencing the drift experienced by the entire structure. The behaviour of middle stories is characterised by varying drift values depending on the model, though the trend is less consistent than seen in the upper or lower levels. This inconsistency is attributed to the complex interaction between mass distribution and the building's inherent stiffness and damping properties at different levels.

In conclusion, the MRSP analysis conducted on various models with MI that altered the increased mass location across the structure has exposed significant insights into the structural dynamics under seismic loading. The study uncovered that the location of increased mass within the structure plays a crucial role in its seismic response, with upper levels showing higher sensitivity and demonstrating higher drift when increased mass is located on lower levels. Conversely, when mass is added to upper levels, the drift tends to be more localised to the upper levels, sparing the lower levels from significant effects. This trend highlights the importance of considering mass

distribution when designing buildings for seismic resilience, as the dynamic behaviour of buildings under seismic loading is significantly affected by the location where increased mass is applied.

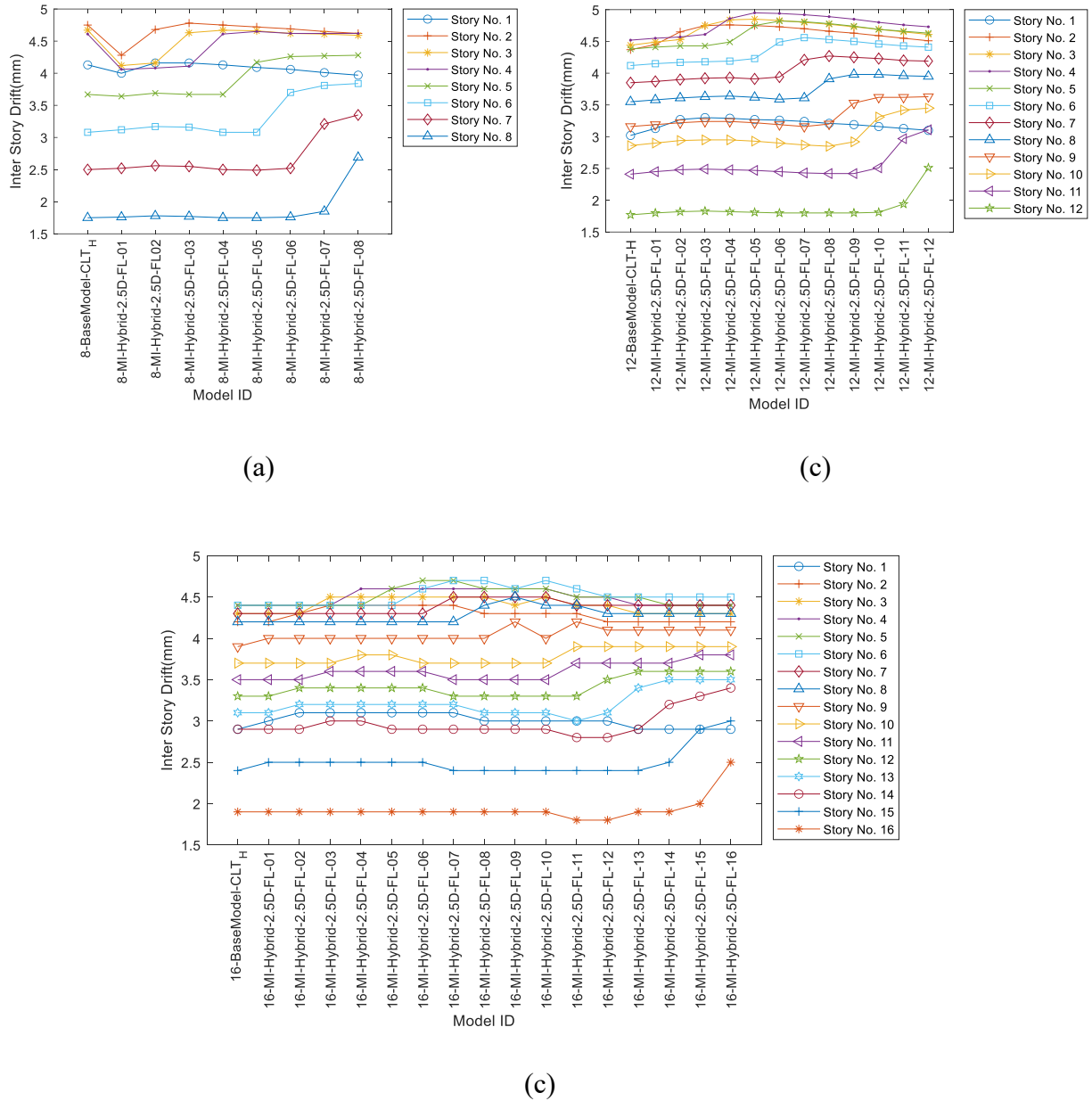(a)   (c)


(c)

Fig. 3-12 Inter-Story Drift Variability with Increased Mass Distribution Along the Building's Elevation: (a) 8-story hybrid structure (b) 12-story hybrid structure (c) 16-story hybrid structure

3.8 Vertical Geometric Irregularity

The MRSP analysis was conducted to investigate the VGI of buildings with different shear wall configurations (Configuration-1 and Configuration-2). Employing the first ten modes to analyse the hybrid structures with VGI. Notably, the MPF for these modes exceeded 90% for all the models, indicating a significant representation of the structure's dynamic behaviour within these modes. Steel columns and beams were also checked per the Steel Design (CSA S16,2019). The inter-story drift distributions along the height of models exhibiting VGI were compared and depicted in Fig. 3-13, with the inter-story drift observed in regular building configurations (base models) recognising the influence of VGI on the overall structural performance under seismic loading conditions.

The results show a notable increase in the drift corresponding to the VGI in buildings, especially in the tower stories, compared to base stories (see Fig. 3-8), notably in the X direction. It revealed that some stories have experienced a remarkable surge in story drift for both shear wall configurations. Further, it was observed that the increase in story drift was more pronounced in Configuration 1 than in Configuration 2. As the analysis widened to include the Y direction, a marked trend was observed, demonstrating that the drift for the buildings with the VGI was substantially increased in configuration 1 than in configuration 2.

This study highlights the significance of directional approaches in the seismic response analysis in the case of VGI buildings. VGI poses a unique set of challenges since the mass and stiffness of buildings often need to be more evenly distributed along the height of the building. The directional responses in the X direction are particularly important and must be considered in seismic design and analysis since this irregularity is an essential factor affecting seismic performance. The research recognises the critical role of incorporating the directional behaviours of the seismic response and how this can result in a scenario where the risk is underestimated.
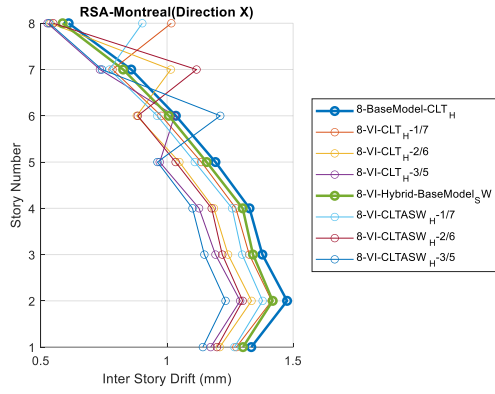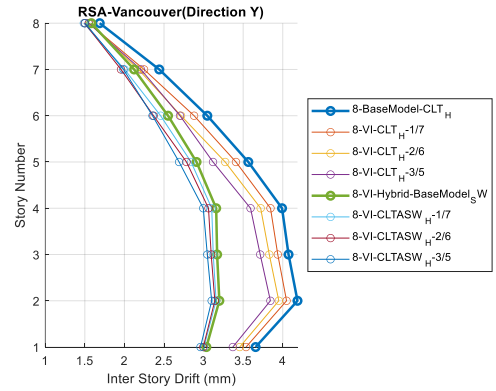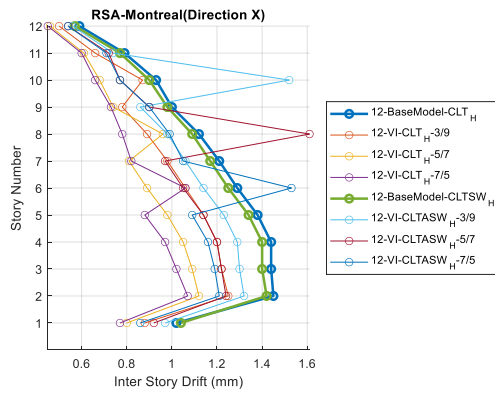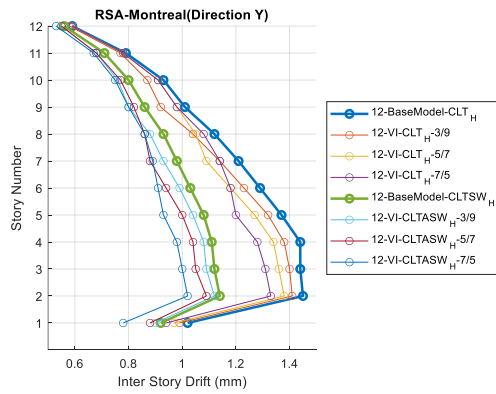
(a)
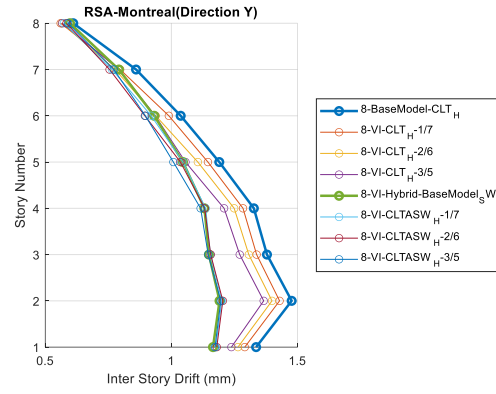
(b)
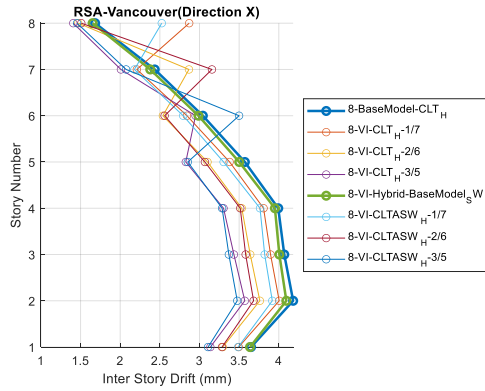
(c)

(d)

(e)

(f)
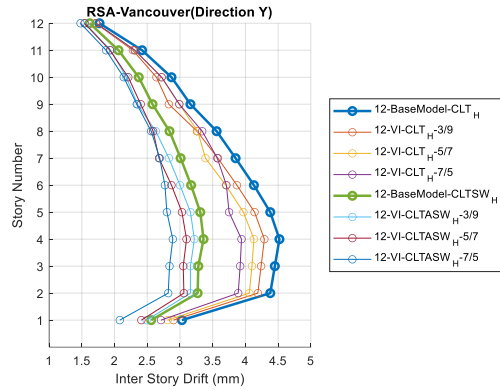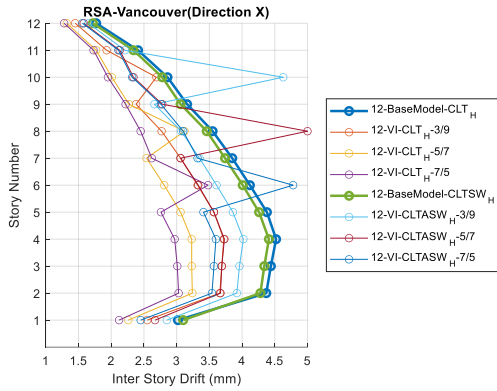
(g)

(h)
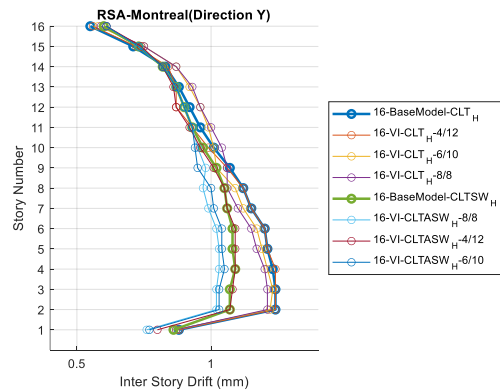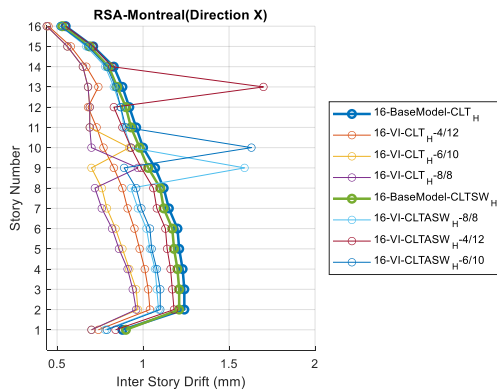
(i)

(j)

(k)

(l)

Fig. 3-13 Maximum Inter-Story Drift Distribution across the Height of Hybrid Models with VGI:
(a) 8 Story -Direction X (RSA- Montreal) (b) 8 Story -Direction Y (RSA- Montreal) (c) 8 Story -
Direction X (RSA- Vancouver) (d) 8 Story -Direction Y (RSA- Vancouver) (e) 12 Story -
Direction X (RSA- Montreal) (f) 12 Story -Direction Y (RSA- Montreal) (g) 12 Story -Direction

X (RSA- Vancouver) (h) 12 Story -Direction Y (RSA- Vancouver) (i) 16 Story -Direction X (RSA- Montreal) (j) 16 Story -Direction Y (RSA- Montreal) (k) 16 Story -Direction X (l) 16 Story -Direction Y

3.9   Conclusion

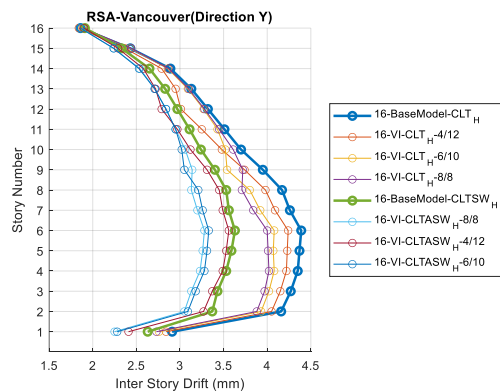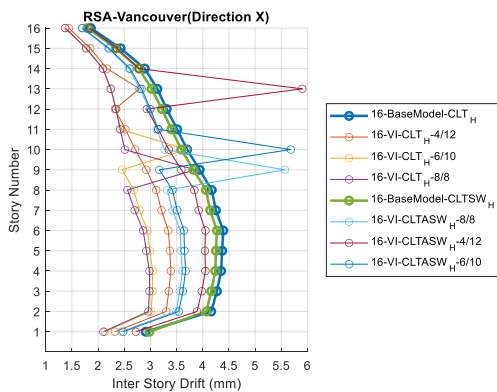In this investigation, the seismic behaviours of structures with Mass Irregularity (MI) and Vertical Geometric Irregularity (VGI) were evaluated through the utilisation of Dlubal RFEM 6.05 software, centring on the implementation of Modal Response Spectrum Analysis (MRSP). The principal findings of this study are as follows:

- ⁻ The investigation revealed a relationship between a hybrid structure with MI, increased mass and the resulting inter-story drift, indicating that mass increment significantly impacts structural behaviour under seismic conditions. Nevertheless, this influence was observed to be diminished at higher-level stories. Higher-level stories demonstrate a negligible correlation with increased mass for all the cases. This observation highlights the importance of mass distribution within the structure and its pivotal role in influencing seismic response, particularly in MI.

- ⁻ The geographical seismic characteristics emerged as a significant determinant of structural behaviour, as evidenced by the case studies conducted in Montreal and Vancouver. Additionally, Vancouver has significantly higher inter-story drift ratios than Montreal. These findings emphasise the region-specific seismic analysis, acknowledging that geographic seismic profiles considerably influence the outcomes of MRSP.

- ⁻ The investigation into the effects of shifting the location of increased mass within the structure exposed that the seismic response is markedly affected by the location of added mass. Increased mass at lower levels induced higher sensitivity and more significant drift in the upper levels, whereas mass additions to upper levels resulted in more localised drift to those upper levels, sparing the lower levels from pronounced impacts emphasising to carefully consider mass distribution in the architectural design phase to enhance seismic resilience.

- ⁻ The research highlighted the importance of directional approaches in seismic response analysis, especially in VGI buildings. The study identified that the directional responses, particularly in the X direction, play a crucial role due to the often-uneven distribution of

mass and stiffness along the height of such buildings. If not adequately accounted for, this irregularity could lead to underestimating seismic risk.

- The analysis highlights that in buildings characterised by VGI, the tower structure is notably affected by a sudden increase in inter-story drift compared to adjacent stories, specifically in the X direction. This phenomenon indicates a difference in how the building's tower structure and base structure respond to external forces, with the tower structure experiencing greater displacement than the base structure. Such findings underscore the importance of considering VGI in the design and evaluation of buildings to ensure structural integrity and resilience against dynamic loads.

3.10 Credit Authorship Contribution Statement

K.G.M. Kandethanthri: Formal Analysis, Validation, Finite Element Models. **Ghazanfarah Hafeez:** Conceptualization, Methodology, Investigation, Formal Analysis, Validation, Writing— original Draft Preparation, Review, and Editing. Supervision, Data Collection, Conceptualization, Methodology, Investigation, Visualization, Writing, Review, and Editing,

3.11 Statements and Declarations

All authors certify that they have no affiliations with or involvement in any organisation or entity with any financial or non-financial interest in the subject matter or materials discussed in this manuscript.

3.12 Declaration of Competing Interest

The authors declare that they have no known competing financial interests or personal relationships that could have appeared to influence the work reported in this paper.

3.13 Data Availability

The raw/processed data required to reproduce these findings cannot be shared as it is also part of an ongoing study.

3.14 References

[1]   E. Ferdosi, Seismic damage assessment for balloon-type shear wall timber structures, University of British Columbia, 2024. https://open.library.ubc.ca/collections/ubctheses/24/items/1.0440683.

[2]   F. Pierobon, M. Huang, K. Simonen, I. Ganguly, Environmental benefits of using hybrid CLT structure in midrise non-residential construction: An LCA based comparative case study in the U.S. Pacific Northwest, Journal of Building Engineering 26 (2019) 100862. https://doi.org/10.1016/j.jobe.2019.100862.

[3]   B. Shin, S. Wi, S. Kim, Assessing the environmental impact of using CLT-hybrid walls as a sustainable alternative in high-rise residential buildings, Energy Build 294 (2023) 113228. https://doi.org/10.1016/j.enbuild.2023.113228.

[4]   A. Opazo-Vega, F. Benedetti, M. Nuñez-Decap, N. Maureira-Carsalade, C. Oyarzo-Vera, Non-destructive assessment of the elastic properties of low-grade CLT panels, Forests 12 (2021) 1734.

[5]   R.E. Thomas, U. Buehlmann, Using low-grade hardwoods for CLT production: a yield analysis, in: Proceedings of the 6th International Scientific Conference on Hardwood Processing, 2017: pp. 25–28.

[6]   R. Cherry, A. Manalo, W. Karunasena, G. Stringer, Out-of-grade sawn pine: A state-of-the-art review on challenges and new opportunities in cross laminated timber (CLT), Constr Build Mater 211 (2019) 858–868.

[7]   E. Karacabeyli, S. Gagnon, Canadian CLT handbook, 2019.

[8]   R. Brandner, P. Dietsch, J. Dröscher, M. Schulte-Wrede, H. Kreuzinger, M. Sieder, Cross laminated timber (CLT) diaphragms under shear: Test configuration, properties and design, Constr Build Mater 147 (2017) 312–327.

[9]   M. Shahnewaz, S. Alam, T. Tannert, In-Plane Strength and Stiffness of Cross-Laminated Timber Shear Walls, Buildings 8 (2018) 100. https://doi.org/10.3390/buildings8080100.

[10]   M. Mohammad, J. Tourrilhes, R. Coxford, M. Williamson, Canadian mass timber demonstration projects initiatives, Modular and Offsite Construction (MOC) Summit Proceedings (2019) 51–58.

[11]   I.C. Council, 2021 International Building Code, International Code Council, 2020. https://books.google.ca/books?id=n8DfzQEACAAJ.

[12]   J. Liu, F. Lam, Experimental test of coupling effect on CLT angle bracket connections, Eng Struct 171 (2018) 862–873. https://doi.org/10.1016/j.engstruct.2018.05.013.

[13]   D. Trutalli, L. Marchi, R. Scotta, L. Pozza, Capacity design of traditional and innovative ductile connections for earthquake-resistant CLT structures, Bulletin of Earthquake Engineering 17 (2019) 2115–2136. https://doi.org/10.1007/s10518-018-00536-6.

[14]   X. Zhang, Y. Pan, T. Tannert, The influence of connection stiffness on the dynamic properties and seismic performance of tall cross-laminated timber buildings, Eng Struct 238 (2021) 112261.

[15]   Z.X. Zhang XiaoYue, M. Popovski, T. Tannert, High-capacity hold-down for mass-timber buildings., (2018).

[16]   X. Zhang, M. Popovski, T. Tannert, Experimental Test on Novel Seismic Hold-Downs for Timber Structures, in: Proc., World Conference on Earthquake Engineering, Santiago, Chile, 2017.

[17]   S. Dires, T. Tannert, S. Tesfamariam, Energy-Based Seismic Design Method for Coupled CLT Shear Walls, in: International Workshop on Energy-Based Seismic Engineering, Springer, 2021: pp. 221–235.

[18]   L. Bathon, O. Bletz-Mühldorfer, J. Schmidt, F. Diehl, Fatigue design of adhesive connections using perforated steel plates, in: Proceedings of the World Conference on Timber Engineering, 2014: pp. 996–1001.

[19]   X. Zhang, M. Popovski, T. Tannert, High-capacity hold-down for mass-timber buildings, Constr Build Mater 164 (2018) 688–703. https://doi.org/10.1016/J.CONBUILDMAT.2018.01.019.

[20]   A. Erdle, I. Smith, J. Weckendorf, A. Asiz, Control of the dynamic performance of hybrid steel frame and cross laminated timber slab buildings, in: Proc., 12th World Conf. on

Timber Engineering (WTCE), P. Quenneville, Ed., Curran Associates, Auckland, New Zealand, 2012.

[21] R. Krisciunas, Ontario's experience with Composite Wood/Steel Bridges, in: National Conference on Wood Transportation StructuresUS Forest Service, Forest Products Laboratory; Federal Highway Administration, 1996.

[22] J. Weckendorf, I. Smith, Multi-functional interface concept for high-rise hybrid building systems with structural timber, in: Proc., 12th World Conf. on Timber Engineering, 2012: pp. 16–19.

[23] J. Schneider, S.F. Stiemer, S. Tesfamariam, E. Karacabeyli, M. Popovski, Damage assessment of cross laminated timber connections subjected to simulated earthquake loads, in: World Conference on Timber Engineering, 2012: pp. 398–406.

[24] M. Yousuf, A. Bagchi, Seismic design and performance evaluation of steel-frame buildings designed using the 2005 National building code of Canada, Canadian Journal of Civil Engineering 36 (2009) 280–294.

[25] S. Tesfamariam, S.F. Stiemer, C. Dickof, M.A. Bezabeh, Seismic Vulnerability Assessment of Hybrid Steel-Timber Structure: Steel Moment-Resisting Frames with CLT Infill, Journal of Earthquake Engineering 18 (2014) 929–944. https://doi.org/10.1080/13632469.2014.916240.

[26] C. Dickof, S.F. Stiemer, M.A. Bezabeh, S. Tesfamariam, CLT–steel hybrid system: Ductility and overstrength values based on static pushover analysis, Journal of Performance of Constructed Facilities 28 (2014) A4014012.

[27] F. Pierobon, M. Huang, K. Simonen, I. Ganguly, Environmental benefits of using hybrid CLT structure in midrise non-residential construction: An LCA based comparative case study in the US Pacific Northwest, Journal of Building Engineering 26 (2019) 100862.

[28] R. Tremblay, L. Poncet, Seismic performance of concentrically braced steel frames in multistory buildings with mass irregularity, Journal of Structural Engineering 131 (2005) 1363–1375.

[29] P. Sarkar, A.M. Prasad, D. Menon, Vertical geometric irregularity in stepped building frames, Eng Struct 32 (2010) 2175–2182.

[30]   S.S. Tezcan, C. Alhan, Parametric analysis of irregular structures under seismic loading according to the new Turkish Earthquake Code, Eng Struct 23 (2001) 600–609. https://doi.org/10.1016/S0141-0296(00)00084-5.

[31]   S. Tesfamariam, M. Saatcioglu, Risk-Based Seismic Evaluation of Reinforced Concrete Buildings, Earthquake Spectra 24 (2008) 795–821. https://doi.org/10.1193/1.2952767.

[32]   M. Khajehpour, Y. Pan, T. Tannert, Seismic analysis of hybrid steel moment frame CLT shear walls structures, Journal of Performance of Constructed Facilities 35 (2021) 04021059.

[33]   M. Pirizadeh, H. Shakib, Probabilistic seismic performance evaluation of non-geometric vertically irregular steel buildings, J Constr Steel Res 82 (2013) 88–98.

[34]   C. Menun, A. Der Kiureghian, A replacement for the 30%, 40%, and SRSS rules for multicomponent seismic analysis, Earthquake Spectra 14 (1998) 153–163.

[35]   P.K. Das, S.C. Dutta, T.K. Datta, Seismic Behavior of Plan and Vertically Irregular Structures: State of Art and Future Challenges, Nat Hazards Rev 22 (2021). https://doi.org/10.1061/(ASCE)NH.1527-6996.0000440.

Four.   Chapter 4.

4   Structural Performance of Balloon-Type Unbounded Post-Tensioned Cross-Laminated Timber Wall System

KTGM Kandethanthri, Ghazanfarah Hafeez, Zhiyong Chen

4.1   Abstract

The structural behaviour of unbonded post-tensioned Cross-Laminated Timber (CLT) shear walls is comprehensively analysed in this study using a combined approach that appreciates numeric simulation and advanced machine learning techniques. It aims to investigate how various structure parameters, such as thickness, aspect ratio, post-tension diameter, and post-tension stress, affect the initial stiffness of unbonded post-tensioned CLT shear walls. The study identified that increasing wall thickness significantly improves resistance to lateral loads while maintaining a constant aspect ratio. Subsequently, the study incorporated machine learning algorithms like eXtreme Gradient Boosting (XGBoost), Gradient Boosting Decision Tree, Random Forest, Catboost, and Decision Tree model to develop machine learning models to make reliable initial lateral and vertical stiffness predictions. Furthermore, SHapley Additive exPlanations (SHAP) are used to explain the machine learning models as they reveal vital connections between these structural factors. Finally, this paper investigates factors contributing to complex dynamics controlling the structural behaviour of unbonded post-tensioned CLT shear walls.

Keywords: Post-Tensioned; Numerical Model; Structural Performance, Cross Laminated Timbers, Balloon-Type

4.2 Introduction

The growing population and environmental concerns necessitate the construction of tall wooden buildings to mitigate these issues. The emergence of Cross-Laminated Timber (CLT) is a significant alternative to address the height limitation associated with light-frame wood construction, including those in the presence of seismic and wind forces. CLT is a widely used engineered wood product for tall wood buildings in the construction industry. CLT comprises orthogonal sawn lumber layers glued together to form panels with high in-plane strength and stiffness. It is used as a full-size wall system, floor element, and structural member throughout mass timber construction. Generally, two primary approaches in constructing CLT buildings involving residential dwellings to mid-rise commercial edifices are balloon frame and platform construction[1–3]. These methods diverge in assembling each building floor, consequently influencing the load pathways for gravity and lateral forces. Platform construction contains the sequential construction of shear walls for each building floor, placing each one atop the previous floor, thereby utilising the last floor as a foundation or platform for the subsequent one. Balloon frame construction entails erecting the shear walls for each floor as a continuous vertical wall spanning the full height of the building. The floors are integrated into this wall at specific heights using angle brackets, wooden ledgers, or other connection methods. Balloon frame construction is less commonly employed with materials other than CLT due to complexities in connection design and load path determination; it offers significant advantages in constructability when paired with CLT [4]. A numerical study by Casagrande et al. (2019) highlighted the flexibility of the platform framing system, which can lead to significant lateral displacement due to the slipping of CLT panels at floor levels. Additionally, the construction of buildings employing CLT walls with traditional connections experienced high accelerations at the floor levels during shake table testing, reaching up to 3.8g[6]. These CLT panels were either connected to the foundation via traditional metal bracket connections[7] or employing unbonded post-tensioning [3,8,9].

Previous studies have been conducted on the lateral performance of single and coupled CLT walls with traditional CLT connections, concentrating on wall-to-floor and wall-to-foundation connections. Discoveries from these studies indicated that walls with suitable height-to-length ratios (not less than 2) demonstrate re-centring capabilities post a significant lateral load event, remaining predominantly elastic and heavily influenced by the connection behaviour [6,7].

However, while offering energy dissipation and ductility, these traditional connection systems are limited [9]. Consequently, building design codes in Canada recommend their use under assumptions of low to zero ductility and modification factors[6,10]. This necessitates an elastic design approach, leading to high shear forces at the base and upper story levels, potentially resulting in uneconomical designs, especially in high seismic regions[11].

A study by Izzi et al. (2018) on multi-story structures using the platform framing system revealed significant flexibility and drift due to the slip of CLT panels at floor levels. In response, researchers started investigating unbonded post-tensioning for CLT shear wall panel-to-foundation connections, drawing inspiration from the PRESSS (PREcast Seismic Structural System) program for concrete structures[13]. In this system, the CLT shear wall is tied to the foundation, utilising an unbonded post-tensioning strand (see Fig. 4-1). This system utilises post-tensioning strands to link the CLT shear wall to the foundation. The wall panel starts rocking when a lateral force is applied to its corner. This causes the post-tension strands to get longer and helps the system return to its centre position after removing the load [14,15].

With developments in timber construction techniques, the Unbounded Post-tensioned Cross-laminated timber (UPTC) shear wall system has appeared as an encouraging solution to increase the ductility of CLT shear walls. This technique offers several advantages, including increased seismic resilience and improved lateral load resistance. CLT shear walls employing this system are tied to the foundation using unbonded post-tensioning strands, as shown in Fig. 4-1.
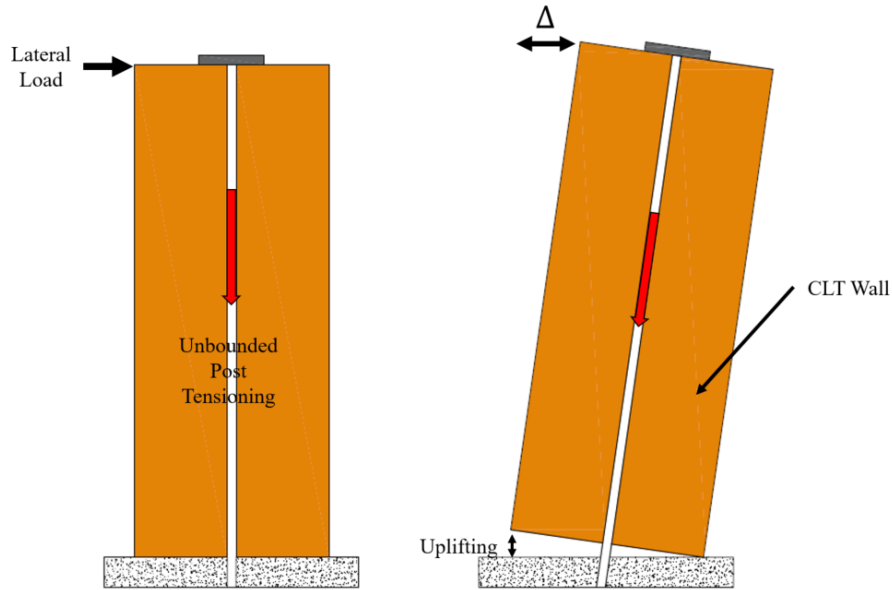
Fig. 4-1 UPTC Shear Wall

The main objective of this study is to investigate the lateral performance of the UPTC balloon-frame shear wall system. It evaluates critical parameters influencing the system, such as shear wall thickness, aspect ratios, post-tension stress and diameter, and unbounded post-tensioned CLT balloon's initial lateral stiffness effect employing traditional sensitivity analysis techniques. The following section discusses a range of Machine Learning (ML) algorithms, including XGBoost, decision trees, gradient-boosted decision trees, random forest, and Catboost, which were implemented in this study.

While numerous studies have utilised ML models to investigate complex matters, only a few have examined how different features or input variables influence the outcomes of these models [16–19]. A significant criticism of ML methods in structural engineering is their "black box" nature, which obscures the understanding of how input features affect outputs, a key aspect for model improvement and reliable decision-making. To address this, SHapley Additive exPlanations (SHAP) were employed in this study. SHAP uses game theory to assess how each feature contributes to a model's overall prediction and for individual samples. This research aimed to create a machine learning (ML) model and identify the critical parameters affecting lateral and vertical stiffness via SHAP analysis.

4.3 Machine Learning

Developments in the field of ML offer a unique benefit in comprehending complex relationships and relationships within the data generated by structural systems, leading to a conspicuous growth in research within the domain [20–22]. This surge in employing ML for research investigations is attributed to several factors, including conventional engineering practices relying heavily on limit criteria-based design and employing deterministic closed-form predictive equations, provided these established models often exhibit substantial variability and inherent biases from the modelling inaccuracies and oversimplifications. Limited access to meticulously curated experimental data and datasets stemming from high-fidelity numerical simulations provides an abundant and invaluable resource for research and analysis in structural and timber engineering. Additionally, the significant progress observed in ML algorithms is partly reinforced by improved computational capabilities and an increasing demand for their application in non-engineering contexts. This expanding demand has consequently driven the adoption of ML techniques in structural and timber engineering research [23]

While previous studies have employed ML models to explore complex problems, only a limited number of studies have delved into the impact of input features on the outcomes predicted by ML models [16,17,19]. An often-cited downside to applying ML in structural engineering is that it's a "black box" nature and needs transparency and comprehension from mechanics-based or empirical regression models [23]. Therefore, it's crucial to understand the cause-and-effect relationships and sensitivities to quantify uncertainties, guide future experiments or model enhancements, and make informed decisions about model deployment. Feature importance, as typically employed, offers a general understanding of how features influence model predictions; nevertheless, it falls short in quantifying individual feature effects on outputs.

4.4 Predictive Model Based on XGBoost, Decision Trees, Gradient Boosted Decision Trees, Random Forest, and Catboost

In Artificial Intelligence (AI) based modelling, a meticulously compiled database is employed to aid in the training of a predictive model using algorithms from the supervised family of ML. This procedure, secured in the principles of supervised learning, involves applying algorithms programmed to learn from a dataset where the correct outputs are already known. The ML model

can establish patterns through this method, thereby equipping it with the capability of predictions employing novel data that has not been encountered previously. The competence of this approach is conditional upon the quality and comprehensiveness of the database used, as it forms the foundation upon which the learning algorithm constructs its predictive understanding. Among the algorithms encompassed within this category, specific attention is directed towards eXtreme gradient boosting, random forest, catboost, gradient boosting decision tree, and decision Trees, with an emphasis on their theoretical foundations [24–26].

eXtreme gradient boosting (XGboost): A notable ensemble learning algorithm, XGBoost is identified for its proficiency in integrating predictions generated by multiple decision trees (XGBoost). Its theoretical keystone centres on gradient boosting, involving the iterative addition of decision trees to minimise the loss function. Remarkably, XGBoost differentiates itself by integrating regularisation techniques and parallel processing capabilities, rendering it resilient against overfitting and exceptionally swift handling of extensive datasets. Real-world applications highlight its efficacy, as evidenced by using XGBoost to construct a dependable machine-learning model for estimating the load-carrying capacity of timber joints under harsh environmental conditions [24]. Similarly, it has been deployed to develop an ML-based fire risk assessment system for historic timber structures, surpassing alternative models and enhancing fire safety inspections at the Palace Museum of China [25].

Random Forest (RF): Another ensemble method, RF, involves the building of multiple decision trees during the training phase, drawing from the theory of capturing to mitigate variance by averaging predictions from recurrent independent trees. Each tree in RF is trained on a random subset of the data, accompanied by a random subset of features, thus mitigating overfitting and balancing bias and variance [27].

CatBoost: CatBoost is a significant addition to the ensemble learning algorithms. It's designed to work with categorical features and boasts gradient boosting, similar to XGBoost and gradient boosting decision tree. Its theory revolves around minimising loss function through gradient descent. Several applications have proven the algorithm [28,29].

Gradient Boosting Decision Tree (GBDT): GBDT, another ensemble method, builds a decision tree and focuses on reducing the loss function using gradient descent. Within the sequence of trees,

each one corrects what its predecessor did wrong. It can easily capture complex relationships within the data, but it requires careful parameter tuning to avoid overfitting.

Decision Trees (DT): Decision trees are critical to the ensemble above methods. They generate a hierarchical structure like a flowchart by recursively splitting data based on informative features. The theoretical basis of decision trees revolves around concepts such as information gain or Gini impurity, which determine the optimal feature for data partitioning at each node [26]. This approach facilitates effective quality control and grading, ultimately reducing variations in mechanical properties for mass timber structures. In summary, XGBoost, RF, CatBoost, GBDT, and DT constitute distinct ML algorithms grounded in unique theoretical principles.

4.4.1 Shapley Additive Explanations (SHAP)

SHAP, a game-theory-based approach recently developed(Lundberg et al., 2018; Lundberg & Lee, 2017), investigates ML models based on the additional feature attribute method. This process defines the input model as the linear addition of input variables, assuming that the input variable of the model is x. For the original model f(x), the interpretation model g(x') of the simplified input x' is expressed as Equation 1.

$$f(x) = g(x') = \emptyset_0 + \sum_{i=1}^{5} \emptyset_i x_i^i \qquad \text{Equation 1}$$

Where x is connected to x' through a mapping function, $x = h_x(x')$, and ϕ_0 maintains a constant value when all inputs are absent. The function h_x signifies the mapping that links x to x'. By adhering to three essential properties, including local accuracy, missingness, and consistency, the solution to Equation 2 can be expressed as follows:

$$\emptyset_i(f, x) = \sum_{z' \subseteq x'} \frac{|z'|! \, (M - |z'| - 1)!}{M!} [f_x(z') - f_x(z'\backslash i)] \qquad \text{Equation 2}$$

Where |z'| denotes the count of non-zero entries in z', and z' is a subset of x', $f_x(z') = f(h_x(z')) = E[f(z) | z_S]$, with S representing the set of non-zero indices in z', known as SHAP values[32]. SHAP can determine whether an input variable positively or negatively influences each prediction. For a

more comprehensive explanation of SHAP in structural engineering, interested readers are referred to the references [19,33].

Subsequent sections conduct a sensitivity study to distinguish the significance of factors influencing the initial lateral stiffness. This is followed by developing various ML models for predicting initial lateral and vertical stiffness and identifying the critical factors influencing UPTC's lateral and vertical stiffness.

4.5 Methodology

4.5.1 Finite Element (FE) Model Creation and Validation

The lateral response of UPTC shear wall under diverse geometric and loading conditions was evaluated, considering the experiment conducted by Hossain et al. (2019). The author reproduces the experimental setup (Fig. 4-2) of the tested UPTC, where the pivotal mechanism for recentering a UPTC shear wall structure after being subjected to lateral loads relies on unbounded post-tensioning stands. These stands were threaded through predrilled holes running along the length of the CLT wall, firmly anchored at the upper extremity of the wall, and affixed to a foundation. Grade 270 (ultimate strength of post-tension strands =1862 MPa) low-relaxation 7-wire post-tensioning strands were selected for deployment in the experimental phase. These strands have a yield strength of 1675.9 MPa and a substantial modulus of elasticity amounting to 196.6 GPa. The current research used finite element modelling to reproduce the geometry of the tested UPTC wall.

The experiment was initially remodelled using commercially available software Abaqus CAE and validated by choosing a three-layer UPTC shear wall measuring 0.61m x 2.44m x 0.10m. The shear wall incorporates a post-tensioned strand with a diameter of 15mm and features a strand force ratio of 0.48 [34]. The accuracy of the FE model was ensured by comparing the results of finite element analysis with empirical data obtained from experimental tests. The elastic properties of the elements in the finite element model are detailed in TABLE 4-1 [35].

TABLE 4-1 Elastic Properties of Elements

Element	Properties	Value
CLT	E_T / E_L	0.038

	E_R / E_L	0.078
	μ_{LT}	0.344
	μ_{RT}	0.410
	μ_{TR}	0.344
	G_{LR} / E_L	0.052
	G_{LT} / E_L	0.048
	G_{RT} / E_L	0.005
	E_L (MPa)	8500
Post Tension Strands	Density (kg/m^3)	7849.13
	E (MPa)	196,500.66
	Poisson's Ratio	0.27
Anchor Element	Density (kg/m^3)	7849.13
	E(MPa)	59,954.43
	Poisson's Ratio	0.27
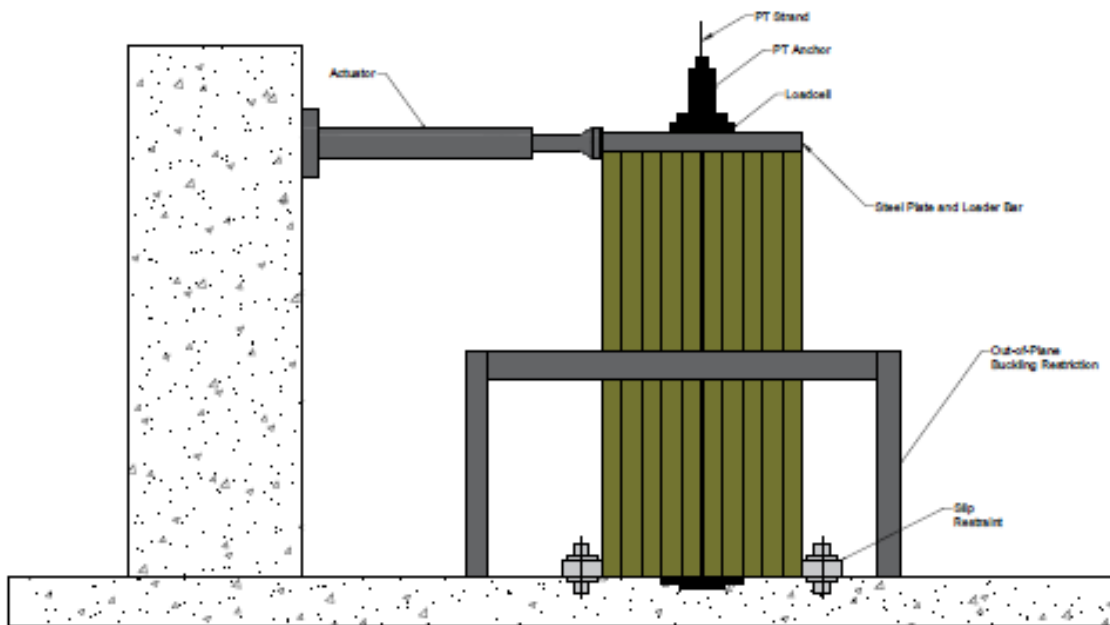
Fig. 4-2 Experimental Setup Performed on UPTC Shear Wall (Hossain et al., 2019)

Contact interaction properties between surfaces of adjacent timber panels in the same layer were defined using both tangential and normal behaviour. A friction coefficient of 0.3 was introduced to replicate these interactions accurately, playing a vital role in modeling the frictional forces governing how these wood surfaces engage with each other and with post-tension strands[35]. This coefficient effectively captured the sliding or gripping behaviour in the tangential direction and the compressive or tensile interactions in the normal direction.

Hard contact was used to capture the pressure-overclosure behaviour. Surface-to-surface tie constraints were used for simulating a bonded connection between adjacent layers and ensured that the nodes at corresponding locations in adjacent layers were wholly tied together in all six degrees of freedom, allowing the layer to deform as a single structural entity. Steel bearing plates were strategically placed in loading and boundary regions to help distribute loads uniformly, mitigate stress concentration, and promote convergence in analysis for improved stability. Post-tensioning strands represented by one-dimensional wire geometry were discretised into B33 beam elements segmented along their length with the two-node cubic beam. Multi-point constraints were employed at the top ends of strands to connect them to nodes at the bottom of steel anchor plates on top of the wall. "Predefined field" functionality offered within Abaqus CAE was used for post-

tensioning stress application to achieve precise control over stress applied along the length of strand geometry.

Fig. 4-3 visually depicts the deviation between the experimental and Finite Element Model load-displacement curves, with a deviation of 6% between the two curves attributable to geometric simplification and boundary conditions. Fig. 4-4 provides insights into the stress distribution within the model, further enhancing the understanding of the UPTC wall's structural behaviour under stress. Higher stress concentrations were noticed at the overturning point and around the post-tension anchor area.
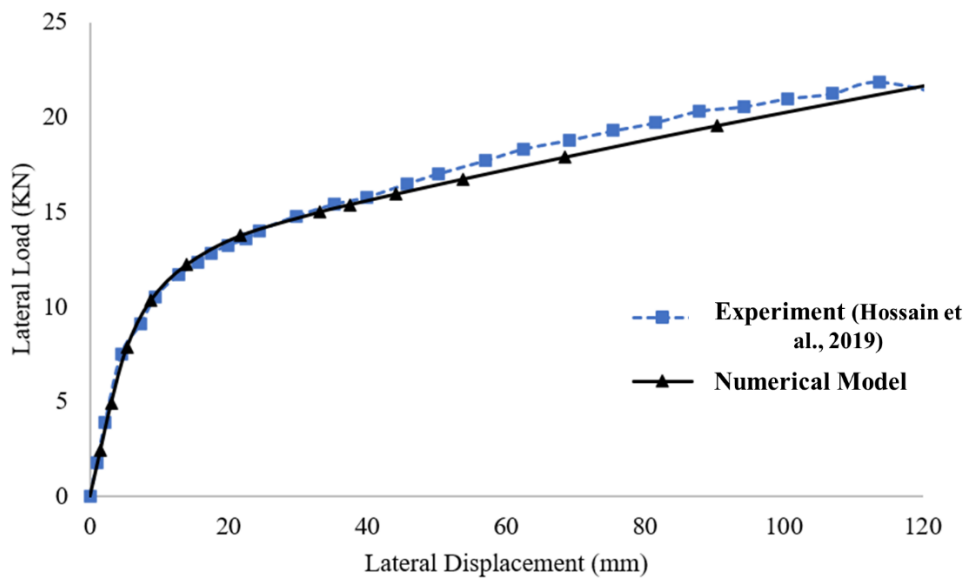
Fig. 4-3 Experimental and Numerical Model Comparison

S, Mises
(Avg: 75%)
```
   +2.239e+05
   +7.000e+03
   +6.417e+03
   +5.833e+03
   +5.250e+03
   +4.667e+03
   +4.083e+03
   +3.500e+03
   +2.917e+03
   +2.334e+03
   +1.750e+03
   +1.167e+03
   +5.836e+02
   +2.611e-01
```

(a)   (b)
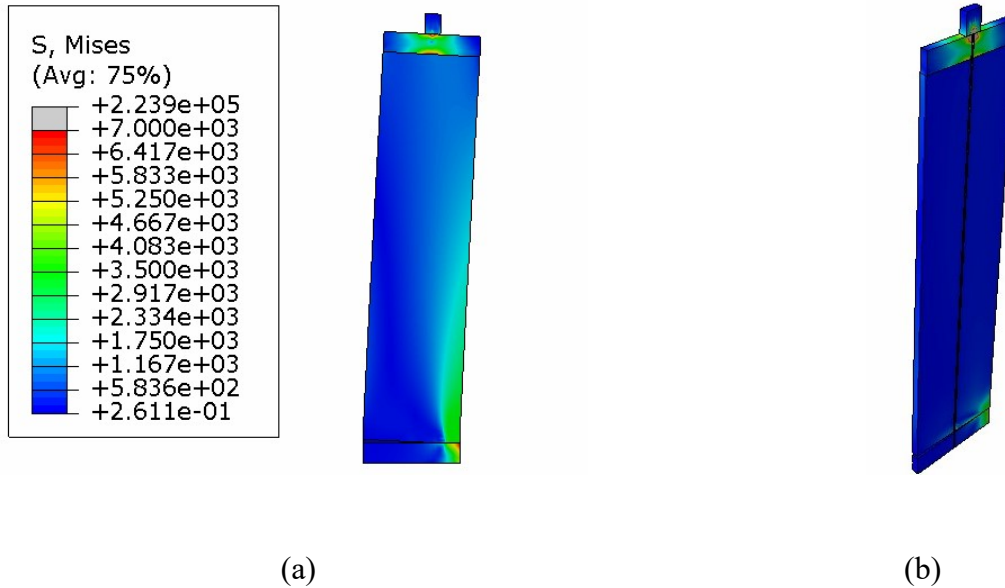
Fig. 4-4 Stress Distribution and Deflections (A) Side View (B) Cross Section

4.6 Assessment of Critical Parameters on Lateral Performance of UPTC Wall System

The parametric study provides insights that can aid in optimising design configurations, improving structural integrity, and promoting sustainable construction practices. A detailed investigation explored the impact of various crucial parameters on the lateral performance of the UPTC shear wall system. Numerical simulations were performed employing the methodology explained earlier, focusing on four key aspects: the influence of panel thickness, the effect of aspect ratio (UPTC wall Height/Width), sensitivity to post-tension stress, and diameter. Fig. 4-5 provides the schematic of the studied parameters.
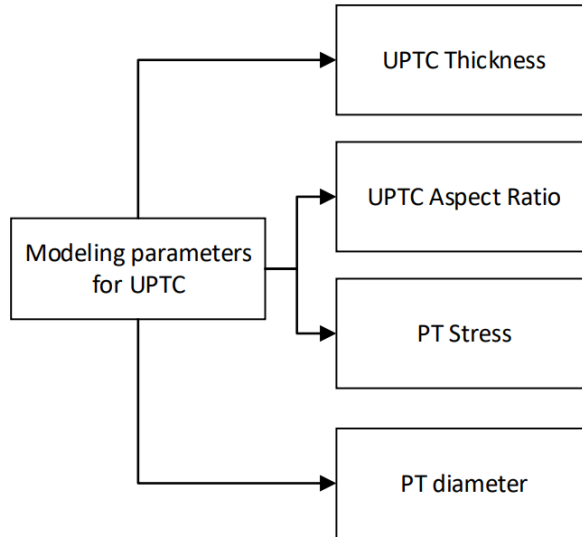
Fig. 4-5 Framework of Parametric Study

4.6.1 Effect of Thickness

The validated FE model was modified by changing the thickness to represent different configurations while maintaining constant UPTC shear wall aspect ratios, stand diameters, and post-tensioning stress levels to investigate the influence of UPTC shear thickness on the lateral performance of UPTC shear walls. Each 3-ply (99.06 mm), 5-ply (165.1 mm), and 7-ply (199.8mm) models were developed to investigate the effect of diverse thicknesses on the lateral resistance of the wall assemblies. This section modelled the UPTC walls using specific dimensions and conditions. The width of the walls was kept consistent at 3 meters while the height was set at 6 meters. A uniform stand diameter of 15 mm was used, and a post-tensioning stress of 770 MPa was applied to the stands.

Fig. 4-6(a) presents the initial stiffness values for the three distinct UPTC wall models with variable thicknesses. At the same time, Fig. 4-6(b) graphically depicts the pivotal relationship between lateral force and lateral displacement, capturing the essence of their interaction.
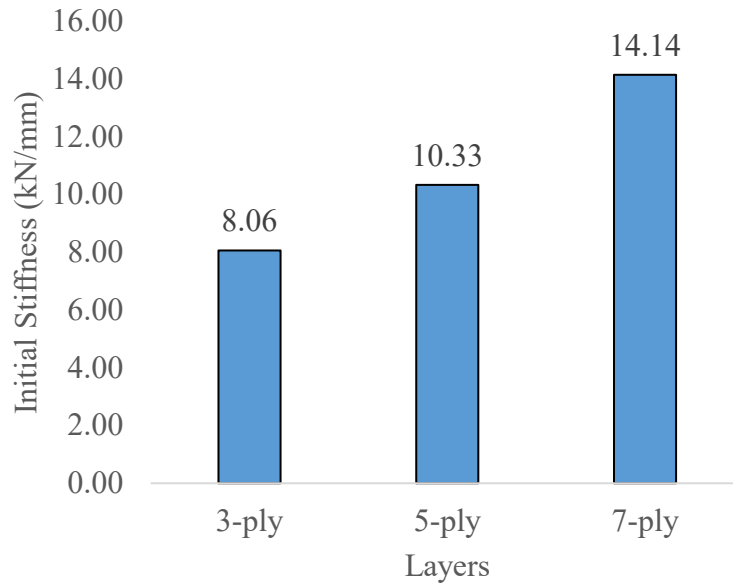
(a)
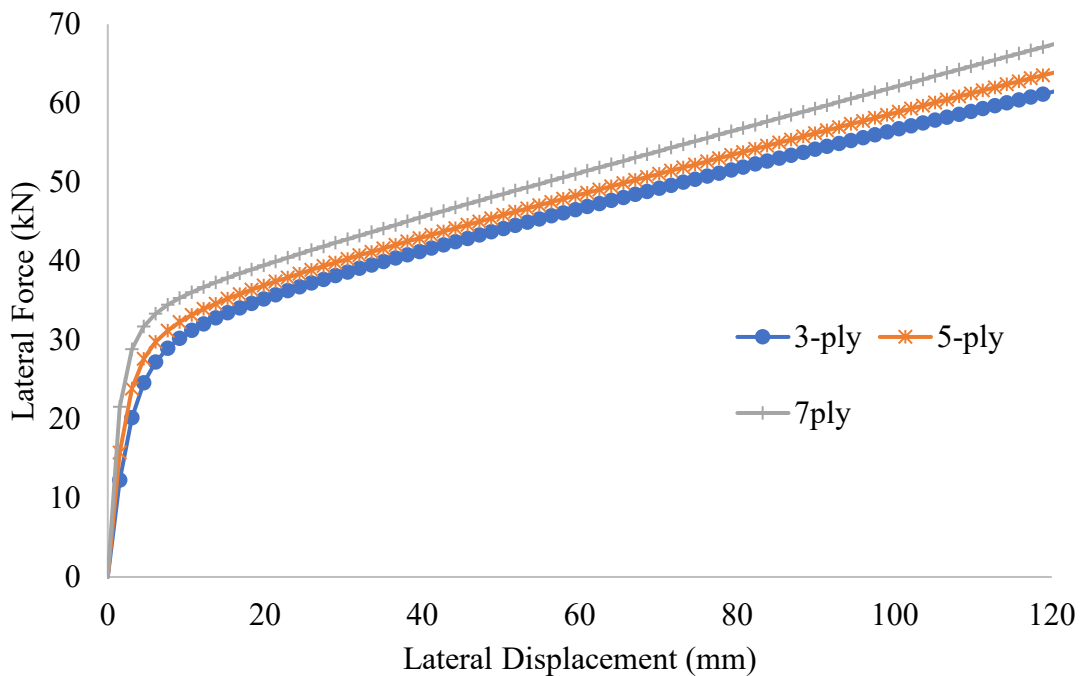
(b)

Fig. 4-6 (a) Thickness vs. Initial Stiffness (kN/mm) ; (b) Lateral Force (kN) vs. Lateral Displacement (mm) for Three Different Thicknesses of UPTC System

The impact of varying thicknesses on the UPTC wall is evident from these figures. For instance, an increase of 28% in initial stiffness is noted when a 5-ply UPTC wall is used, compared to a 3-

ply wall. Meanwhile, with a 7-ply wall, there is an indicated 75% increase in initial stiffness compared to a 3-ply wall. The substantial improvement in initial stiffness in thicker sections is attributed to their enhanced ability to resist deformations caused by lateral loads. Hence, increasing the thickness of UPTC shear walls significantly enhances their lateral performance. Specifically, transitioning from 3-ply to 7-ply wall configurations results in a 75% increase in initial stiffness, underscoring the critical role of panel thickness in optimising wall resistance to lateral forces.

4.6.2 Effect of Aspect Ratio

Each model was remodelled to investigate the influence of aspect ratio on lateral stiffness. Three different thicknesses, 3-ply, 5-ply, and 7-ply were paired with two different wall widths and heights. The widths were 3 meters and 2 meters, and the heights were 6 meters and 7 meters. These models also maintained a consistent prestress level of 775 MPa during analysis.

The initial stiffness values for the walls with variable thicknesses and aspect ratios are illustrated in Fig. 4-7. While Fig. 4-8 illustrates the lateral force and displacement graphs, revealing that the changes in the aspect ratio result in noticeable alterations in the initial stiffness of the UPTC wall models. As such, increases in the aspect ratio from 2 to 3 lead to an average reduction of 56% across all thicknesses. This dynamic relationship emphasises the interaction between aspect ratios and structural rigidity, offering valuable insights that can significantly contribute to the design and engineering practices of UPTC shear walls, ultimately achieving the highest performance standards.
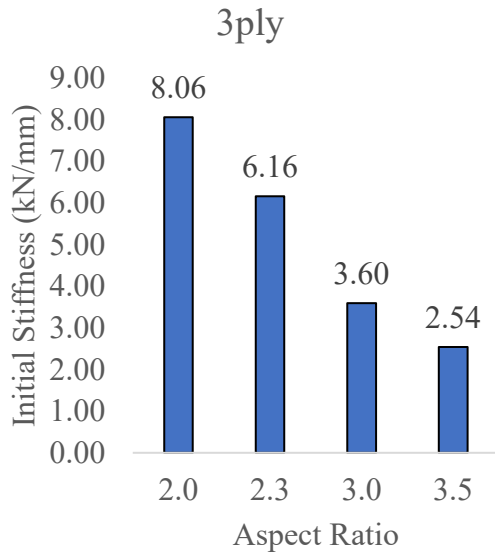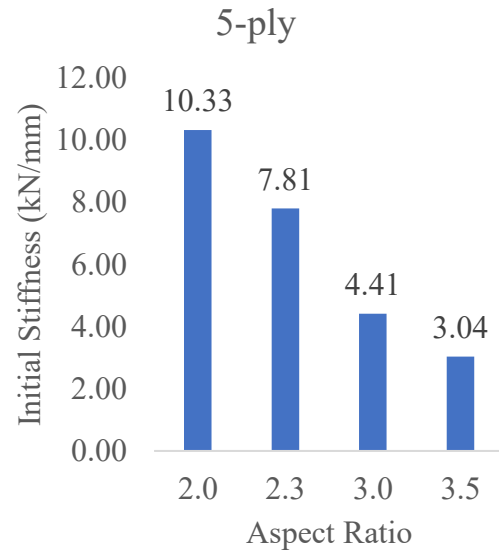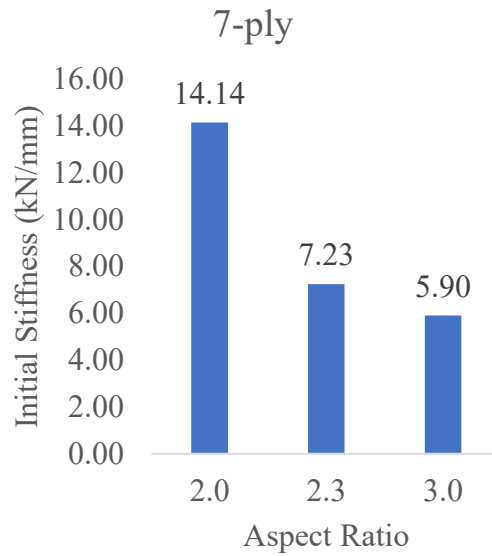
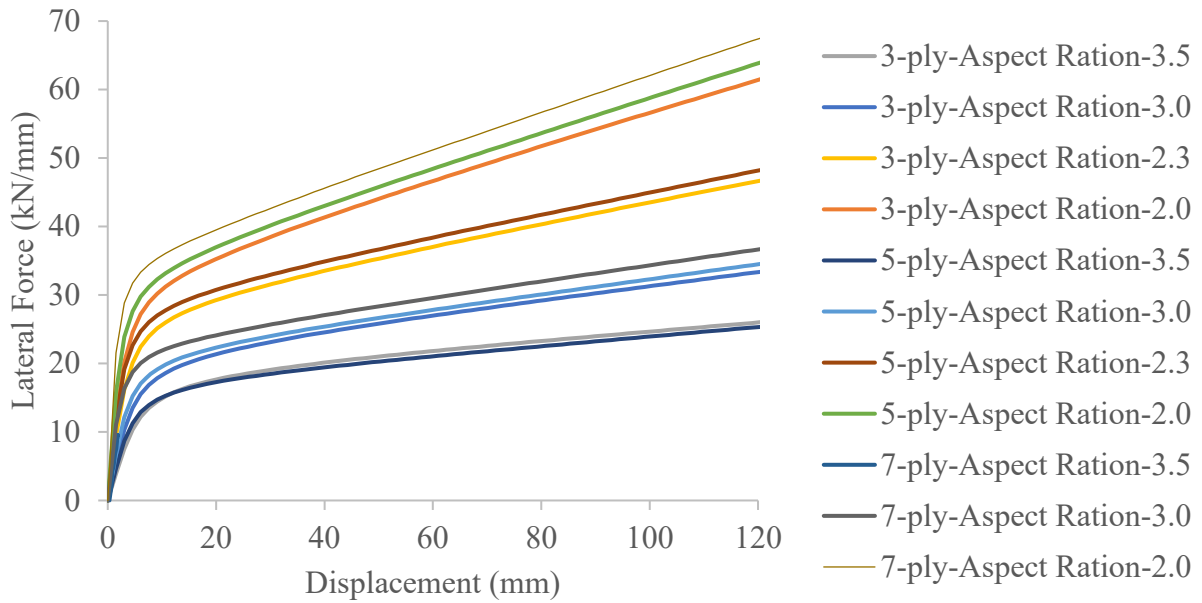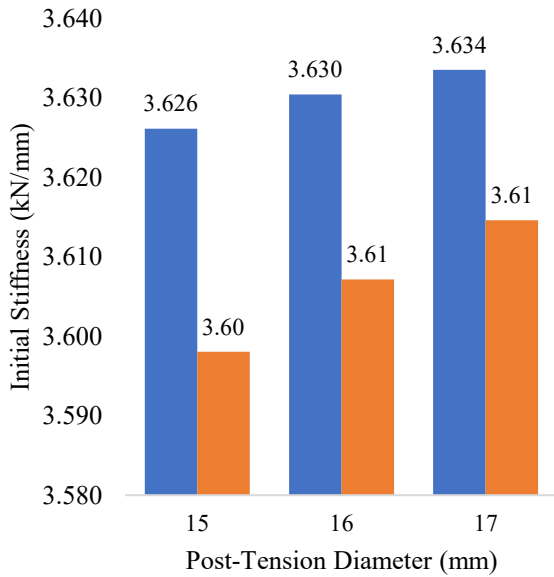Fig. 4-7 Initial Stiffness vs. Aspect Ratio (a) 3-ply (b) 5-ply (c)7-ply

Fig. 4-8 Lateral Force (kN) vs. Lateral Displacement (mm) for Three Different Aspect Ratios of UPTC System

4.6.3 Effect of Post-Tension Stress and Diameter on the Lateral Performance of UPTC Shear Wall

The validated FE models were modified to include post-tension cables with 15mm, 16mm, and 17 mm diameters and post-tension varying from 770 MPa to 1160 MPa to investigate the influence of post-tension stress and diameters on the lateral stiffness of the UPTC Wall. The method was consistent with the previous models used in the study. Fig. 4-9 presents initial stiffness values for walls that experience post-tension stress and post-tension diameter changes while Fig. 4-10 represents the lateral force and displacement graphs.

The analysis indicates that for 3-ply configurations, increasing the strand diameter from 15mm to 17mm results in a minimal initial stiffness increase of 0.12%. Further, the post-tension stress at 780 MPa experiences a marginal rise of 0.46% across this diameter range. Meanwhile, 5-ply configurations exhibit a slight decrease in stiffness with increasing diameter, down by 0.30% at 773 MPa and 0.17% at 1150 MPa, suggesting a stable structural response. Yet the 7-ply configurations present a more considerable change, with stiffness escalating by 4.23% at 770 MPa and by 0.85% at 1145 MPa when the diameter is increased from 15mm to 17 mm, indicating a

greater sensitivity to diameter in higher-ply configurations. Hence, for all the CLT configurations, initial stress is increased with higher post-tension diameters and post-tension stresses, and the increment is higher with more layers in the UPTC shear wall.
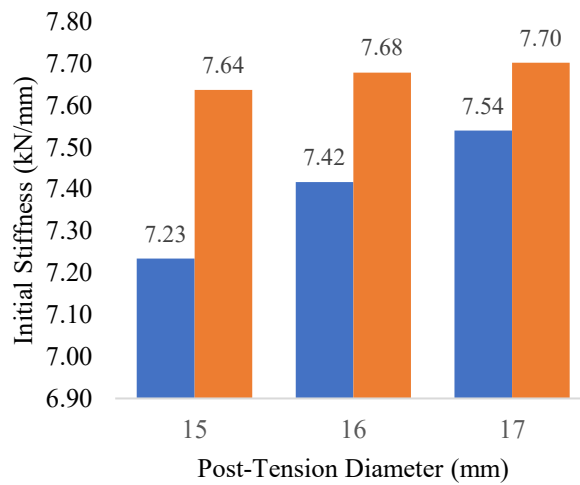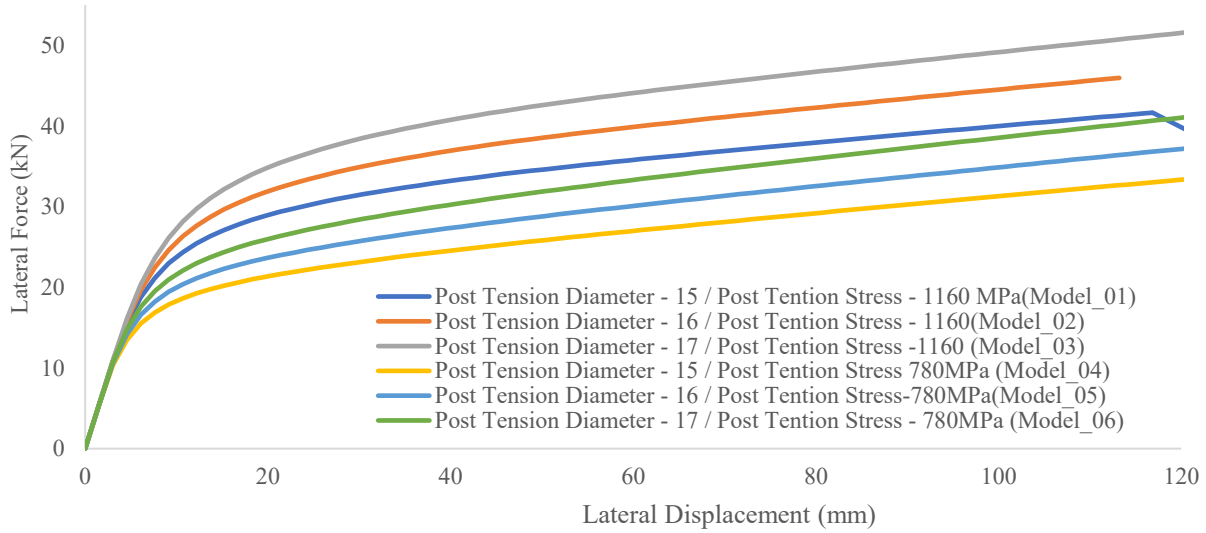

(a)

(b)

(c)
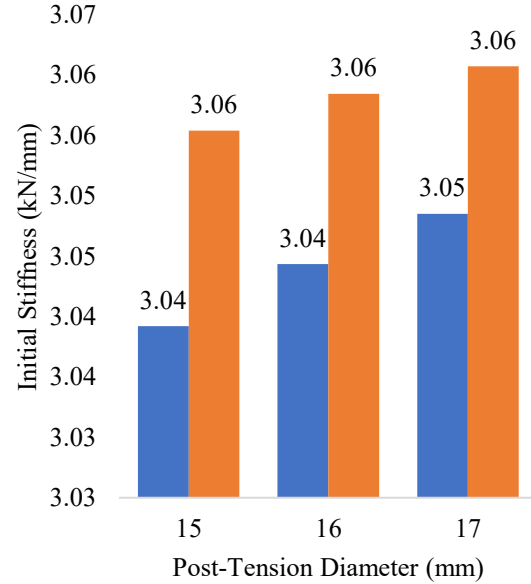
Fig. 4-10 Lateral Force (kN) vs. Lateral Displacement (mm) for Three Different Post Tension
Stresses and Post Tension Diameters of the UPTC System

4.7 Initial Lateral and Vertical Stiffness of UPTC Wall System Employing Informational Models

The study introduced Equation 3, as initial vertical stiffness is integral to structural engineering and aids in measuring the system's immediate response under lateral load. Due to the lateral force, there is a vertical uplift, and from the equation, the authors analysed the uplift behaviour of this structure. It is worth emphasising that this equation assumes its applicability under linear elastic behaviour, considering the material's response within the elastic limit to prevent permanent deformation. Additionally, the structure's performance under various loading conditions requires computing initial lateral stiffness (Equation 4) as one of the critical parameters for assessing the UPTC's performance, providing insights into how the structure responds to lateral forces and ensuring safety and reliability in building design and construction. The vertical displacements and lateral displacements that occurred due to the lateral force are illustrated in Fig. 4-11.

$$\text{Initial Vertical Stiffnss(IVS)} = \frac{\text{Lateral Force}(F_l)}{\text{Vertical Displacement }(D_v)} \qquad \text{Equation 3}$$

$$\text{Initial Lateral Stiffness(ILS)} = \frac{\text{Lateral Force}(F_l)}{\text{Lateral Displacement }(D_l)} \qquad \text{Equation 4}$$
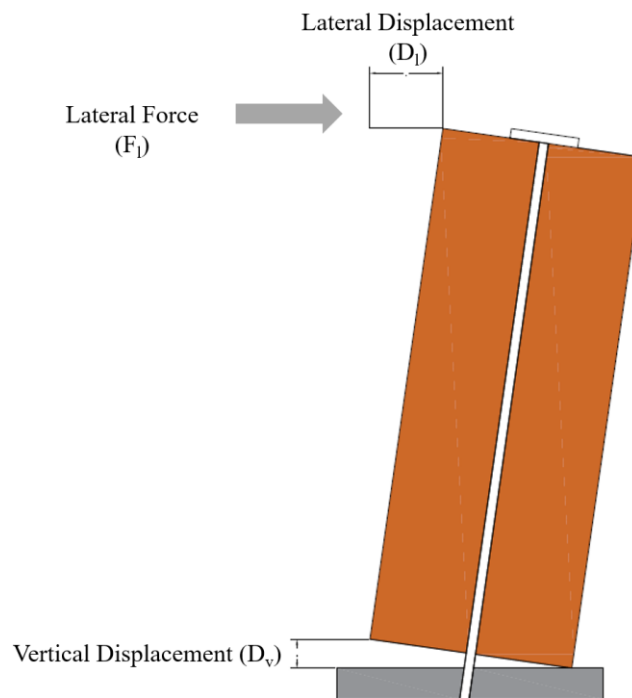

Fig. 4-11 Diagrammatic Representation of a UPTC Shear Wall Under Lateral Loading: ILS and IVS

Further, this study develops an ML model for predicting ILS and initial IVS to establish a quantifiable relationship between the model's predictions and the input variables. The SHAP method ensures the interpretability of the model's decision-making process.

4.8 Establishing a Stiffness Database for the UPTC wall system

A comprehensive finite element model database validated through an experimental program was created to develop a precise stiffness model for the UPTC wall system. The data set comprising 128 distinct models, each utilising a unique set of input variables, underwent simulation to determine each model's ILS and Initial IVS. The input variables for these models cover a range of critical factors, including Shear Wall Height (H_{sw}), Shear Wall Width (W_{sw}), Shear Wall Thickness

(T$_{sw}$), Post-Tension Stress (PT$_s$), Post-Tension Diameter (PT$_d$), and Friction Coefficient (FC) collectively defining the characteristics and properties of the UPTC shear wall. For a more comprehensive understanding of the input variables, TABLE 4-2 provides descriptions and statistical attributes, whereas Fig. 4-12 shows the statistical distributions of input variables.

The data is randomly divided into two subsets, following the conventional practice of a 70%–30% split to serve the training and testing phases of the modelling. The ML model is trained on the training set (70%) and then assessed on the testing set (30%) to evaluate its predictive accuracy.

TABLE 4-2 Statistic Distribution of the Database

| Variable	Units	Minimum	Maximum	Mean	Standard Deviation	Type
Shear wall height (H$_{sw}$)	mm	6000.00	7000.00	6492.19	501.90	Input
Shear wall width (W$_{sw}$)	mm	2000.00	3000.00	2375.00	486.03	Input
Shear wall thickness (T$_{sw}$)	mm	99.06	231.14	154.78	53.35	Input
Post-tension Stress (PT$_s$)	MPa	767.50	1162.73	956.27	189.64	Input
Post-tension Diameter (PT$_d$)	mm	15.00	17.00	15.97	0.82	Input
Friction Coefficient (FC)	no units	0.30	0.50	0.40	0.08	Input
Initial Vertical Stiffness (IVS)	kN/m	12439.54	2757761.46	155236.66	402960.19	Output
Initial Lateral Stiffness (IVS)	kN/m	2212.86	17242.06	5972.03	3388.78	Output
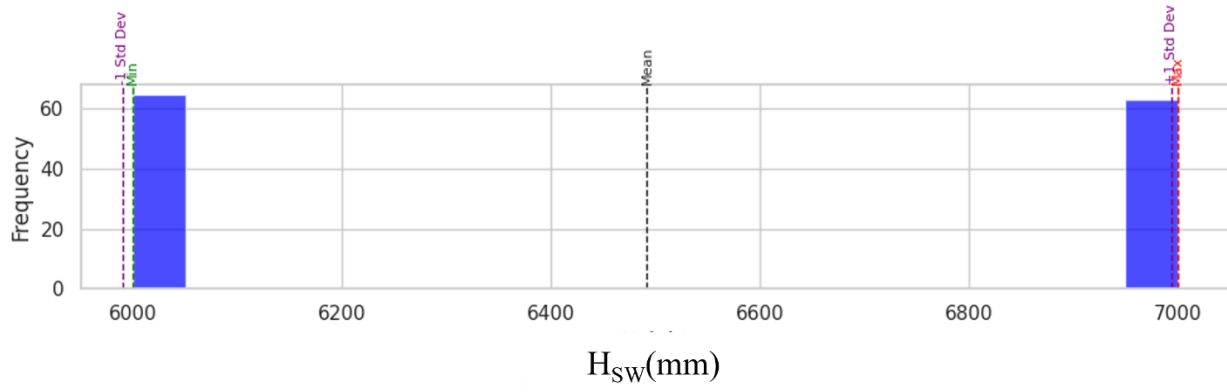
(a)
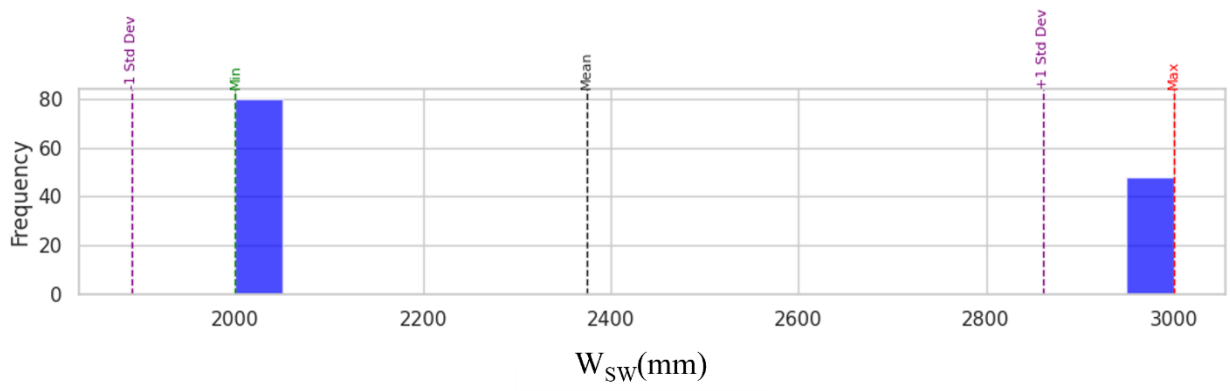
(b)
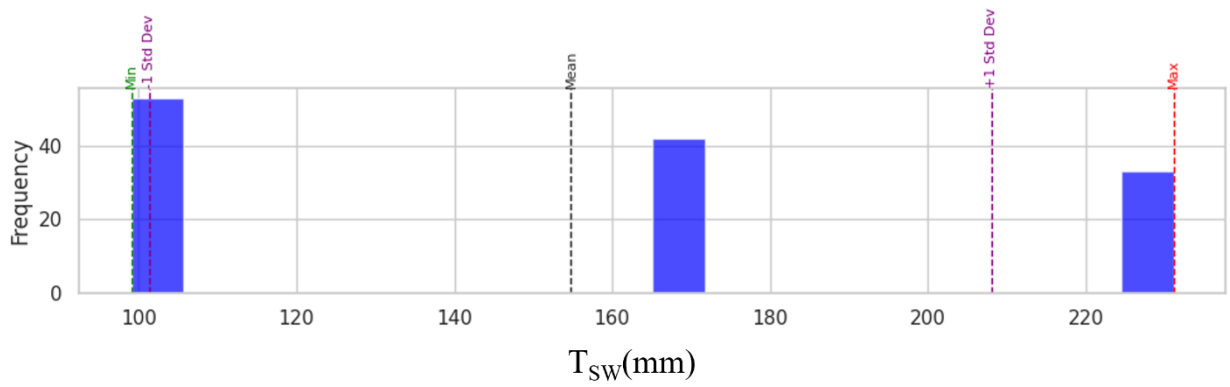
(c)
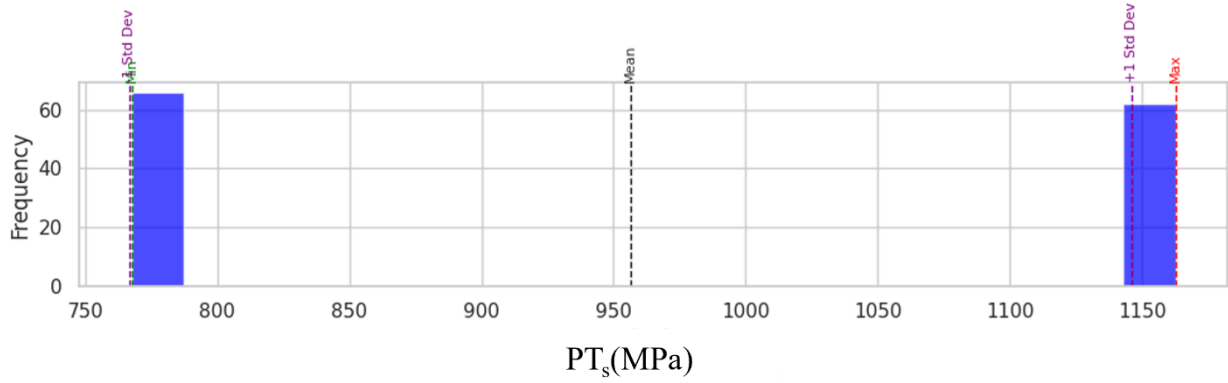
(d)
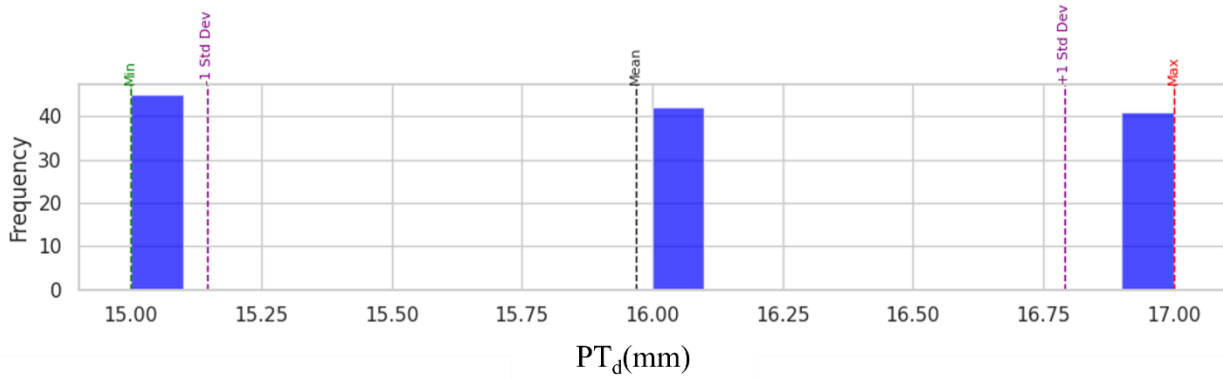
(e)
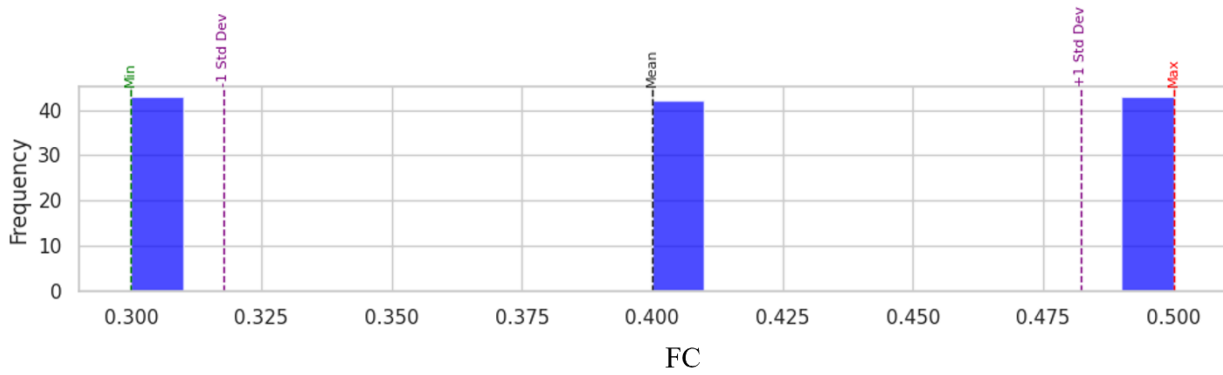
(f)

Fig. 4-12 Frequency Distribution of the Database: (a) Shear Wall Height (Hsw); (b) Shear Wall Width (Wsw); (c) Shear Wall Thickness (Tsw); (d) Post-Tension Stress (PTs); (e) Post-Tension Diameter (PTd); (f) Friction Coefficient (FC)

4.9 Prediction Performance of Various Analysed ML-Based Models

Various ML-based algorithms, including XGBoost, DT, GBDT, RF, and CatBoost, were implemented on the established database to assess their performance for estimating the ILS and IVS of UPTC wall systems. These algorithms were meticulously adjusted through hyperparameter optimisation employing grid search and a 10-fold cross-validation procedure during model training [23]. The resulting hyperparameters are illustrated in TABLE 4-3

TABLE 4-3 Algorithm Settings for Different ML Models

Model	Hyper Parameters	Optimised Values for ILS	Optimised Values for IVS
XGBoost	Number of trees	200	400
	Learning rate	0.3	0.1
	Maximum depth of the trees	6	6
RF	Number of trees	200	500
	Maximum tree depth	20	None
	Minimum samples per leaf	1	1
	Minimum samples to split	2	2
GBDT	Number of trees	500	200
	Learning rate	0.3	0.3
	Maximum depth of trees	3	6
DT	Maximum depth of the decision tree.	None	None
	Min Samples to Split	2	5
	Min Samples in Leaf	1	1
CatBoost	Iterations	660	761
	Maximum depth of trees	4	6
	Learning rate	0.13	0.22
	L2 Leaf Reg	6.24	1.56

The assessment of these algorithms was compared based on four performance metrics, including R-squared, which elucidates the models' ability to explain the variance in the data, with values

approaching 1 indicating a solid fit. RMSE (Root Mean Square Error) measures the average disparity between predicted and actual values, favouring smaller values for enhanced accuracy. MAE (Mean Absolute Error) offers an alternative perspective on prediction accuracy by calculating the average absolute difference. Lastly, MAPE (Mean Absolute Percentage Error) scrutinises the average percentage disparity, with reduced MAPE values signifying a more precise model. The results of these performance metrics of five ML-based algorithms for predicting IVS and ILS are included in TABLE 4-4.

TABLE 4-4 Comparison of Model Results for Different ML Models

| Model | | ILS | | | | IVS | | |
	R² (ILS)	RMSE (ILS)	MAE (ILS)	MAPE (ILS)	R² (IVS)	RMSE (IVS)	MAE (IVS)	MAPE (IVS)
XGBoost	0.9997	52.8	38.0	0.9%	0.8819	24907	15823	24%
CatBoost	0.9993	69.5	51.9	1.2%	0.8070	36595	26108	40%
GBDT	0.9998	27.3	19.4	0.4%	0.8824	35675	20935	22%
DT	0.9996	52.4	35.8	0.6%	0.7154	44437	24013	28%
RF	0.9970	169.9	103.5	2.0%	0.74	37047	24996	42.3%

Further, the ML-based predictive models are assessed by generating prediction-to-test ratios for all the samples in the testing dataset. This provides a comparative understanding of these models while predicting ILS and IVS. Fig. 4-13 Predict-to-Test Ratios: (a) XGBoost Model; (b) Random Forest Model; (c) GBDT Model; (d) Decision Tree Model; (e) CATBooster Model

TABLE 4-5 Prediction Performance for ML Models

 illustrates the predict-test ratios for each ML model for IVS and ILS, while Table 5 provides a detailed summary of the associated statistics measures.

XGBoost established a remarkable predictive precision rating for both IVS and ILS, as validated by its high R² values of 0.9997 for ILS and 0.8819 for IVS. This ML model establishes accuracy across a wide range of initial stiffness values, as indicated by the lowest RMSE (52.8 for ILS and 24907 for IVS) and MAE (38.0 for ILS), signifying its ability to produce consistent and reliable predictions that closely associate with actual observations. The slight deviation from the valid

values, denoted by the low MAPE (0.9% for ILS), underscores XGBoost's capacity to capture the intricacies of stiffness in diverse situations accurately. While presenting commendable predictive strength, CatBoost exhibits a slightly broader range in its predictions, especially for IVS, with a higher MAPE of 40%, suggesting that CatBoost may offer unique insights in certain scenarios where its prediction pattern aligns with specific structural characteristics. However, it may not consistently match the precision of XGBoost. The DT model displays more concentrated predictive behaviour, with a relatively lower R^2 of 0.9996 for ILS and 0.7154 for IVS, indicating a more focused yet slightly less accurate prediction range than XGBoost. It seems to be a reliable model but doesn't capture the variability as effectively as XGBoost. The GBDT nearly parallels the performance of XGBoost, especially in ILS predictions, with an outstanding R^2 of 0.9998, the highest among all models. This similarity suggests that GBDT shares a closely aligned predictive approach with XGBoost, highlighting its capability to model structural stiffness accurately. On the other hand, Random Forest showcases a broader range of predictions with substantial accuracy, as reflected by its R^2 values (0.9970 for ILS and 0.74 for IVS). Despite not reaching the accuracy of XGBoost, it validates consistent reliability within its predictive range, making it a valuable model for scenarios where a balance between prediction diversity and accuracy is desired.

Fig. 4-13 illustrate predicted-to-test ratios for each model. XGBoost notices itself with remarkable accuracy, especially in predicting ILS. It demonstrates a commendable consistency in IVS predictions, evident from a relatively narrow range (0.34 to 1.96), centring around a mean of 1.01 with a moderate spread indicated by a standard deviation of 0.28. This precision escalates notably in ILS predictions, where XGBoost exhibits remarkable accuracy. The predictions are tightly clustered around the actual value (mean of 1.00), reflected by an extremely narrow range (0.97 to 1.04) and an impressively low standard deviation of 0.01, highlighting the model's exceptional reliability in this dimension. CatBoost emerges as a robust predictor with a broader spectrum in its predictions for IVS, spanning a range from 0.41 to 3.94. It gravitates towards a slightly higher mean of 1.18, accompanied by a more significant standard deviation of 0.69, indicating a wider dispersion of predictions. Despite this broader range, CatBoost maintains a commendable precision in ILS predictions, mirroring the trend of concentrated predictions with a mean of 1.00, showcased by a narrow range (0.97 to 1.05) and a modest standard deviation of 0.02. The DT model reveals a broad variability in IVS predictions, with values spanning from 0.20 to 3.37 and centring around a mean of 1.11. This is complemented by a standard deviation of 0.55, pointing to

a substantial but controlled dispersion of predictions. In contrast, its ILS predictions are highly focused, as indicated by a tight range (0.98 to 1.01), a mean of 1.00, and a minimal standard deviation of 0.01, highlighting its precision in this domain. GBDT showcases a balanced predictive performance, particularly in IVS, with a range extending from 0.29 to 2.01 and converging around a mean of 1.01. The standard deviation of 0.34 suggests a moderate spread of predictions, affirming a consistent predictive behaviour. ILS predictions by GBDT are exact, almost perfectly aligning with the actual values, denoted by an extremely narrow range (0.99 to 1.01), a precise mean of 1.00, and a negligible standard deviation. Lastly, the RF model offers insights into a diverse range of predictions for IVS, which is evident from the broadest range (0.52 to 6.59) among the models and a higher mean of 1.28. This diversity is further emphasised by the most significant standard deviation of 0.96, indicating a substantial spread of predictions. In ILS predictions, RF maintains a reasonable level of accuracy, with a range of 0.88 to 1.08, a mean of 0.99, and a standard deviation of 0.03, suggesting a balance between predictive diversity and precision.
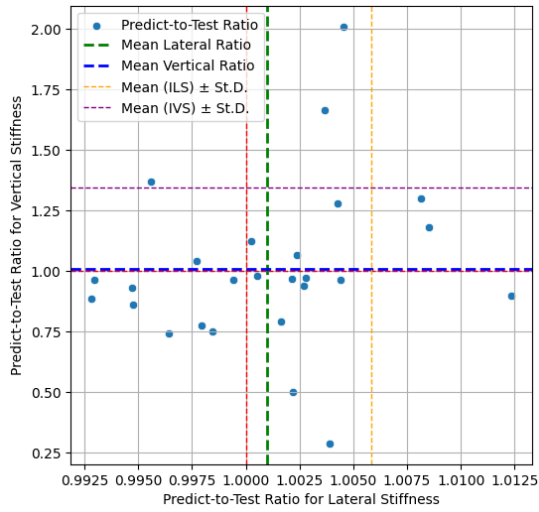
While each model exhibits distinct predictive characteristics, XGBoost and GBDT are particularly identified in their precision and consistency across IVS and ILS predictions, underlining their robustness and reliability in structural stiffness modelling.
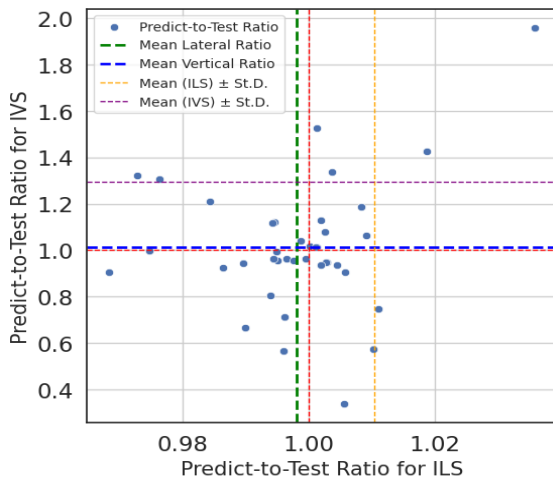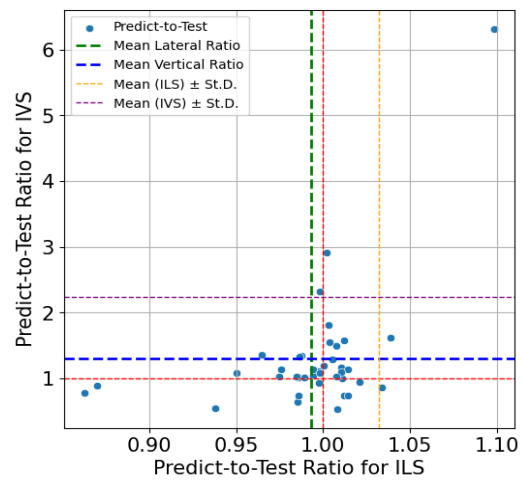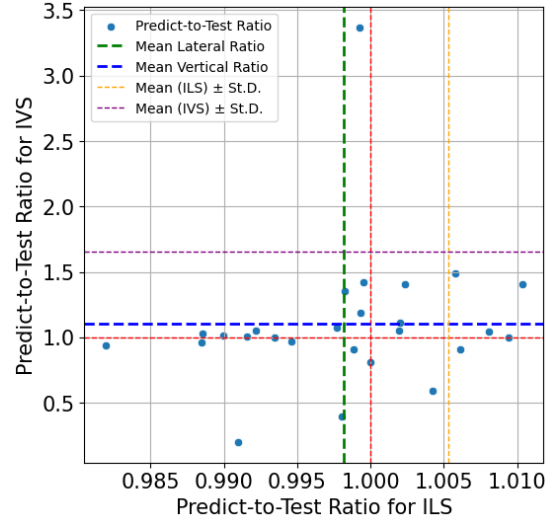

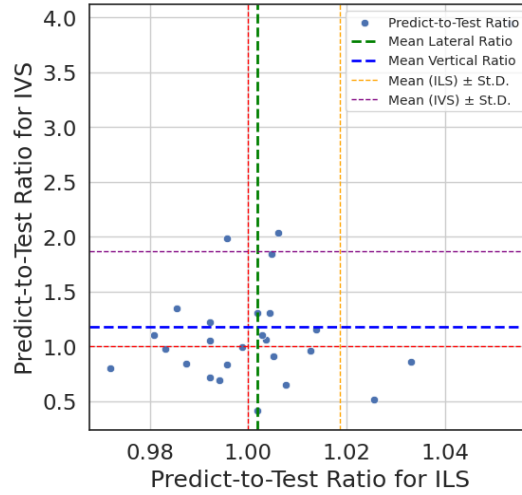(a)   (b)

(c)

(d)

(e)

Fig. 4-13 Predict-to-Test Ratios: (a) XGBoost Model; (b) Random Forest Model; (c) GBDT Model; (d) Decision Tree Model; (e) CATBooster Model

TABLE 4-5 Prediction Performance for ML Models

Model	Minimum	Maximum	Mean	Standard Deviation
XGBoost				
IVS	0.34	1.96	1.01	0.28
ILS	0.97	1.04	1.00	0.01

	CATboost			
IVS	0.41	3.94	1.18	0.69
ILS	0.97	1.05	1.00	0.02
	Decision Tree			
IVS	0.20	3.37	1.11	0.55
ILS	0.98	1.01	1.00	0.01
	GBDT			
IVS	0.29	2.01	1.01	0.34
ILS	0.99	1.01	1.00	0.00
	Random Forest			
IVS	0.52	6.59	1.28	0.96
ILS	0.88	1.08	0.99	0.03

4.10 Identification of Crucial Input Parameters

The XGBoost ML model was identified as superior for predicting the IVS and ILS of the UPTC shear wall system in both directions, as indicated by various performance measures, shown in TABLE 4-4 and TABLE 4-5. The ML model's highly complex and non-linear architecture, such as XGBoost, can be categorised as a black-box model [19], provided such a tree-based model inherently possesses an explainable hierarchical structure that is difficult to visualise easily. Hence, the study employs SHAP as a model-agnostic tool for interpreting the XGBoost ML model by harnessing the internal structure of the tree-based model while conducting calculations specific to the leaf nodes of the tree model, ultimately achieving low-order polynomial complexity [32]. Fig. 4-14 illustrates the mean SHAP values of various features, including H_{sw}, W_{sw}, T_{sw}, PT_s, and PT_d, and associated with the predictions of ILS and IVS obtained from the XGBoost tree ensemble model. The SHAP value analysis for ML model predictions of ILS and IVS reveals distinct patterns of feature importance. The feature with the most substantial impact in predicting ILS is W_{sw}, with a mean absolute SHAP value approaching 2500, suggesting that this parameter is crucial for predicting ILS in the model. T_{sw} comes in next, with a value of just over 1000, indicating a significant but notably lesser impact than W_{sw}. H_{sw} shows a moderate influence with a SHAP value of around 750, which is substantial but still less than T_{sw}. The features PT_s and PT_d demonstrate relatively more minor SHAP values in the range of approximately 250-500, implying that these

factors have a relatively minor effect on the model's ILS predictions. Lastly, FC, with a SHAP value close to 250, has the most negligible influence on the projections. Despite its lower ranking, it is essential to note that FC still plays a role in the model's output.

In predicting IVS, the feature T_{sw} is the dominant feature, with a SHAP value that dramatically surpasses the others, situated at the pinnacle of influence with a value close to 20,000. This suggests that T_{sw} is the most critical predictor of IVS within the model. The next feature, PT_s, also shows substantial importance, with a mean absolute SHAP value of around 5,000, yet it is significantly less influential than T_{sw}. Following this, W_{sw} displays a moderate impact, with its value near 2,500. Further, in influence, FC shows a more negligible contribution to the model's output, with a SHAP value of approximately 1,500. PT_d follows closely with a value slightly below 1,500, indicating a near-similar impact on IVS as FC. Lastly, H_{sw} is depicted as having the most minor influence on the predictions of IVS, with a SHAP value of just over 500.


(a)
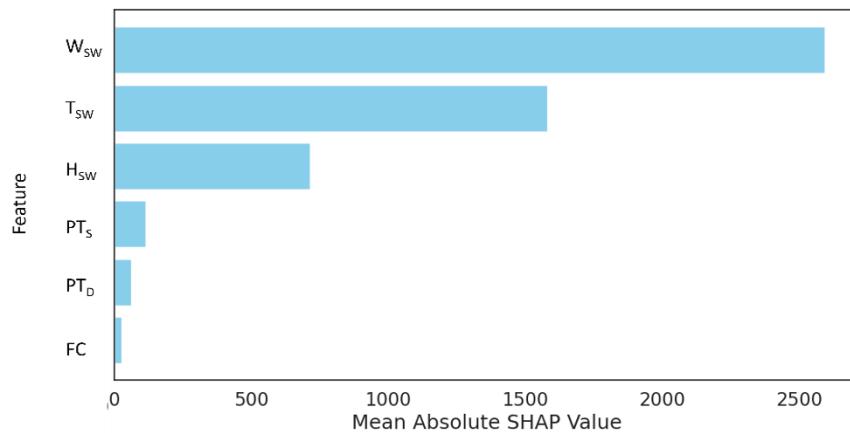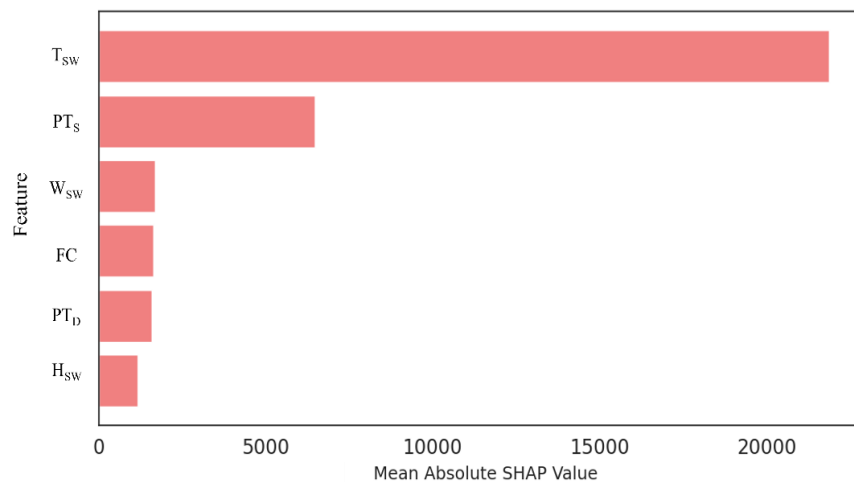
Fig. 4-14 Mean Absolute SHAP Values (Ascending Order) (a) ILS (b) IVS

Fig. 4-15 is presented as a visual depiction of the SHAP violin plots, illustrating the SHAP values for each feature considered in predicting the IVS and ILS of UPTC using the XGBoost model. Within these plots, the colour coding of each feature indicates its value, while the corresponding position on the x-axis (representing SHAP values) signifies the feature's contribution to the predicted output.

The W_{SW} has the most extensive range of SHAP values, from approximately -4000 to 4000. This wide distribution indicates a strong influence on ILS, with higher W_{SW} generally associated with an increase in ILS and lower W_{SW} with a decrease. T_{sw} has SHAP values ranging roughly between -2000 to 2000, showing a moderate influence. Its symmetrical distribution around zero suggests that T_{SW} can positively or negatively affect ILS, depending on other factors within the model. H_{sw} shows a narrower spread of SHAP values, from about -1000 to 1000, and a slight skew towards positive values. This indicates that greater heights tend to reduce ILS moderately. Other features, such as PT_s, PT_d, and FC, have SHAP values concentrated closer to zero, implying a more subtle effect on the model's output. PT_d notably has a cluster of positive values, suggesting a strong positive correlation with increased ILS. FC has a balanced distribution of SHAP values, indicating its influence on stiffness can vary greatly depending on the specific value. In aggregate, the plot reveals that W_{sw}, T_{sw}, and H_{sw} are critical drivers in the model's prediction of ILS, with W_{sw} displaying the most significant variability in impact. For T_{SW}, the SHAP values display a wide range, indicating that this feature can positively and negatively affect IVS, and its impact varies widely across different instances. PT_S shows primarily positive SHAP values, with a significant concentration in the 20,000 to 40,000 range, suggesting a strong positive association with increased IVS. W_{SW} has SHAP values that are positively skewed, although centred close to zero. This indicates a general trend of W_{SW} having a moderate positive effect on IVS. FC presents a very tight cluster of SHAP values around zero, suggesting it has a minimal impact on IVS. PT_D has SHAP values that are mostly positive, with some outliers, signifying a generally positive influence on IVS, with instances of significant impact. Lastly, H_{SW} shows a narrow spread of predominantly positive SHAP values, indicating a consistent and possibly substantial positive impact on increasing IVS.
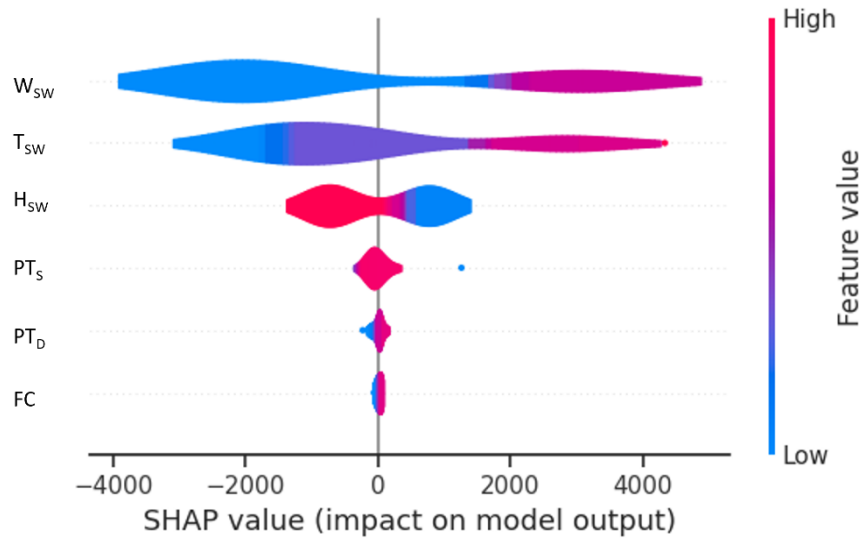
(a)
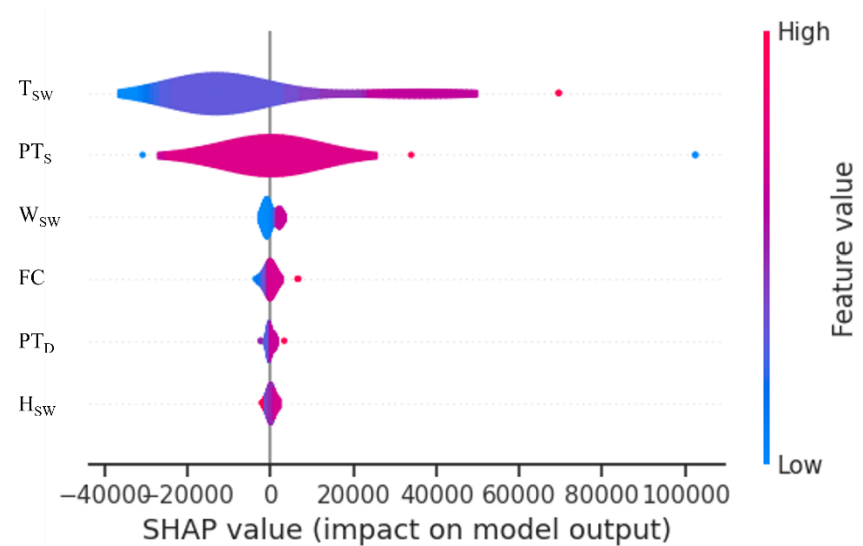
(b)

Fig. 4-15 SHAP Violin Summary Plot (a) XGBoost-ILS Model (b) XGBoost-IVS Model

4.11 Conclusion

This study investigates the performance of Unbounded tension laminated Timber (UPTC) shear walls using an integrated approach that combines numerical simulations with advanced Machine Learning (ML) techniques. This innovative approach has enabled a thorough examination of the influence of structural parameters on the performance of UPTC shear walls, providing valuable insights for constructing earthquake-resistant buildings. The research meticulously explored the

impact of wall thickness, aspect ratio, post-tension diameter (PT_d), and post-tension stress (PT_s) on the initial lateral stiffness of UPTC shear walls. It quantitatively demonstrated that increasing wall thickness considerably enhances the wall's resistance to lateral loads, evidenced by a 75% increase in initial stiffness when transitioning from a 3-ply to a 7-ply configuration. Further, the study highlighted the importance of aspect ratio in structural rigidity, as seen in the significant reduction in initial stiffness with increased aspect ratio, emphasising the necessity of careful structural design.

Enhancing the study's strength, advanced ML algorithms like XGBoost and Gradient Boosting Decision Tree (GBDT) were employed, showcasing remarkable precision and consistency in predicting Initial Lateral Stiffness (ILS) and Initial Vertical Stiffness (IVS). The performance of these ML models was rigorously evaluated, with metrics such as R-squared values nearing perfection and other indicators like RMSE, MAE, and MAPE demonstrating a strong predictive alignment within the observed data.

The research contributed critically by integrating the SHAP method, adding a profound level of interpretability to the ML models. The SHAP analysis unveiled various input parameters' significance and intricate interdependency, providing a clear, quantifiable perspective on feature contributions to UPTC shear wall performance. W_{sw} was identified as the most impactful feature in ILS prediction, followed by T_{sw} and H_{sw}. For IVS prediction, T_{sw} was pinpointed as the dominant feature, with PT_s, W_{sw}, and FC also playing substantial roles in the model's predictions. The SHAP violin plots visually depicted these findings, detailing each feature's range and distribution of SHAP values. These plots emphasised the considerable variability in the impact of features like W_{sw} and T_{sw} on ILS and IVS predictions, revealing the nuanced and complex nature of structural behaviour in UPTC shear walls.

Finally, this research marks a significant advancement in applying ML to structural engineering, showcasing how ML models can enhance predictive analysis and offer a transparent understanding of structural systems. The insights gained are poised to direct future research, fostering the evolution of more intricate, precise, and clear structural predictions and analyses, focusing mainly on earthquake-resistant construction. This study establishes a benchmark for blending numerical simulation with ML and SHAP analysis, setting the stage for improved structural designs and championing resilient, sustainable building methodologies.

4.12 Statements and Declarations

All authors certify that they have no affiliations with or involvement in any organisation or entity with any financial or non-financial interest in the subject matter or materials discussed in this manuscript.

4.13 Credit Authorship Contribution Statement:

K.G.M. Kandethanthri: Formal Analysis, Validation, Finite Element Models. **Ghazanfarah Hafeez:** Conceptualization, Methodology, Investigation, Formal Analysis, Validation, Writing—original Draft Preparation, Review, and Editing. Supervision, Data Collection, Conceptualization, Methodology, Investigation, Visualization, Writing, Review, and Editing, **Zhiyoung Chen** Methodology, Investigation, Visualization, and Review.

4.14 Declaration of Competing Interest

The authors declare that they have no known competing financial interests or personal relationships that could have appeared to influence the work reported in this paper.

4.15 Data Availability

The raw/processed data required to reproduce these findings cannot be shared at this time as it is also part of an ongoing study.

4.16 References

[1]   Z. Chen, M. Popovski, Structural performance of balloon mass timber shear walls under in-plane lateral loads, in: Structures, Elsevier, 2023: p. 105643.

[2]   Z. Chen, M. Popovski, Theoretical Building Height Limits of Balloon Mass Timber Shear Wall Systems, Journal of Structural Engineering 150 (2024). https://doi.org/10.1061/JSENDH.STENG-12726.

[3]   Z. Chen, M. Popovski, Material-based models for post-tensioned shear wall system with energy dissipators, Eng Struct 213 (2020) 110543.

[4]   Karacabeyli E, Douglas B, CLT Handbook: cross-laminated timber, FPInnovations, Pointe-Claire, 2013.

[5]   D. Casagrande, G. Doudak, A. Polastri, A proposal for the capacity-design at wall-and building-level in light-frame and cross-laminated timber buildings, Bulletin of Earthquake Engineering 17 (2019) 3139–3167.

[6]   A. Ceccotti, C. Sandhaas, M. Okabe, M. Yasumura, C. Minowa, N. Kawai, SOFIE project–3D shaking table test on a seven-storey full-scale cross-laminated timber building, Earthq Eng Struct Dyn 42 (2013) 2003–2021.

[7]   I. Gavric, M. Fragiacomo, A. Ceccotti, Cyclic behavior of CLT wall systems: Experimental tests and analytical prediction models, Journal of Structural Engineering 141 (2015) 04015034.

[8]   Z. Chen, M. Popovski, A. Iqbal, Structural performance of post-tensioned CLT shear walls with energy dissipators, Journal of Structural Engineering 146 (2020) 04020035.

[9]   R. Ganey, J. Berman, T. Akbas, S. Loftus, J. Daniel Dolan, R. Sause, J. Ricles, S. Pei, J. van de Lindt, H.-E. Blomgren, Experimental investigation of self-centering cross-laminated timber walls, Journal of Structural Engineering 143 (2017) 04017135.

[10]   T. Connolly, C. Loss, A. Iqbal, T. Tannert, Feasibility study of mass-timber cores for the UBC tall wood building, Buildings 8 (2018) 98.

[11]   S. Pei, J.W. van de Lindt, M. Popovski, Approximate R-factor for cross-laminated timber walls in multistory buildings, Journal of Architectural Engineering 19 (2013) 245–255.

[12]   M. Izzi, A. Polastri, M. Fragiacomo, Investigating the hysteretic behavior of Cross-Laminated Timber wall systems due to connections, Journal of Structural Engineering 144 (2018) 04018035.

[13]   M.J.N. Priestley, S. (Sri) Sritharan, J.R. Conley, S. Stefano Pampanin, Preliminary Results and Conclusions From the PRESSS Five-Story Precast Concrete Test Building, PCI Journal 44 (1999) 42–67. https://doi.org/10.15554/pcij.11011999.42.67.

[14]   A. Palermo, S. Pampanin, A. Buchanan, M. Newcombe, Seismic design of multi-storey buildings using laminated veneer lumber (LVL), (2005).

[15]   A. Iqbal, S. Pampanin, A. Palermo, A.H. Buchanan, Performance and Design of LVL Walls Coupled with UFP Dissipaters, Journal of Earthquake Engineering 19 (2015) 383–409. https://doi.org/10.1080/13632469.2014.987406.

[16]   S. Mangalathu, J.-S. Jeon, Ground motion-dependent rapid damage assessment of structures based on wavelet transform and image analysis techniques, Journal of Structural Engineering 146 (2020) 04020230.

[17]   X. Zhao, R. Lovreglio, D. Nilsson, Modelling and interpreting pre-evacuation decision-making using machine learning, Autom Constr 113 (2020) 103140.

[18]   A. Gondia, M. Ezzeldin, W. El-Dakhakhni, Mechanics-Guided Genetic Programming Expression for Shear-Strength Prediction of Squat Reinforced Concrete Walls with Boundary Elements, Journal of Structural Engineering 146 (2020). https://doi.org/10.1061/(ASCE)ST.1943-541X.0002734.

[19]   D.-C. Feng, B. Fu, Shear strength of internal reinforced concrete beam-column joints: intelligent modeling approach and sensitivity analysis, Advances in Civil Engineering 2020 (2020) 1–19.

[20]   M.Z. Naser, Fire resistance evaluation through artificial intelligence-A case for timber structures, Fire Saf J 105 (2019) 1–18.

[21]   M. Nikoo, G. Hafeez, P. Cachim, Using Optimization Algorithms-Based ANN to Determine the Temperatures in Timber Exposed to Fire for a Long Duration, Buildings 12 (2022) 2265.

[22]   A.T.G. Tapeh, M.Z. Naser, Artificial intelligence, machine learning, and deep learning in structural engineering: a scientometrics review of trends and best practices, Archives of Computational Methods in Engineering 30 (2023) 115–159.

[23]   D.-C. Feng, W.-J. Wang, S. Mangalathu, E. Taciroglu, Interpretable XGBoost-SHAP machine-learning model for shear strength prediction of squat RC walls, Journal of Structural Engineering 147 (2021) 04021173.

[24]   N. Tajik, A. Mahmoudian, M. Mohammadzadeh Taleshi, M. Yekrangnia, Explainable XGBoost machine learning model for prediction of ultimate load and free end slip of

GFRP rod glued-in timber joints through a pull-out test under various harsh environmental conditions, Asian Journal of Civil Engineering (2023) 1–17.

[25] Y. Lei, Z. Shen, F. Tian, X. Yang, F. Wang, R. Pan, H. Wang, S. Jiao, W. Kou, Fire risk level prediction of timber heritage buildings based on entropy and XGBoost, J Cult Herit 63 (2023) 11–22.

[26] S. Rahimi, V. Nasir, S. Avramidis, F. Sassani, Wood moisture monitoring and classification in kiln-dried timber, Struct Control Health Monit 29 (2022) e2911.

[27] M.Z. Esteghamati, T. Gernay, S. Banerji, Evaluating fire resistance of timber columns using explainable machine learning models, Eng Struct 296 (2023) 116910.

[28] J. Chonghyo, P. Hyundo, H. Seokyoung, L. Jongkoo, H. Insu, C. Hyungtae, K. Junghwan, Prediction for heat deflection temperature of polypropylene composite with Catboost, in: Computer Aided Chemical Engineering, Elsevier, 2022: pp. 1801–1806.

[29] S. Kookalani, B. Cheng, J.L.C. Torres, Structural performance assessment of GFRP elastic gridshells by machine learning interpretability methods, Frontiers of Structural and Civil Engineering 16 (2022) 1249–1266.

[30] S.M. Lundberg, S.-I. Lee, A unified approach to interpreting model predictions, Adv Neural Inf Process Syst 30 (2017).

[31] S.M. Lundberg, G.G. Erion, S.-I. Lee, Consistent individualized feature attribution for tree ensembles, ArXiv Preprint ArXiv:1802.03888 (2018).

[32] S.M. Lundberg, G. Erion, H. Chen, A. DeGrave, J.M. Prutkin, B. Nair, R. Katz, J. Himmelfarb, N. Bansal, S.-I. Lee, Explainable AI for trees: From local explanations to global understanding, ArXiv Preprint ArXiv:1905.04610 (2019).

[33] S. Mangalathu, S.-H. Hwang, J.-S. Jeon, Failure mode and effects analysis of RC members based on machine-learning-based SHapley Additive exPlanations (SHAP) approach, Eng Struct 219 (2020) 110927.

[34] K. Hossain, M.E. Kreger, K.J. Fridley, T.N. Dao, M.E. Barkey, EXPERIMENTAL INVESTIGATION OF LONG TERM AND LATERAL LOAD BEHAVIOR OF CLT SHEAR WALLS FOR MID-RISE WOOD BUILDINGS, 2019.

[35] F.A. Chowdhury, Experimental and FEA Study of Structural Behavior of CLT Shear Walls for Wood Building Applications, The University of Alabama, 2021.

Five.   Chapter 5.

5   Additional Investigation of Hybrid Structures with Balloon-Type CLT Shear Wall Systems

This chapter provides a comparative investigation into the seismic performance of hybrid buildings by analysing 12 case studies of hybrid buildings featuring two types of balloon-type CLT shear wall configurations (different from those considered in Chapter 3) to investigate the effect of the location of the CLT balloon-type shear wall on the seismic performance following the procedure discussed in Chapter 3. The buildings were grouped based on with and without mass irregularities. The case studies comprise seismic performance assessments of 12-, 16- and 20-story buildings. Modal Response Spectrum Analysis (MRSA) was employed to assess these buildings' seismic performance while examining the impact of mass irregularities on their performance.

5.1   Building Layout

The prototype buildings were symmetrically structured with a footprint of 45 m by 45 m, with five bays, each spanning 9 m, in two orthogonal directions and a story height of 3 meters. The construction of the buildings incorporated a 175-mm thick (5-ply) CLT floor, each topped with a 100-mm concrete layer. To resist the lateral loads, 7-ply CLT panels, each 245 mm thick, 3 m wide, and 12 m tall, shear walls were provided in two orthogonal directions. The layout of the shear walls of Configuration-01 and Configuration-02 is depicted in Fig 5-1. In Configuration-01, the building core is CLT balloon-type shear walls; in Configuration-02, the core is replaced with steel beams.

The steel beams-to-columns connections were considered fixed. Holz-Stahl-Komposit (HSK) connection technology was employed between CLT panels to steel columns, CLT-CLT panels and CLT panels to the foundation of the buildings. The HSK connections and the loading configurations were consistent with the analyses performed in Chapter 3. Each model was assigned a unique label, and those labels were illustrated in Fig. 5-2.

TABLE 5-1 Model Labels

| Model ID	Description
12-Hybrid-Base-Con-01	12-story structure, hybrid CLT shear wall, standard configuration, no irregularities, configuration 01
12-MI-Hybrid-2.5D-Con-01	12-story structure, hybrid CLT shear wall, increased mass at 6th floor, configuration 01
12-Hybrid-Base-Con-02	12-story structure, hybrid CLT shear wall, standard configuration, no irregularities, configuration 02
12-MI-Hybrid-2.5D-Con-02	12-story structure, hybrid CLT shear wall, increased mass at 6th floor, configuration 02
16-Hybrid-Base-Con-01	16-story structure, hybrid CLT shear wall, standard configuration, no irregularities, configuration 01
16-MI-Hybrid-2.5D-Con-01	16-story structure, hybrid CLT shear wall, increased mass at 8th floor, configuration 01
16-Hybrid-Base-Con-02	16-story structure, hybrid CLT shear wall, standard configuration, no irregularities, configuration 02
16-MI-Hybrid-2.5D-Con-02	16-story structure, hybrid CLT shear wall, increased mass at 8th floor, configuration 02
20-Hybrid-Base-Con-01	20-story structure, hybrid CLT shear wall, standard configuration, no irregularities, configuration 01
20-MI-Hybrid-2.5D-Con-01	20-story structure, hybrid CLT shear wall, increased mass at 10th floor, configuration 01
20-Hybrid-Base-Con-02	20-story structure, hybrid CLT shear wall, standard configuration, no irregularities, configuration 02
20-MI-Hybrid-2.5D-Con-02	20-story structure, hybrid CLT shear wall, increased mass at 10th floor, configuration 02

(a)   (b)
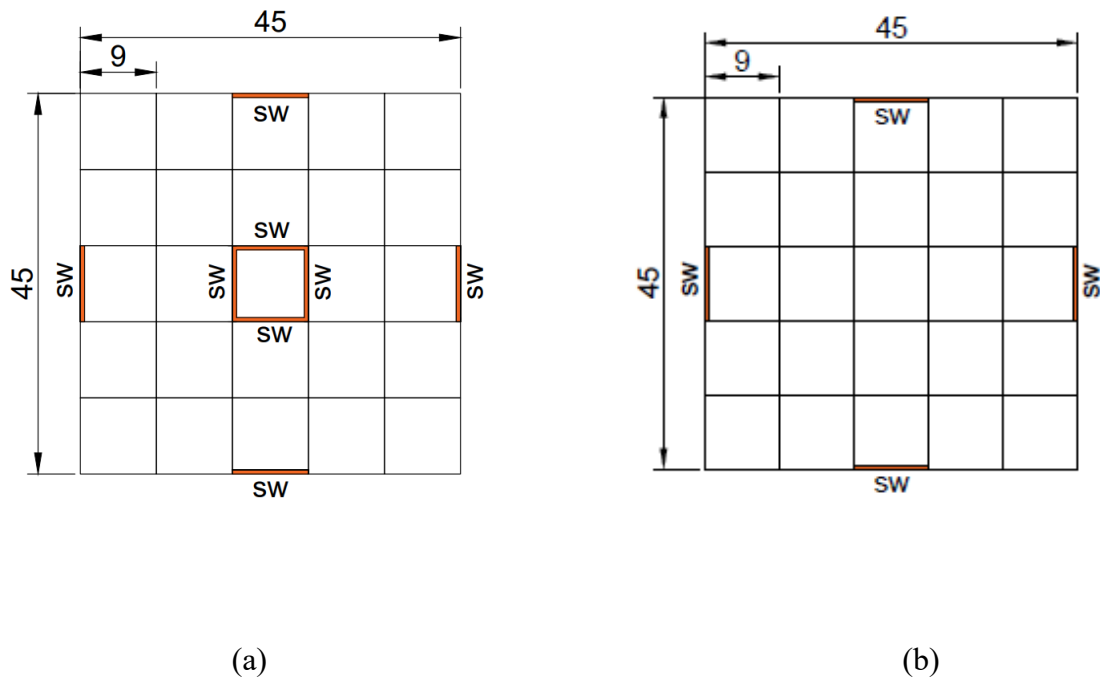
Fig 5-1 Location of the Shear Walls (a) Configuration-01 (Con-01) (b) Configuration-02
(Con-02)

5.2 Methodology

MRSA was employed to evaluate the seismic performance of the buildings modelled in Dlubal RFEM 6.05. MRSA leverages a dynamic analysis technique to ascertain the peak responses of the buildings, thereby capturing the comprehensive seismic impact on the considered buildings. The buildings were assumed to be located at Vancouver City Hall, with seismic response design data sourced from Table 4, following the NBCC [1]. The analyses were carried out assuming a normal importance factor with a Site Class C, a ductility-related modification factor (Rd) of 3.87 and an overstrength-related modification factor (Ro) of 1.57 [2].

The SRSS Modal Combination Rule was applied for periodic responses, with the response spectrum analysis being conducted in both the X and Y directions considering the orthogonal effect. The 100/30 rule stipulates that 100% of the prescribed seismic forces must be applied in one direction, with an additional 30% of the forces in the perpendicular direction. The first six modes were selected due to their significant contribution to the overall dynamic response, with a

Modal Participation Factor (MPF) for these modes exceeding 90% [3]. Steel columns and beams were also checked per the steel design (CSA S16, 2019).

TABLE 5-2 Seismic Design Data for RSA-Vancouver

Spectral Acceleration Parameters	RSA-Vancouver
Spectral Response Acceleration for period 0.2 s	0.848
Spectral Response Acceleration for period 0.5 s	0.751
Spectral Response Acceleration for period 1.0 s	0.425
Spectral Response Acceleration for period 2.0 s	0.257
Spectral Response Acceleration for period 5.0 s	0.08
Spectral Response Acceleration for period 10.0 s	0.029

5.3   Results and Conclusion

The maximum displacement and the inter-story drifts of the analysed buildings are illustrated in Fig. 5-2, and Fig. 5-3.
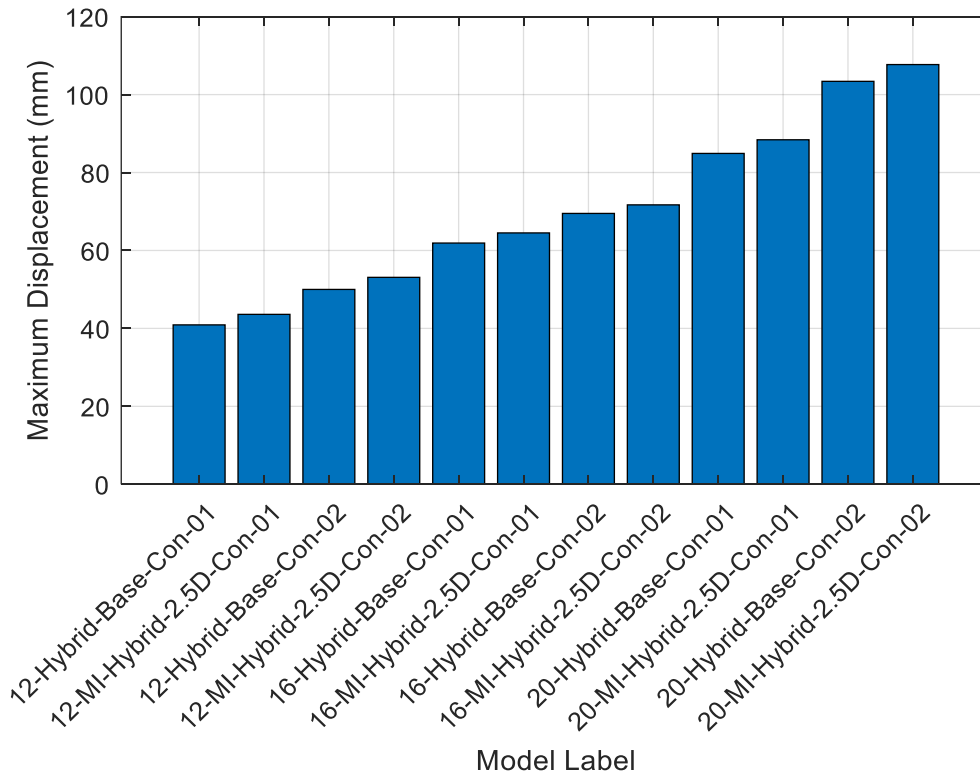
Fig. 5-2 Maximum Displacement of Each Building

According to the Fig. 5-2 in 12-story hybrid building structures, the base model showed a maximum displacement of 40.9 mm, while adding additional mass on the 6th floor led to a 7% increase in maximum displacement to 43.6 mm. Similarly, 16-story hybrid buildings without mass irregularities experienced a maximum displacement of 61.9 mm; adding mass to the 8th story raised the maximum displacement by 4% to 64.5 mm. The 20-story base model initially displaced 84.9 mm, increasing to 88.4 mm after mass was added to the 10th floor, marking a 4% rise maximum displacement. The comparison between the inter-story drift distributions for CLT shear wall configuration-01 and configuration-02 of the buildings with and without mass irregularities along the height is illustrated in Fig. 5-3. For all the building cases (12-story, 16-story, 20-story) with and without mass irregularities, when the core of the hybrid structure is replaced by the steel beam, the maximum displacement is increased by 21%-22%.
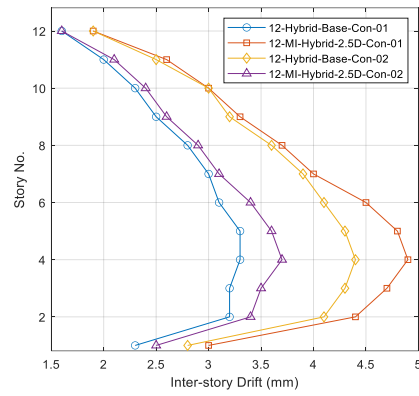
(a)
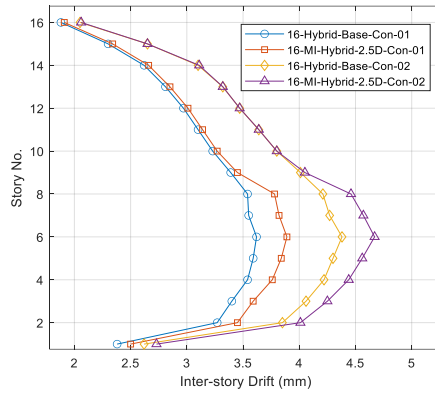
(b)
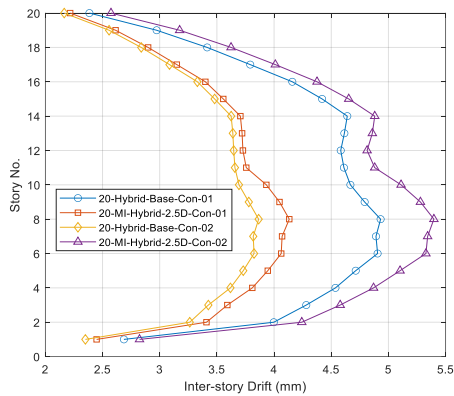
(c)

Fig. 5-3 Inter-Story Drift Comparison between the Base Model and MI Model (a) 12-story structure (b) 16-story structure (c) 20-story structure

The figure shows that the buildings with both CLT shear wall confirmations with mass irregularity show higher inter-storey drifts in the lower storeys, attributing a mass anomaly located at the mid-height of the building. Further, notable inflexions at specific story levels—sixth for a 12-story building, eighth for a 16-story building, and tenth for a 20-story building—emphasise a localised disturbance in the modal properties. These disruptions alter the mass-stiffness distribution, impacting the dynamic response of the buildings, including drift amplification.

5.4   Conclusion

This study employed MRSA to examine the seismic performance of prototype hybrid buildings featuring balloon-type CLT with Mass Irregularity (MI). the study focused on assessing the impact of mass irregularities on seismic behaviour while influencing the buildings' dynamic responses, including inter-story drifts and overall building displacement.

The research findings indicate that buildings with mass irregularities experience more significant displacement than those with regular mass distribution for both shear wall configurations. These results demonstrate mass distribution's crucial role in buildings' seismic resilience.

Further, the study revealed inflexions in the middle stories of the 12-, 16-, and 20-story buildings, representing a localised disturbance in the modal properties. This disturbance mainly affects the mass-stiffness distribution and, consequently, the dynamic response, resulting in an uniform amplification of drift demands.

5.5   References

[1]   C.C. on B. and F. Codes, N.R.C. of Canada, National Building Code of Canada, 2015, National Research Council Canada, 2015. https://books.google.ca/books?id=1H61DAEACAAJ.

[2]   M. Khajehpour, Y. Pan, T. Tannert, Seismic analysis of hybrid steel moment frame CLT shear walls structures, Journal of Performance of Constructed Facilities 35 (2021) 04021059.

[3]   C. Menun, A. Der Kiureghian, A replacement for the 30%, 40%, and SRSS rules for multicomponent seismic analysis, Earthquake Spectra 14 (1998) 153–163.

Six.   Chapter 6.

6   General Conclusions and Recommendations

The main objective of this research is to evaluate the lateral performance of balloon-type CLT at component and building levels. The finite element programs Dlubal RFEM and ABAQUS CAE were explicitly used to create the finite element models of balloon-type CLT shear walls to accomplish the thesis objectives. The first part of the study is focused on evaluating mass and vertical geometric irregularities of hybrid buildings combining CLT shear walls and steel moment frame employing Modal Response Spectrum Analysis, followed by assessing the lateral performance of unbounded post-tensioned balloon-type CLT shear walls through traditional sensitivity analysis and Machine learning techniques in the second half of this thesis.

The principal outcomes of this thesis are summarised below.

Building Level:

- This study investigated the effect of mass on the inter-story drift in hybrid structures and concluded a direct relationship between the investigated parameters (increased mass and inter-story drift). The investigation found that increasing mass in the middle of 8-story, 12-story, and 16-story buildings by 2.5% of the dead load led to an increase in average inter-story drift by 10%, 6%, and 3%, respectively. The inter-story drift of building models with various mass irregularity configurations is illustrated in Fig. 6-1.

(a)

(b)

(c)
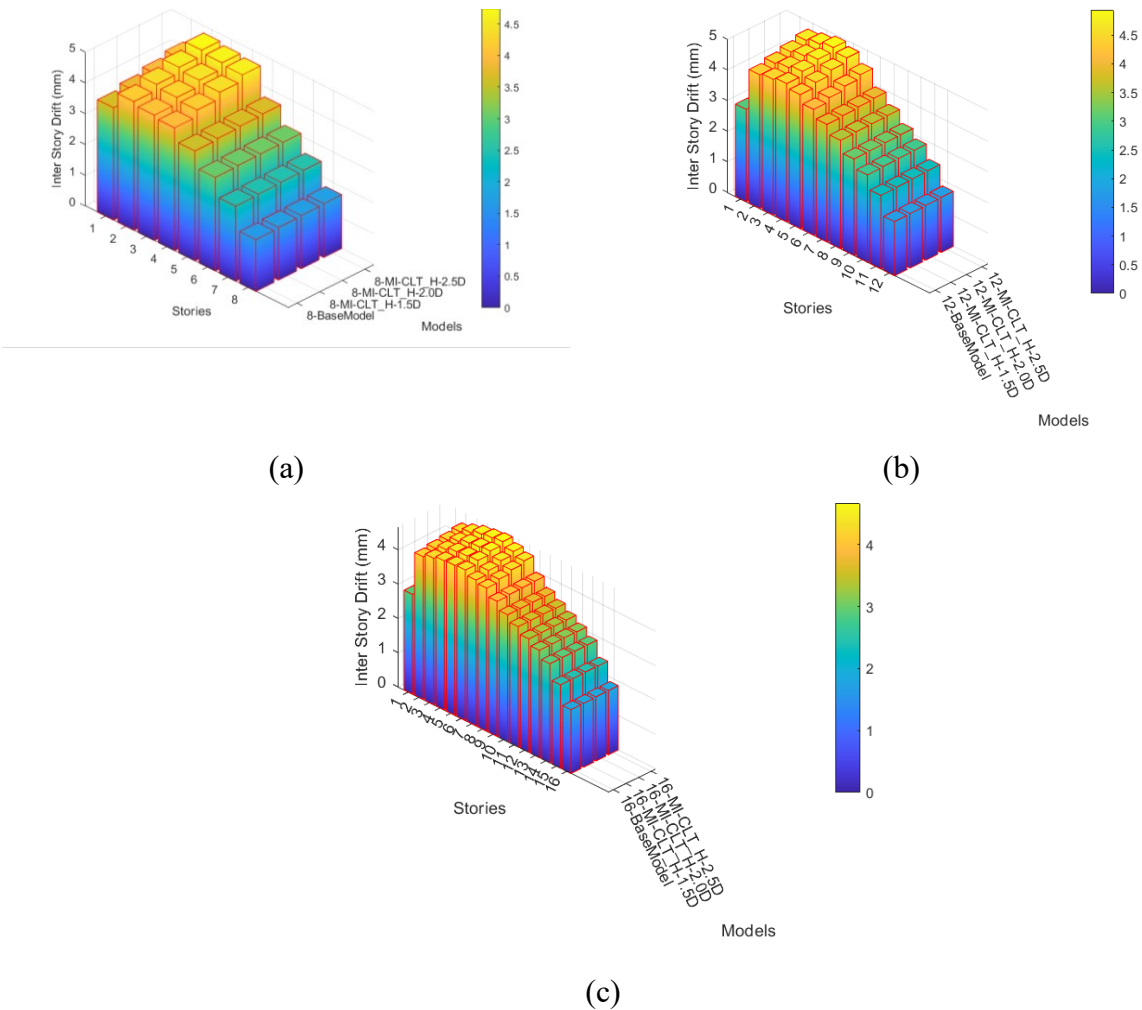
Fig. 6-1 Inter-Story Drifts Variation with Different Mass Irregular Configurations

- The influence of adding mass to different locations within a structure is also assessed. The outcomes of the MRSA suggested that the location of added mass profoundly impacts the seismic response, such that adding mass to lower levels provoked higher sensitivity and significant drift in the lower levels, whereas adding mass to upper levels resulted in localised drift in those levels, sparing the lower levels from pronounced impacts (see Fig. 6-2). For instance, placing additional mass on the second level of an 8-story building yielded 4% of the average inter-story drift for the top stories (fifth to the eighth story) and 7% for the bottom stories (first to the fourth story) compared to the building without mass irregularity. Conversely, placing additional mass on the seventh story of an 8-story building yielded an average inter-story drift of 22% for the top stories (fifth to the eighth story) and 13% for the bottom stories (first to the fourth story) compared to the building without mass

110

irregularity. These results emphasise carefully considering mass distribution during the design phase to enhance seismic resilience.
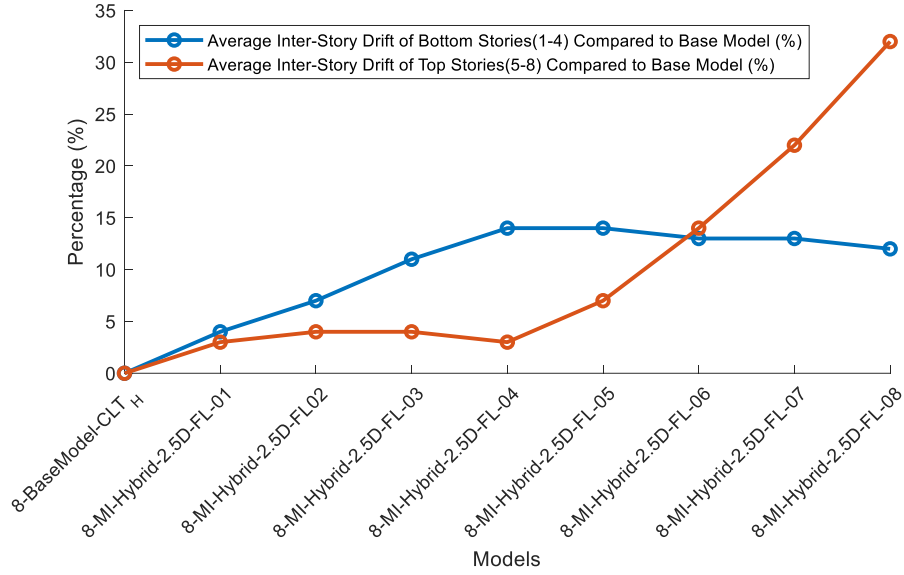
(a)
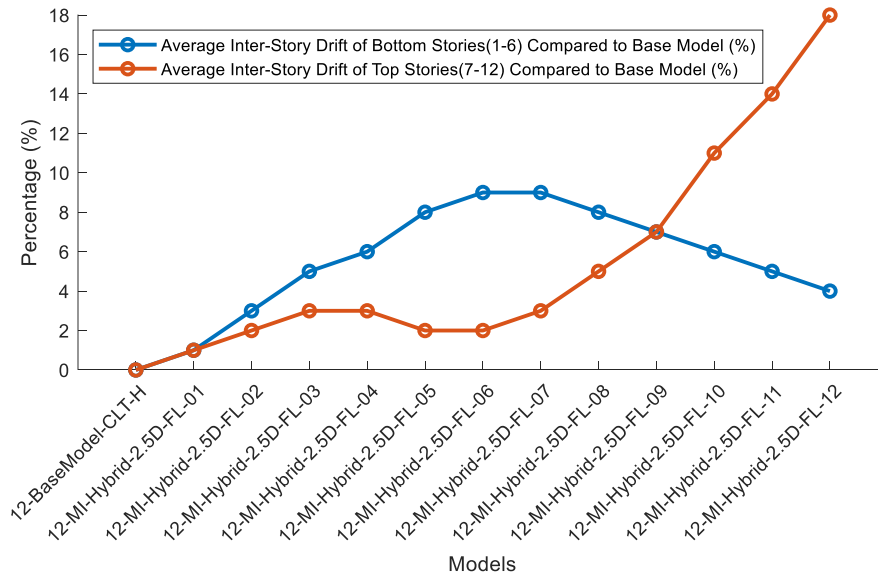
(b)
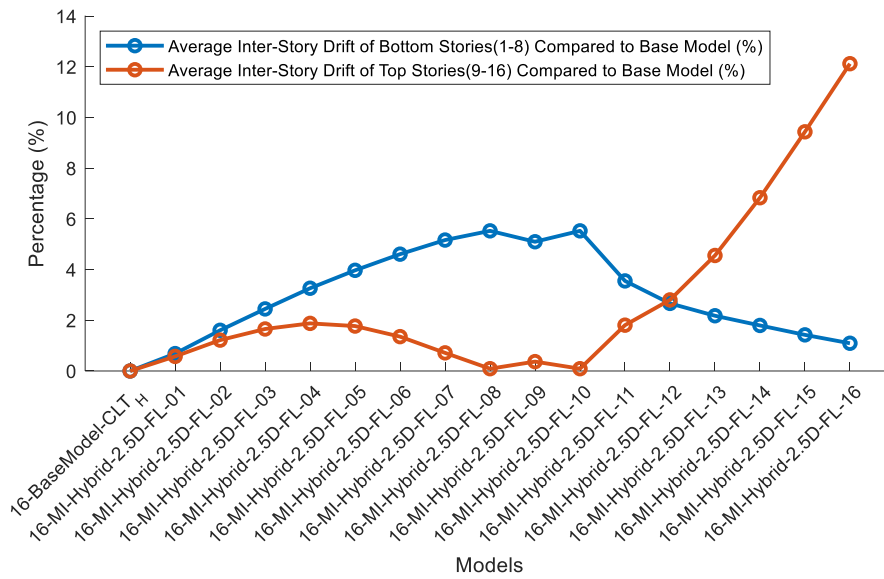
(c)

Fig. 6-2 Averaged Inter-Story Drift Variation (Top Stories vs. Bottom Stories) with Increased Mass Distribution along the Hybrid Structures

– Several models were created with various vertical geometric irregularities, exploring the influence of these irregularities on the inter-story drift of the hybrid building. The study revealed the unique response of the building in two orthogonal directions (X and Y), emphasising the significance of directional approaches in seismic response analysis. Fig. 6-3 illustrates the building model with directional seismic response in two orthogonal directions. Further, the study found that the directional responses, particularly in the X direction, play a crucial role due to an uneven distribution of mass and stiffness along the height of such buildings.

(a)

(b)

(c)
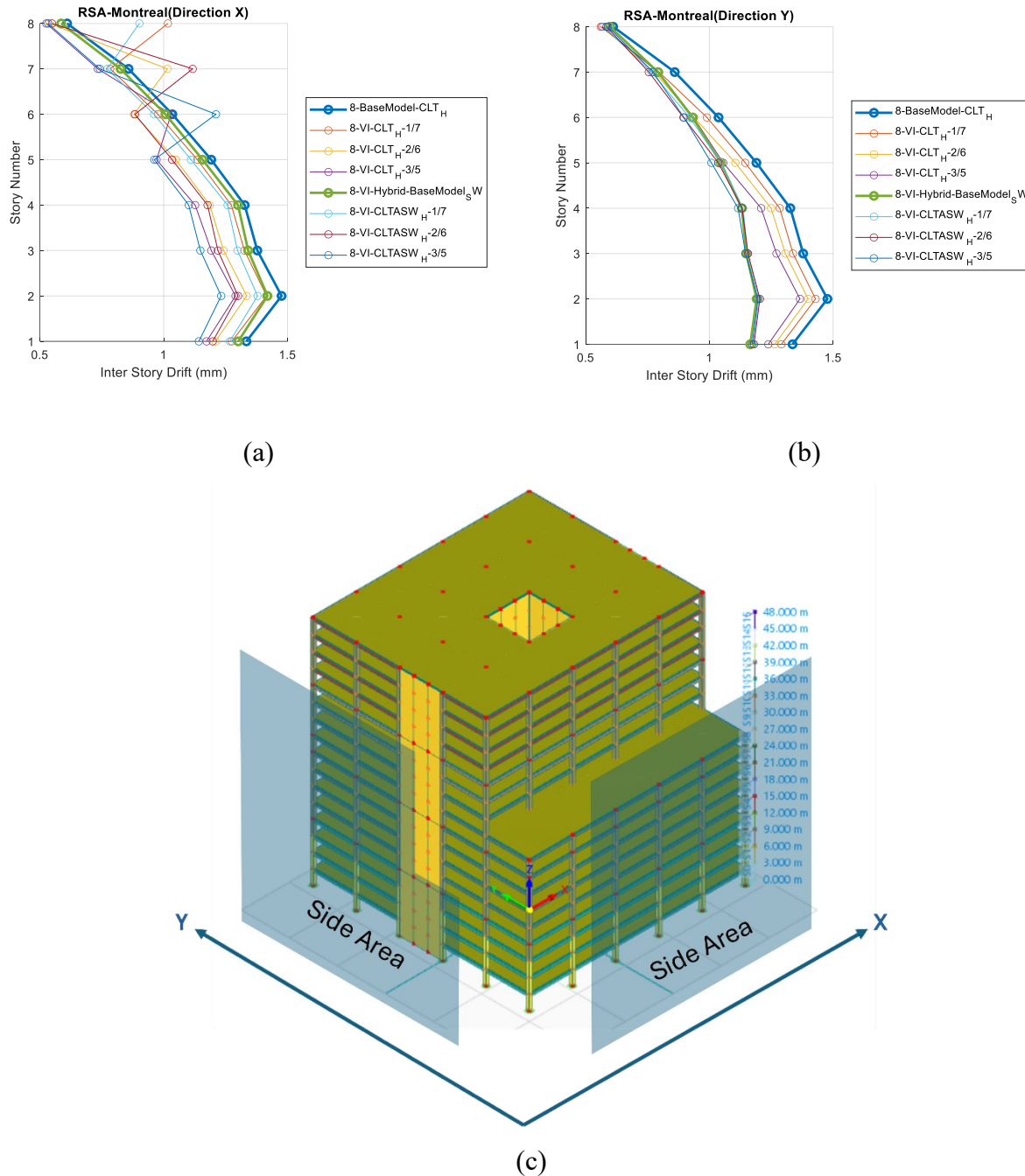
Fig. 6-3 (a) Inter-Story Drift in X Direction in Structures with Vertical Geometric Irregularities; (b) Inter-Story Drift in Y Direction in Structures with Vertical Geometric Irregularities; (c) Definition of the Directional Axes (X and Y Directions)

‾ The research further determined that buildings with vertical geometric irregularities experience a sudden increase in inter-story drift in the tower structure, particularly in the X direction (see Fig. 6-2), indicating a divergence in the base and tower structure response to lateral seismic forces. The tower structure experienced greater displacement than the

base structure, emphasising the significance of considering vertical geometric irregularities in the design phase of buildings to ensure structural integrity and resilience against dynamic loads.

Component Level:

- When the performance was evaluated at the component level, the study concluded that increasing UPTC shear wall thickness markedly improved their lateral performance. For instance, a 28% increase in initial lateral stiffness is observed when a 5-ply UPTC wall is used compared to a 3-ply wall. Additionally, a 7-ply wall showed a 75% increase in initial lateral stiffness compared to a 3-ply wall. This substantial improvement in the initial stiffness of the thicker sections is attributed to their enhanced ability to better resist deformations caused by the lateral loads.
- The initial lateral stiffness values for the walls with variable thicknesses and aspect ratios were investigated. Variations in the aspect ratio significantly varied the initial lateral stiffness of the UPTC wall models. Increasing the aspect ratio from 2 to 3 resulted in an average reduction of 56% across all thicknesses, including 3-ply, 5-ply, and 7-ply.
- Further, a direct relationship was observed between post-tension diameters, post-tension stresses, and the initial lateral stiffness. Increasing the post-tension diameters and post-tension stresses caused an increase in initial lateral stiffness for all CLT configurations, with the surge being higher for more layers in the UPTC shear wall. However, this increase was negligible compared to other factors, such as aspect ratios and thickness.
- A unique model database was created utilising ABAQUS/Standard with different unbounded post-tension CLT shear wall parameters (thickness, width, height, post-tension stress, and post-tension diameter), and stiffnesses were recorded using ABAQUS/Standard. Subsequently, five machine learning algorithms (Extreme Gradient Boosting, Categorical Boosting, Gradient Boosting Decision Tree, Random Forest, and Decision Tree) were explored to predict the stiffness. The Extreme Gradient Boosting (XGBoost) algorithm was identified as the most accurate algorithm for predicting initial lateral and vertical stiffness UPTC shear walls within the dataset created in this study.
- Additionally, the critical parameters impacting the lateral and uplifting behaviour of the UPTC shear wall system were identified through Shapley additive explanations (SHAP).

Fig. 6-4 illustrates the mean absolute SHAP values for both models. The width and thickness of the UPTC shear walls were concluded to be the most critical factors affecting the initial lateral stiffness. While the thickness and post-tension stress were identified as the factors influencing the initial vertical stiffness the most.
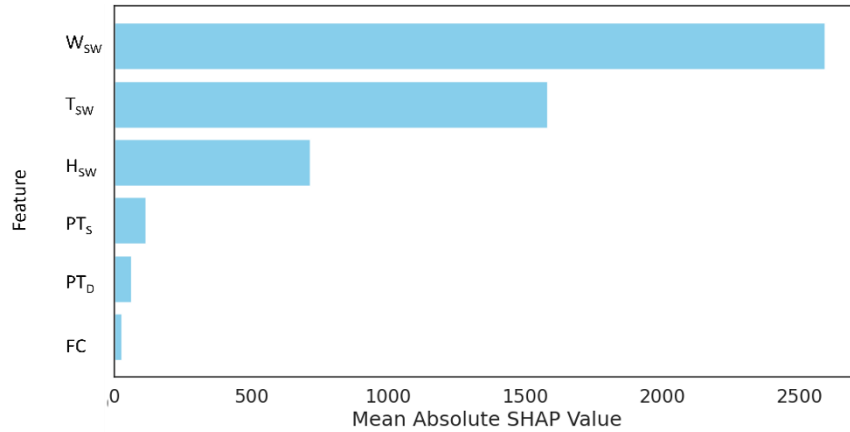
(a)
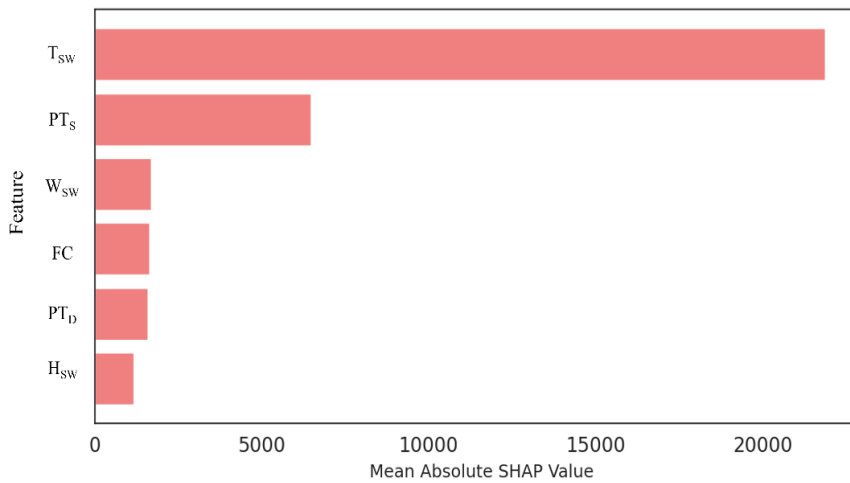
(b)

Fig. 6-4 Mean Absolute SHAP Values (a) XGBoost-Initial Lateral Stiffness Model (b) XGBoost-Initial Vertical StiffnessS Model

6.1 Limitations of This Study and Future Work

The current thesis investigates the linear elastic behaviour of a balloon-type CLT system. The first part of the study focuses on mass and vertical geometric irregularities to evaluate the structure's seismic performance. However, the scope of the research is limited, excluding the torsional building response under seismic loads to simplify the analysis. Torsional behaviour can

115

significantly impact a structure's response to seismic loads; hence, further study on the invested topic is recommended, considering evaluating the torsional response under seismic loading, which will significantly enhance the understanding of this topic.

The second part of the study primarily focused on post-tension balloon-type CLT at the component level. It is recommended that the behaviour of the post-tension system at the building level be explored.

Seven. Appendix

A Appendix A: Analysing Seismic Performance of Hybrid Structures: The Impact of Vertical and Mass Irregularities on Buildings with Ballone Type Cross-laminated Timber Shear Walls

A.1 Model Labeling

TABLE A-1 Model Labelling for Base Models

Number of Stories	Description	Model Label
8	CLT-Steel Hybrid Structure without VI or MI	8-BaseModel-CLT_H
8	CLT-Steel with Additional Shear Wall without VI or MI	8-BaseModel-CLTSW_H
12	CLT-Steel Hybrid Structure without VI or MI	12-BaseModel-CLT_H
12	CLT-Steel with Additional Shear Wall without VI or MI	12-BaseModel-CLTSW_H
16	CLT-Steel Hybrid Structure without VI or MI	16-BaseModel-CLT_H
16	CLT-Steel with Additional Shear Wall without VI or MI	16-BaseModel-CLTSW_H

TABLE A-2 Vertical Geometric Irregularity

Number of Stories	Increased Mass	Description	Label
8	1.5D	CLT-Steel Hybrid I Increased mass on the 4th Floor	8-MI-CLT_H-1.5D
	2.0D	CLT-Steel Hybrid I Increased mass on the 4th Floor	8-MI-CLT_H-2.0D
	2.5D	CLT-Steel Hybrid I Increased mass on the 4th Floor	8-MI-CLT_H-2.5D
12	1.5D	CLT-Steel Hybrid I Increased mass on the 6th Floor	12-MI-CLT_H-1.5D
	2.0D	CLT-Steel Hybrid I Increased mass on the 6th Floor	12-MI-CLT_H-2.0D

	2.5D	CLT-Steel Hybrid I Increased mass on the 6th Floor	12-MI-SM-1.5D
16	1.5D	CLT-Steel Hybrid I Increased mass on the 8th Floor	16-MI-CLT_H-1.5D
	2.0D	CLT-Steel Hybrid I Increased mass on the 8th Floor	16-MI-CLT_H-2.0D
	2.5D	CLT-Steel Hybrid I Increased mass on the 8th Floor	16-MI-SM-1.5D

TABLE A-3 Model Labeling for a model with Mass Irregularity (Variation of Increased Mass Along the Height Of The Structure)

Number of Stories	Setback Ratio (R_h)	Description	Model Label
8	1/7	CLT-Steel Hybrid (Configuration-01)	8-VI-CLT_H-1/7
	2/6	CLT-Steel Hybrid (Configuration-01)	8-VI-CLT_H-2/6
	3/5	CLT-Steel Hybrid (Configuration-01)	8-VI-CLT_H-3/5
	1/7	CLT-Steel Hybrid (Configuration-02)	8-VI-CLTASW_H-1/7
	2/6	CLT-Steel Hybrid (Configuration-02)	8-VI-CLTASW_H-2/6
	3/5	CLT-Steel Hybrid (Configuration-02)	8-VI-CLTASW_H-3/5
12	3/9	CLT-Steel Hybrid (Configuration-01)	12-VI-CLT_H-3/9
	5/7	CLT-Steel Hybrid (Configuration-01)	12-VI-CLT_H-5/7
	7/5	CLT-Steel Hybrid (Configuration-01)	12-VI-CLT_H-7/5
	3/9	CLT-Steel Hybrid (Configuration-02)	12-VI-CLTASW_H-3/9
	5/7	CLT-Steel Hybrid (Configuration-02)	12-VI-CLTASW_H-5/7
	7/5	CLT-Steel Hybrid (Configuration-02)	12-VI-CLTASW_H-7/5
16	8/8	CLT-Steel Hybrid (Configuration-01)	16-VI-CLT_H-8/8
	4/12	CLT-Steel Hybrid (Configuration-01)	16-VI-CLT_H-4/12

6/10	CLT-Steel Hybrid (Configuration-01)	16-VI-CLT_H-6/10
8/8	CLT-Steel Hybrid (Configuration-02)	8-VI-CLTASW_H-1/7
4/12	CLT-Steel Hybrid (Configuration-02)	8-VI-CLTASW_H-2/6
6/10	CLT-Steel Hybrid (Configuration-02)	8-VI-CLTASW_H-3/5

TABLE A-4 Model Labeling for a model with Mass Irregularity (Variation of Increased Mass Along the Height of The Structure)

No. of Stories	The floor that increased mass of 2.5D	Model ID
8	Floor 1	8-MI-Hybrid-2.5D-FL-01
	Floor 2	8-MI-Hybrid-2.5D-FL02
	Floor 3	8-MI-Hybrid-2.5D-FL-03
	Floor 4	8-MI-Hybrid-2.5D-FL-04
	Floor 5	8-MI-Hybrid-2.5D-FL-05
	Floor 6	8-MI-Hybrid-2.5D-FL-06
	Floor 7	8-MI-Hybrid-2.5D-FL-07
	Floor 8	8-MI-Hybrid-2.5D-FL-08
12	Floor 1	12-MI-Hybrid-2.5D-FL-01
	Floor 2	12-MI-Hybrid-2.5D-FL-02
	Floor 3	12-MI-Hybrid-2.5D-FL-03
	Floor 4	12-MI-Hybrid-2.5D-FL-04
	Floor 5	12-MI-Hybrid-2.5D-FL-05
	Floor 6	12-MI-Hybrid-2.5D-FL-06
	Floor 7	12-MI-Hybrid-2.5D-FL-07
	Floor 8	12-MI-Hybrid-2.5D-FL-08
	Floor 9	12-MI-Hybrid-2.5D-FL-09
	Floor 10	12-MI-Hybrid-2.5D-FL-10
	Floor 11	12-MI-Hybrid-2.5D-FL-11
	Floor 12	12-MI-Hybrid-2.5D-FL-12
16	Floor 1	16-MI-Hybrid-2.5D-FL-01
	Floor 2	16-MI-Hybrid-2.5D-FL-02
	Floor 3	16-MI-Hybrid-2.5D-FL-03
	Floor 4	16-MI-Hybrid-2.5D-FL-04
	Floor 5	16-MI-Hybrid-2.5D-FL-05
	Floor 6	16-MI-Hybrid-2.5D-FL-06
	Floor 7	16-MI-Hybrid-2.5D-FL-07
	Floor 8	16-MI-Hybrid-2.5D-FL-08
	Floor 9	16-MI-Hybrid-2.5D-FL-09
	Floor 10	16-MI-Hybrid-2.5D-FL-10

Floor 11	16-MI-Hybrid-2.5D-FL-11
Floor 12	16-MI-Hybrid-2.5D-FL-12
Floor 13	16-MI-Hybrid-2.5D-FL-13
Floor 14	16-MI-Hybrid-2.5D-FL-14
Floor 15	16-MI-Hybrid-2.5D-FL-15
Floor 16	16-MI-Hybrid-2.5D-FL-16

A.2 Evaluation of Mass Irregularity (Increased Mass at the Mid-Level of the Structure)

(a)

(b)

(c)
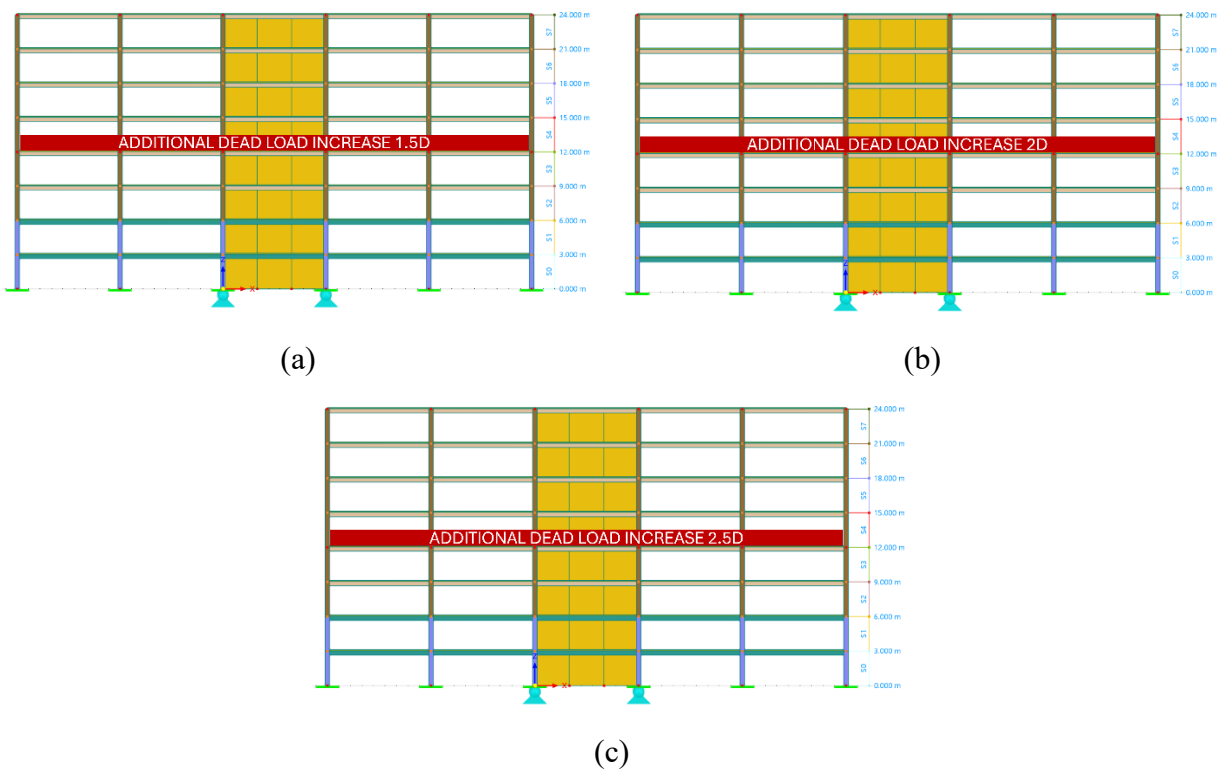
Fig. A-1 (a) 8-MI-CLT_H-1.5D (b) 8-MI-CLT_H-2.0D (c) 8-MI-CLT_H-2.5D
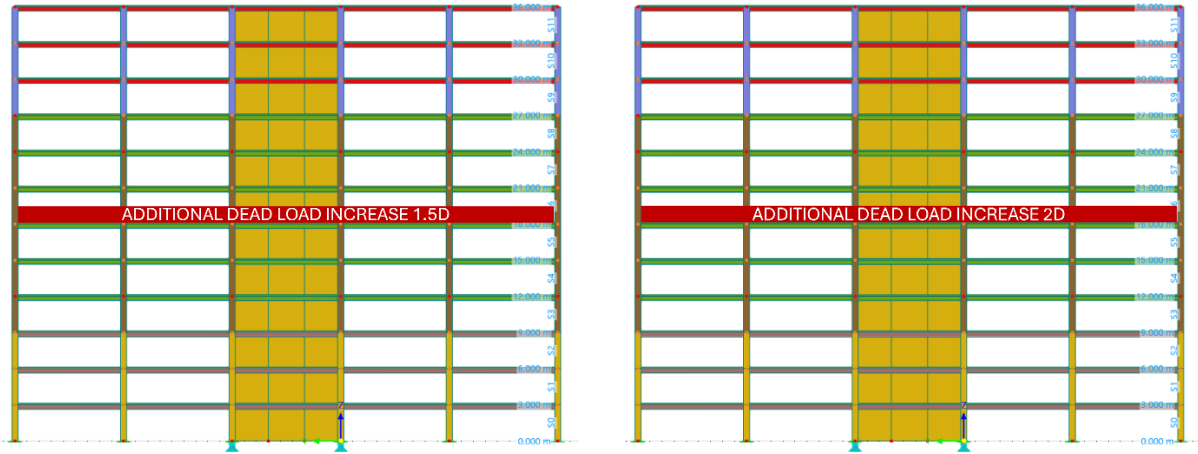
(a)

(b)
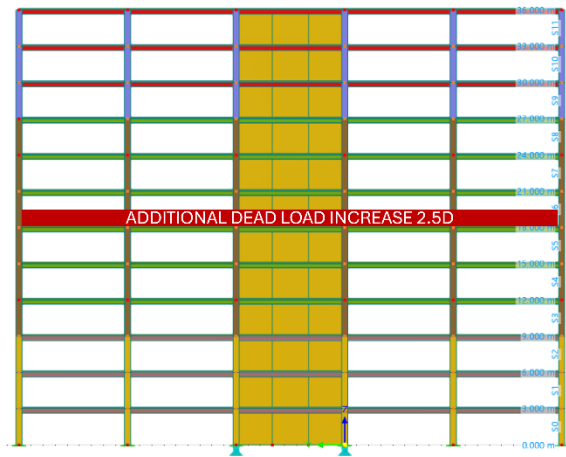
(c)

Fig. A-2 (a) 12-MI-CLT_H-1.5D (b) 12-MI-CLT_H-2.0D (c) 12-MI-CLT_H-2.5D
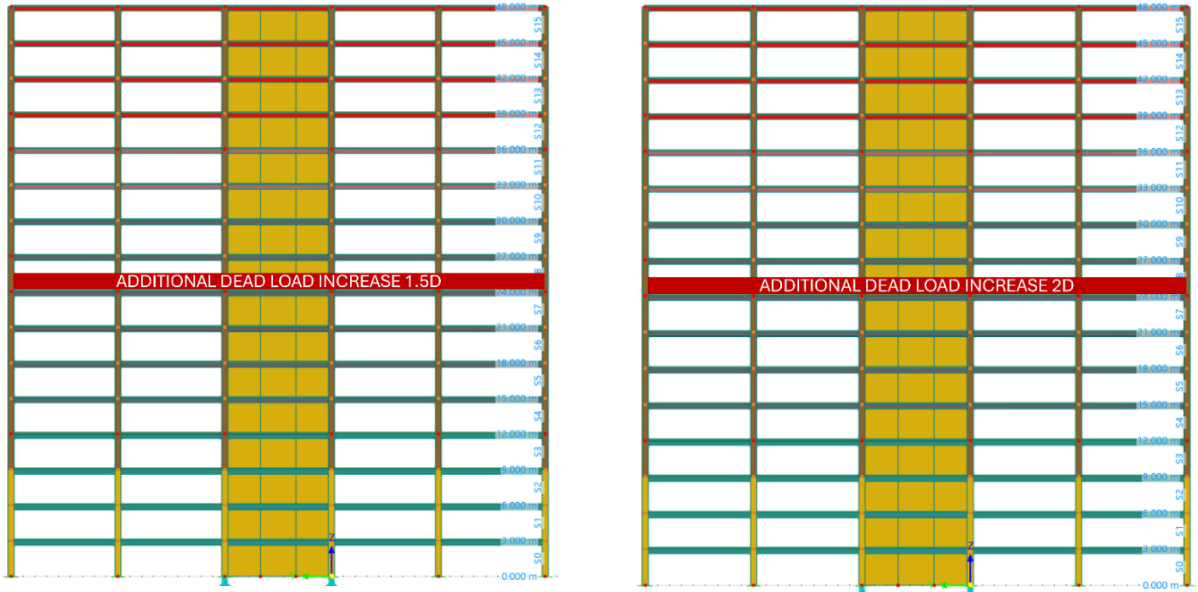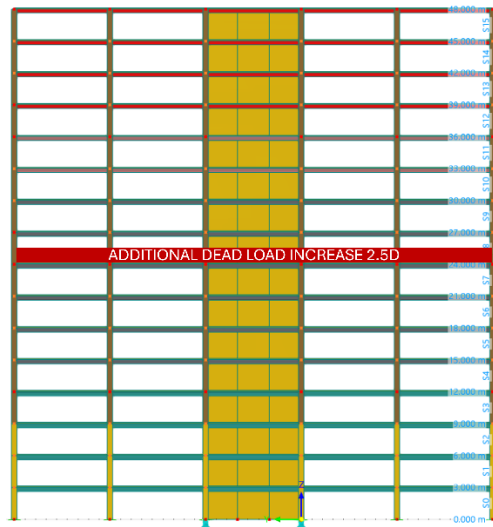
Fig. A-3 (a) 16-MI-CLT_H-1.5D (b) 16-MI-CLT_H-2.0D (c) 16-MI-CLT_H-2.5D

A.3   Assessment of Vertical Geometric Irregularity
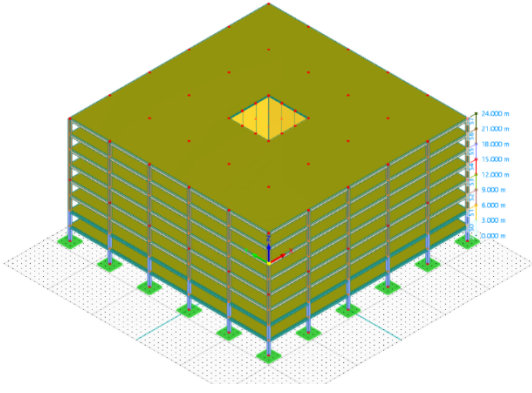
(a)
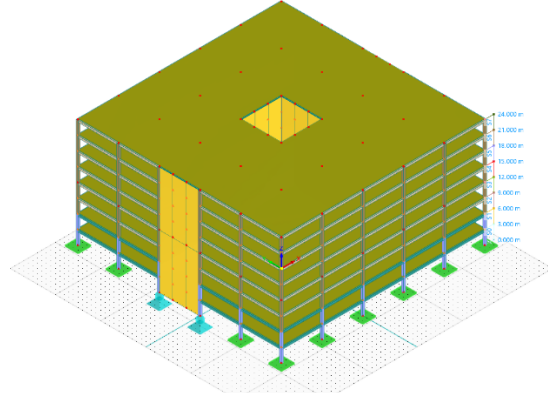
(b)
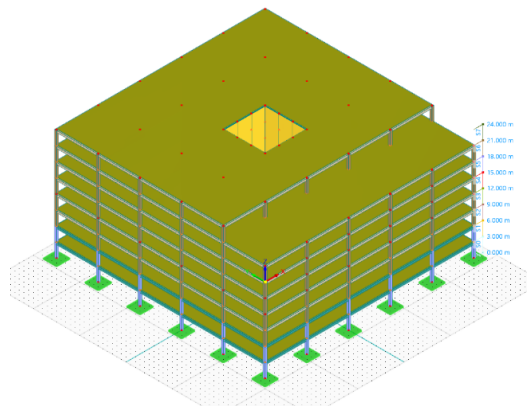
(c)
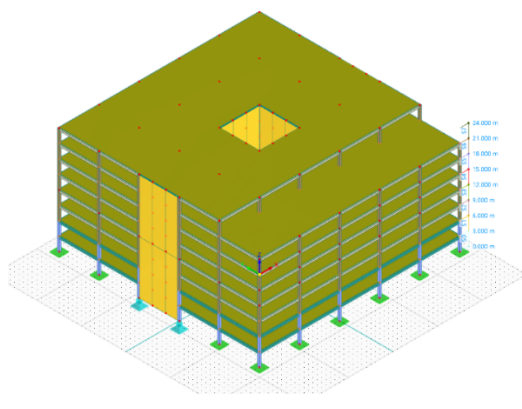
(d)
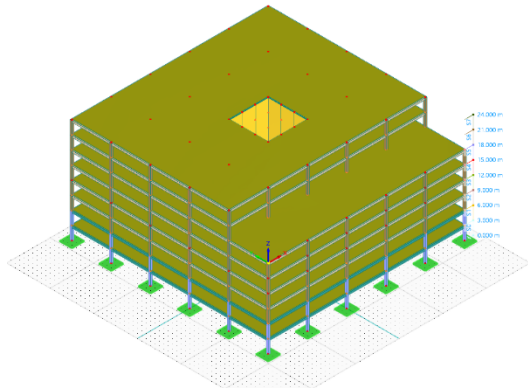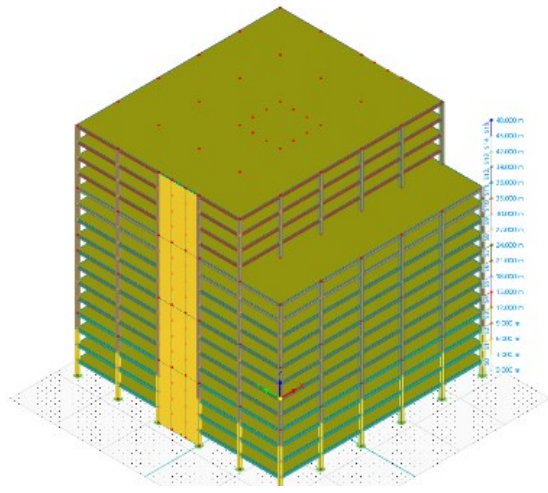
(e)
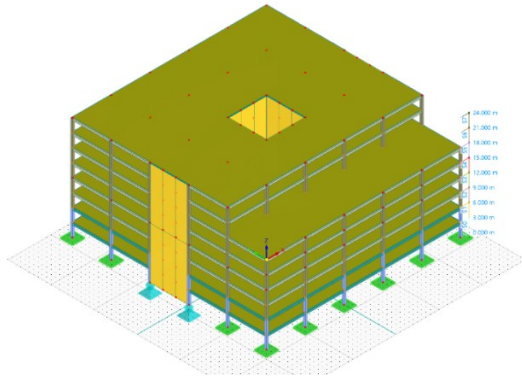
(f)
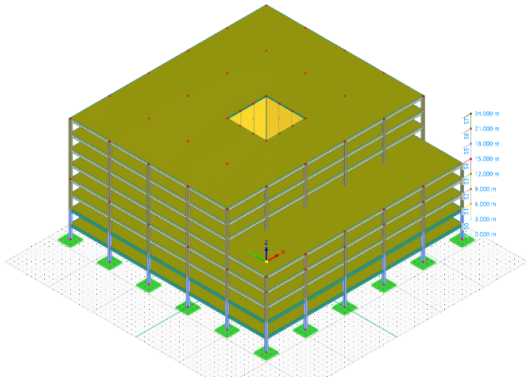
(g)
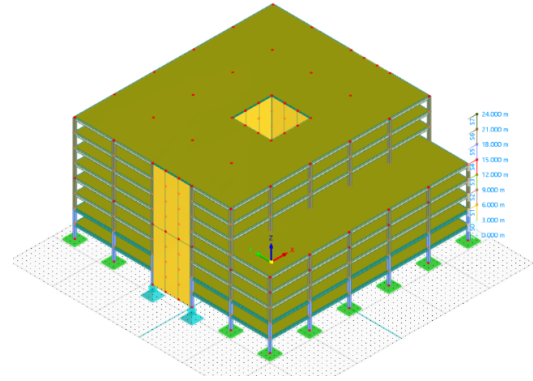
(h)

Fig. A-4 (a) 8-BaseModel-CLT_H (b) 8-BaseModel-CLTSW_H (c) 8-VI-CLT_H-1/7 (d) 8-VI-CLT_H-2/6 (f) 8-VI-CLT_H-3/5 (g) 8-VI-CLTASW_H-1/7 (h) 8-VI-CLTASW_H-2/6 (i) 8-VI-CLTASW_H-3/5
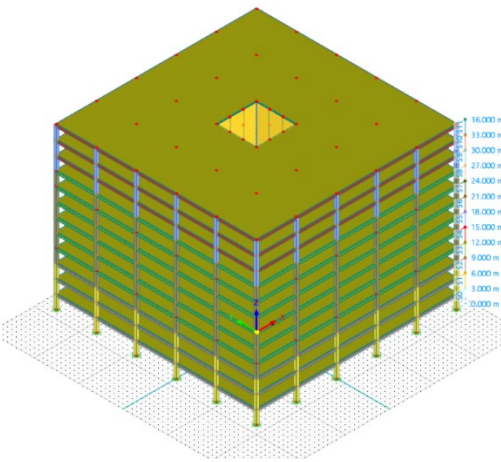
(a)
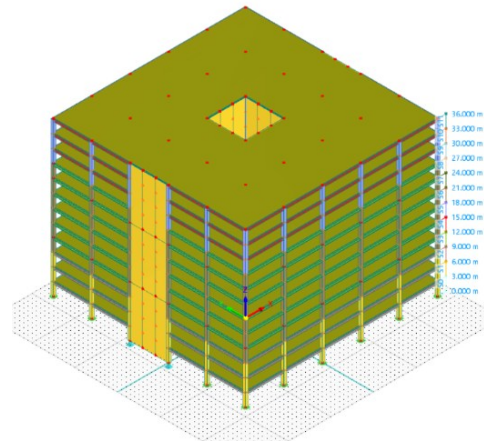
(b)
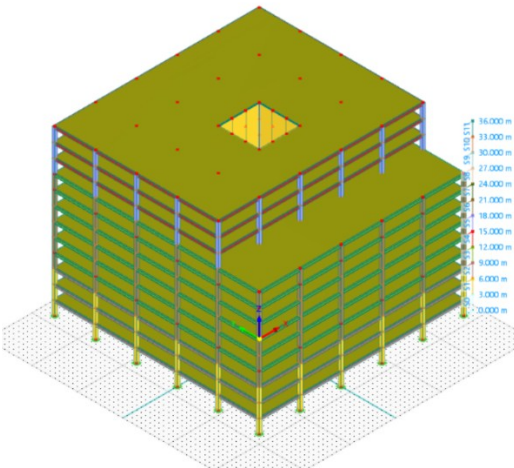
(c)
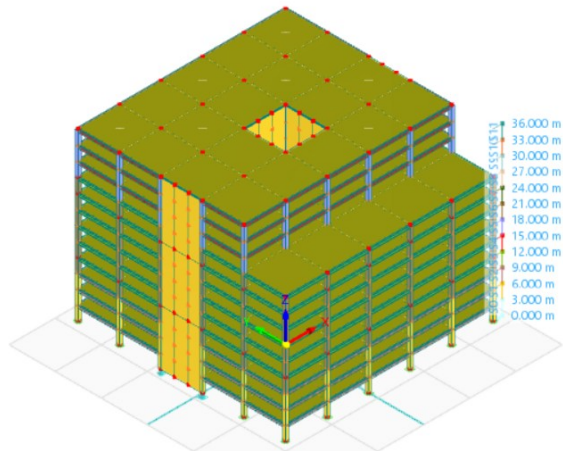
(d)
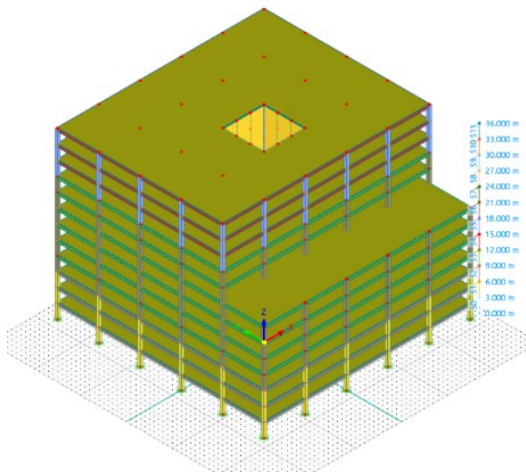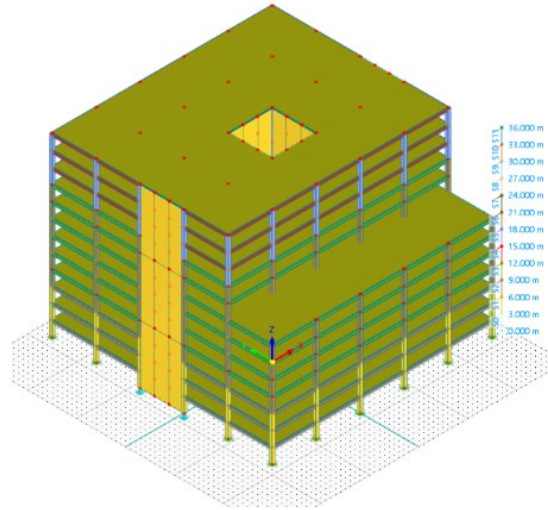
(e)　　　　　　　　　　　　　　　　(f)
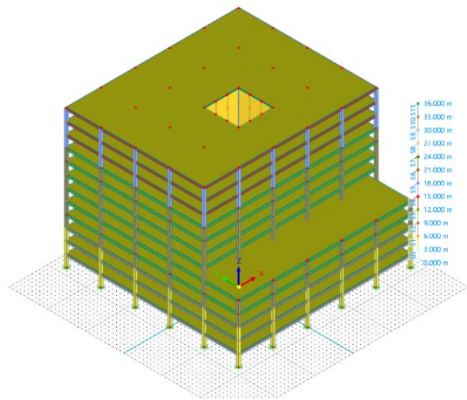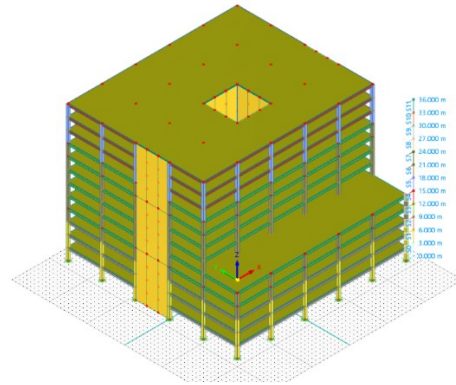
(g)　　　　　　　　　　　　　　　　(h)

Fig. A-5 (a)12-BaseModel-CLT_H (b)12-BaseModel-CLTSW_H (c) 12-VI-CLT_H-3/9 (d) 12-VI-CLT_H-5/7 (e) 12-VI-CLT_H-7/5 (f)12-VI-CLTASW_H-3/9 (g) 12-VI-CLTASW_H-5/7 (h) 12-VI-CLTASW_H-7/5
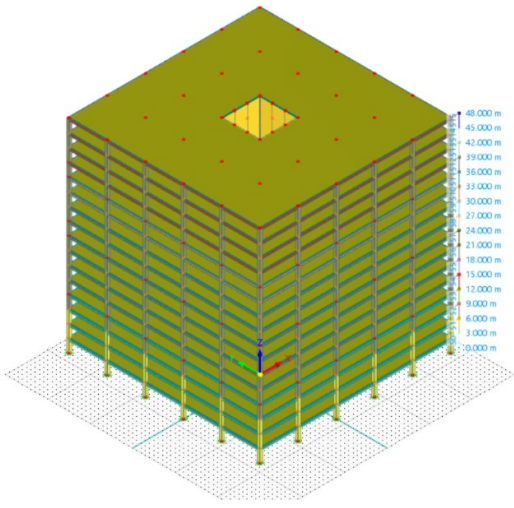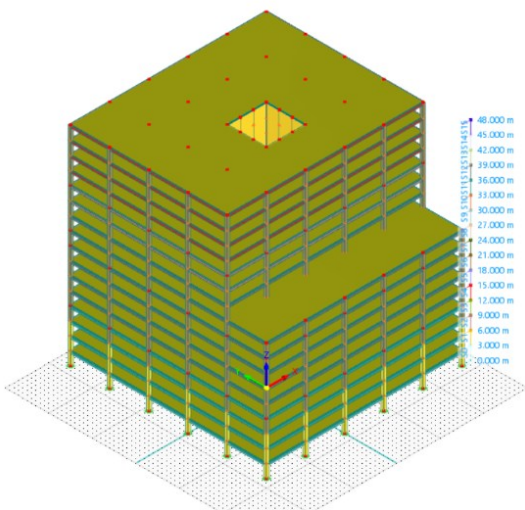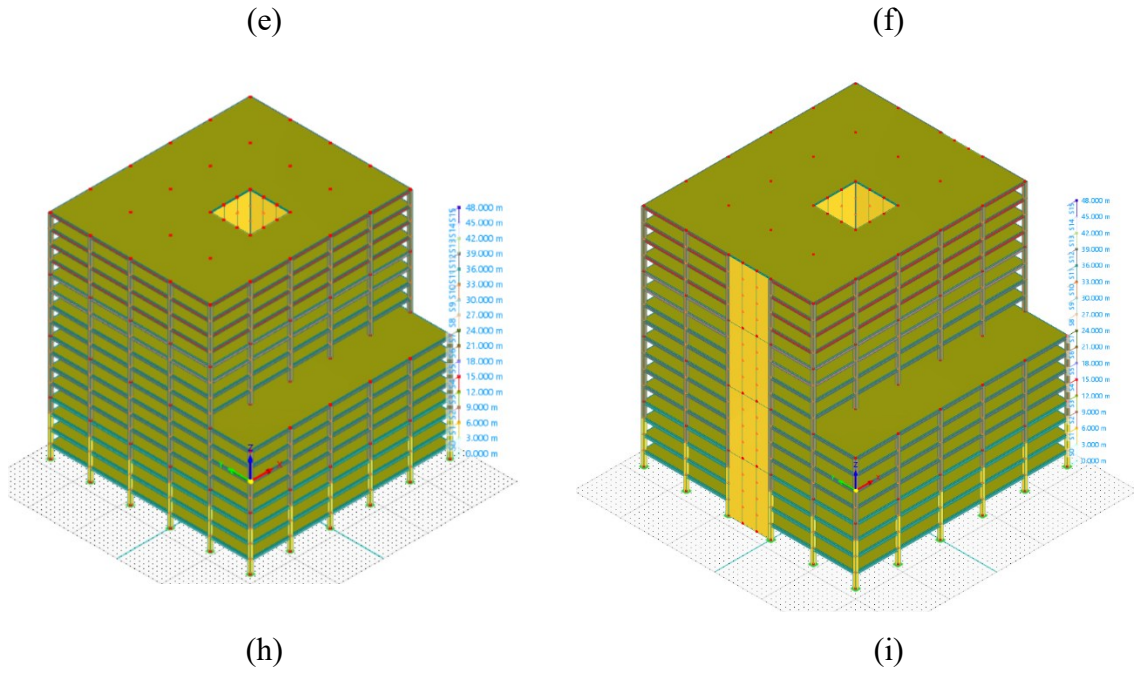
(a)
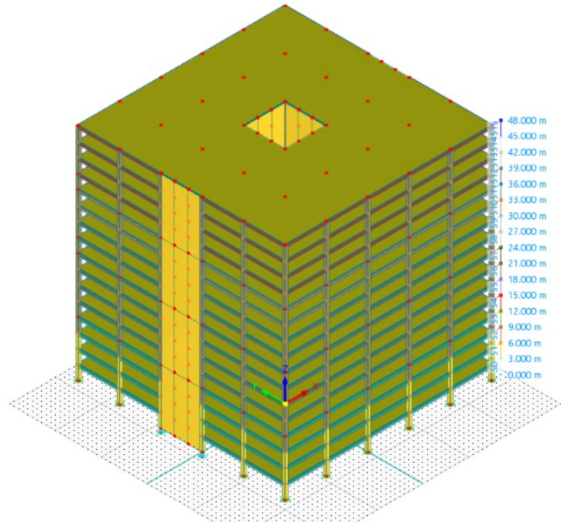
(b)
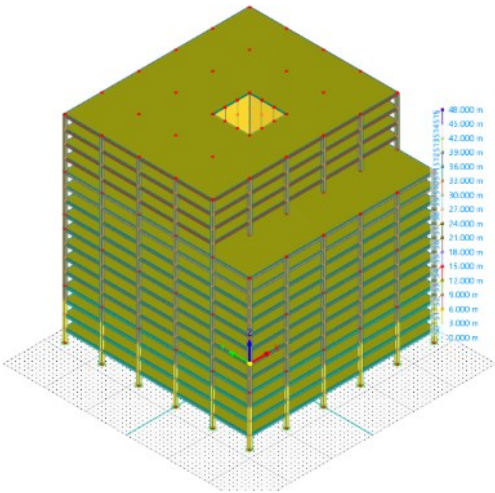
(c)

(d)
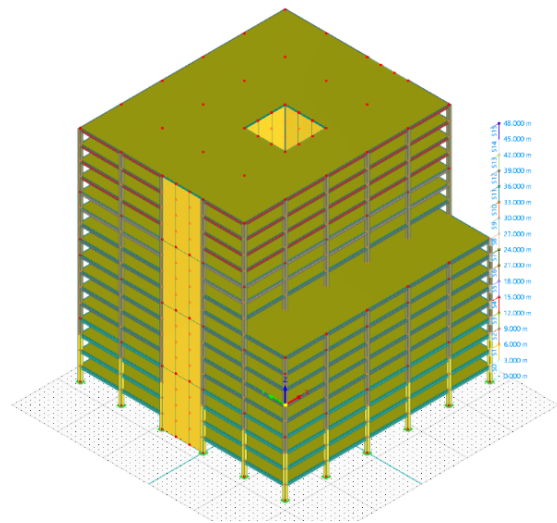
Fig. A-6 (a) 16-BaseModel-CLT_H (b) 16-BaseModel-CLTSW_H (c) 16-VI-CLT_H-8/8 (d) 16-VI-CLT_H-4/12 (e) 16-VI-CLT_H-6/10 (f) 16-VI-CLTASW_H-8/8 (g) 16-VI-CLTASW_H-4/12 (h) 16-VI-CLTASW_H-6/10

B   Appendix B: Structural Performance of Balloon-Type Unbounded Post-Tensioned Cross-Laminated Timber Wall System

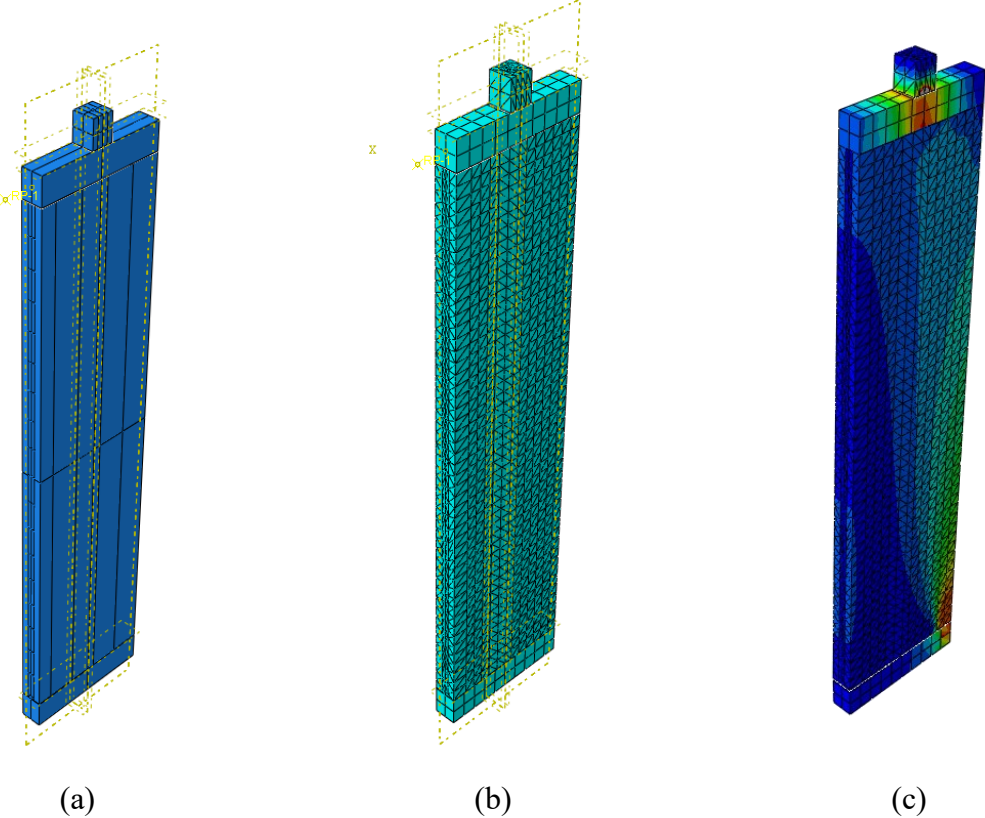(a)   (b)   (c)

Fig. B-1 Validated Model(Abaqus) (a) Undeformed UPTC model (b) Mesh (c) Deformed Shape

C Appendix C: Additional Investigation of Hybrid Structures with Balloon-Type CLT Shear Wall Systems: A Comparative Study
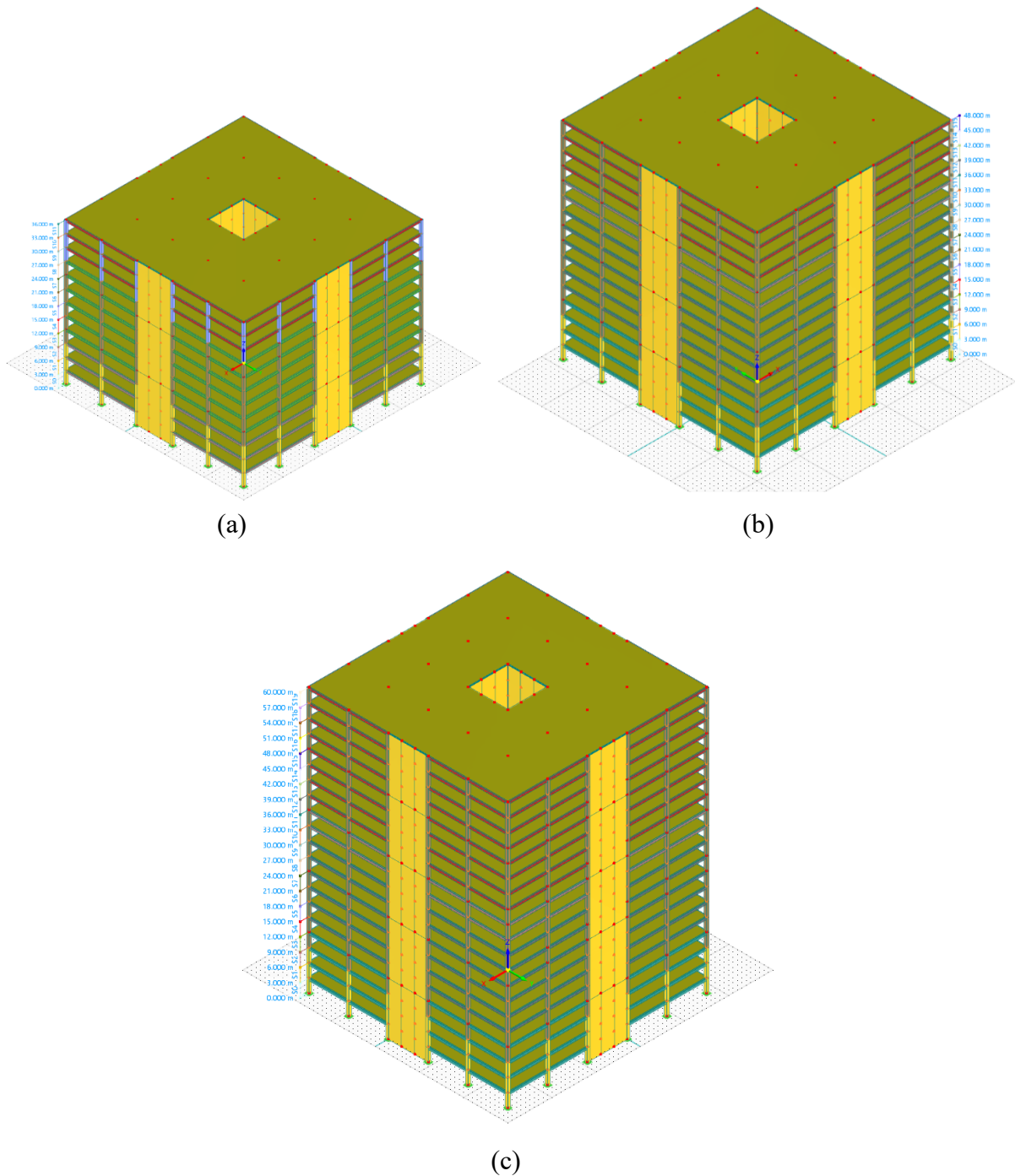

(a)

(b)

(c)

Fig. C-1 (a) 12-MI-Hybrid-2.5D (b) 12-MI-Hybrid-2.5D (c) 12-MI-Hybrid-2.5D